UNIVERSIDADE DE BRASÍLIA

INSTITUTO DE CIÊNCIAS BIOLÓGICAS

PROGRAMA DE PÓS-GRADUAÇÃO EM BIOLOGIA MOLECULAR

ANÁLISE DE FLUXO METABÓLICO DE LEVEDURAS QUE NATURALMENTE

FAZEM A CONVERSÃO DE XILOSE EM ETANOL

HENRIQUE CÉSAR TEIXEIRA VERAS

BRASÍLIA – DF
2018

UNIVERSIDADE DE BRASÍLIA

INSTITUTO DE CIÊNCIAS BIOLÓGICAS

PROGRAMA DE PÓS-GRADUAÇÃO EM BIOLOGIA MOLECULAR

Análise de fluxo metabólico de leveduras que naturalmente fazem a conversão de xilose em etanol

Henrique César Teixeira Veras

Orientadora: Prof. Dra. Nádia Skorupa Parachin
Coorientador: Dr. João Ricardo Moreira de Almeida

Tese apresentada ao programa de Pós-Graduação em Biologia Molecular da Universidade de Brasília, como parte dos requisitos para obtenção do título de Doutor.

Brasília – DF
Março / 2018

Análise de fluxo metabólico de leveduras que naturalmente fazem a conversão de xilose em etanol

Henrique César Teixeira Veras

Tese de Doutorado

Banca Examinadora

Prof^a. Dr^a. Nádia Skorupa Parachin (Orientadora - Presidente)
Programa de Pós-Graduação em Biologia Molecular (IB) - UnB

Prof^a. Dr^a. Eliane Ferreira Noronha (Vinculado)
Programa de Pós-Graduação em Biologia Molecular (IB) - UnB

Prof. Dr. José Gregório Cabrera Gomes (Externo Não Vinculado)
Universidade de São Paulo (ICB) - USP

Pesq^a. Dr^a. Sílvia Belém Gonçalves (Não Vinculado)
EMBRAPA Agroenergia

Prof^a. Dr^a. Talita Souza Carmo (Suplente)
Programa de Pós-Graduação em Biologia Molecular (IB) - UnB

Brasília, DF 09 de março de 2018.

EPÍGRAFE

" Destino é a soma de determinação e desespero. "

Autor desconhecido

RESUMO

A demanda mundial por combustível continua crescendo. Entre as fontes alternativas de energia a produção de etanol tem lugar de destaque. No entanto, está produção ainda pode aumentar com o aproveitamento da xilose proveniente da biomassa lignocelulósica. Vários estudos estão sendo realizados para identificar os mecanismos moleculares envolvidos no metabolismo de xilose. Neste estudo é proposto a integração dados fisiológicas e moleculares para caracterizar o fluxo metabólico de leveduras. Foi avaliado a capacidade fermentativa entre diferentes leveduras naturalmente consumidoras de xilose: *Scheffersomyces stipitis*, *Spathaspora passalidarum*, *Spathaspora arborariae* e *Candida tenuis*. Para entender o metabolismo dessas leveduras foi construído um modelo de fluxo metabólico utilizando as taxas de produção para restringir o modelo e calcular a distribuição interna de carbono. Pela primeira vez, é estimado o fluxo metabólico nas leveduras *Spathaspora*. O modelo de fluxo metabólico de xilose até a formação de etanol foi inicialmente validado a partir do teste de correlação entre fluxos calculados e medidos. O modelo de fluxo metabólico foi útil para aumentar a acurácia de dados de metaboloma. 74% das taxas de fluxos calculados e medidos apresentaram semelhanças acima de 90%. O modelo caracterizou a *S. stipitis* e *S. passalidarum* como tendo as melhores propriedades naturais para fermentar xilose e produzir etanol.

Palavras-chaves:

Biomassa Lignocelulósica, Leveduras Fermentadoras de Xilose, Fluxos Metabólicos, Metaboloma, Etanol.

ABSTRACT

Global demand for fuel continues to grow. Among the alternative sources of energy, the production of ethanol has a prominent place. However, this production can yet increase with the use of xylose from the lignocellulosic biomass. Several studies are being carried out to identify the molecular mechanisms involved in the metabolism of xylose. In this study it is proposed the integration of physiological and molecular data to characterize the metabolic flux of yeasts. It was assessed the fermentative capacity among different yeasts naturally consuming xylose: *Scheffersomyces stipitis*, *Spathaspora passalidarum*, *Spathaspora arborariae* and *Candida tenuis*. To understand the metabolism of these yeasts a metabolic flux model was constructed using the production rates to constrain the model and to calculate the internal carbon distribution. For the first time, is estimated the metabolic flux into *Spathaspora* yeasts. The metabolic flux model was initially validated from a correlation test between calculated and measured fluxes. The metabolic flux model was useful to increase accuracy of metabolome data. 74% of calculated and measured fluxes rate shown similarity above 90%. The model characterized *S. stipitis* and *S. passalidarum* as having the best natural properties for fermenting xylose and producing ethanol.

Keywords:
Lignocellulosic Biomass, Xylose-fermenting Yeast, Metabolic Flux, Metabolome, Ethanol.

LISTA DE ARTIGOS

A tese é baseada nestes três artigos.

- Comparative assessment of fermentative capacity of different xylose-consuming yeasts a. **Henrique César Teixeira Veras**, Nádia Skorupa Parachin, João Ricardo Moreira de Almeida. Microbial Cell Factories 16:153

- New protocol based on UHPLC-MS/MS for quantitation of metabolites in xylose-fermenting yeasts (2017). Christiane Gonçalves Campos, **Henrique César Teixeira Veras**, José Antônio de Aquino Ribeiro, Patrícia Pinto Kalil Gonçalves Costa, Katiúscia Pereira Araújo, Clenilson Martins Rodrigues, João Ricardo Moreira de Almeida, Patrícia Verardi Abdelnur. J. Am. Soc. Mass Spectrometry - doi: 1007/s13361-017-1786-9

- Utilization of metabolic flux analysis for metabolome data validation of xylose-fermenting yeasts (2018). **Henrique César Teixeira Veras**, Christiane Gonçalves Campos, Igor Ferreira Nascimento, Patrícia Verardi Abdelnur, João Ricardo Moreira de Almeida, Nádia Skorupa Parachin. ACS Systems Biology (manuscrito)

SUMÁRIO

1. INTRODUÇÃO

A percepção de que as fontes de energia fóssil são esgotáveis e que a demanda mundial por energia continua aumentando, motivou o desenvolvimento de processos mais produtivos e limpos de energias renováveis (Pereira *et al.*, 2015). Uma estimativa da demanda mundial por energia para o ano de 2040, mostra que o mundo irá requerer 56% a mais de energia do que no ano de 2010. Esse aumento, possivelmente, estará relacionado com o crescimento econômico de países densamente habitados como China e Índia (Mme, 2016). Entre as fontes de energia, as renováveis serão as que apresentarão maior demanda. No ano de 2010 a demanda por fontes renováveis de energia foi de 10,7%, a estimativa é que no ano de 2040 essa demanda seja de 14.5% (Fig. 1). Além disso, espera-se que o consumo de energia derivada do petróleo e carvão diminua. Isso pode ocorrer devido as flutuações do preço do petróleo e pela tentativa de minimizar os efeitos poluidores resultante da queima do petróleo. Energia proveniente de gás natural e energia nuclear também aumentará, mas em pequena proporção, apenas 1% e 2%, respectivamente (Eia, 2016).

Figura 1. Projeções da futura demanda mundial por fontes de energia no ano de 2040 (Eia, 2016).
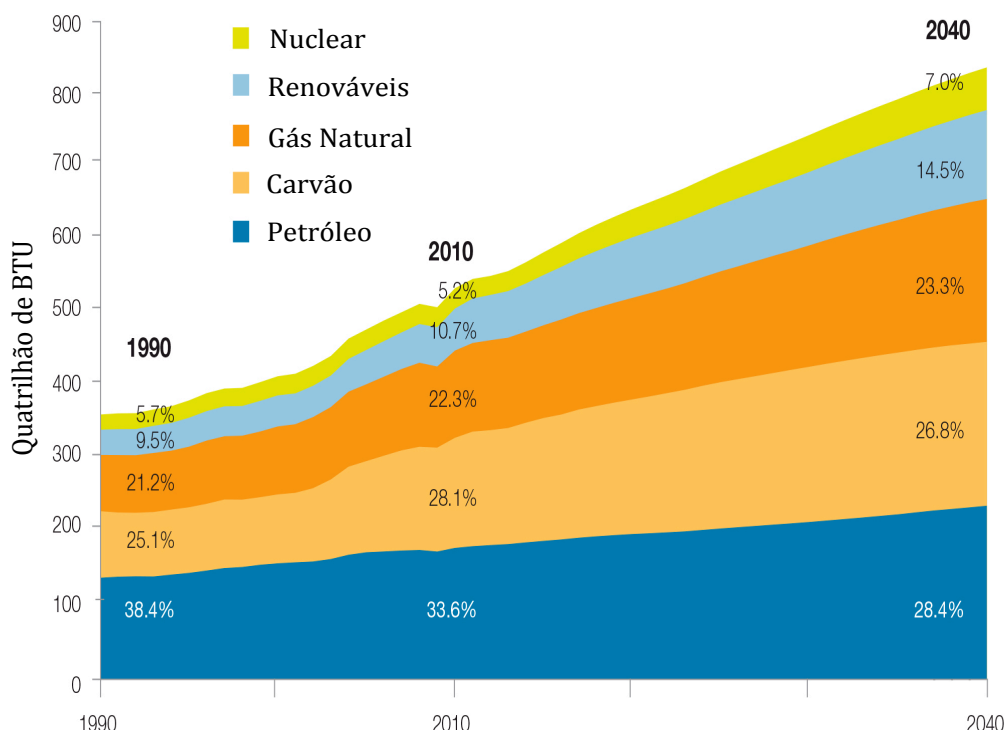
Aliado ao desejo de atender o aumento do consumo de energia, também existe o desejo de que o desenvolvimento dessas tecnologias estejam em sintonia com a necessidade de preservar o meio ambiente. A produção de etanol tem lugar de destaque entre as energias renováveis. O Brasil produziu cerca de 30 bilhões de litros de etanol no ano de 2015. O volume total foi 6% superior ao produzido em 2014 (Mme, 2016). Este biocombustível é produzido a partir da fermentação realizada por microrganismos que utilizam carboidratos como a glicose como fonte de carbono (Hou, 2012).

Com o avanço da biotecnologia é possível investigar uma ampla variedade de microrganismos a fim de identificar bioprocessos mais viáveis. Além do etanol existem outras fontes de energia como biodiesel, butanol entre outros produtos que podem ser produzidos a partir de bioprocessos. Tornando o uso de microrganismos em bioprocessos uma alternativa a síntese química de produtos a partir de fonte fóssil (Li and Borodina, 2014). As leveduras estão entre os microrganismos unicelulares amplamente estudados. Algumas espécies são utilizadas em atividades econômicas, tais como a produção de bebidas fermentadas e pães (Kavscek *et al.*, 2015). A levedura *Saccharomyces cerevisiae* é um dos principais microrganismos utilizados na produção de bioquímicos pela indústria. Um dos principais produtos é o etanol (Kavscek *et al.*, 2015; Radecka *et al.*, 2015; Moyses *et al.*, 2016).

Um dos principais desafios, no entanto, é melhorar a capacidade fermentativa de produção de etanol realizando fermentação de açúcares hexoses e pentoses derivados da lignocelulose (Radecka *et al.*, 2015). A limitação da *S. cerevisiae* em fermentar xilose, torna a produção de etanol a partir da biomassa lignocelulósica menos viável economicamente (Hou, 2012). Embora seja observado que a *S. cerevisiae* possua as enzimas responsáveis pela conversão de xilose, elas não são funcionais a ponto de converter a xilose (Almeida *et al.*, 2011; Liao *et al.*, 2016). Portanto, o uso da biomassa lignocelulósica para produção de etanol, desperta o interesse de entender o funcionamento do metabolismo de leveduras que foram descobertas com a capacidade de consumir açúcares como a xilose (Jeffries *et al.*, 2007; Wohlbach *et al.*, 2011; Cadete *et al.*, 2012).

1.1 Biomassa Lignocelulósica

A biomassa lignocelulósica é composta por polímeros como celulose e hemicelulose e compostos fenólicos que formam a lignina (Fig. 2). A celulose e hemicelulose podem ser

convertidas em açúcares para futura utilização em processos fermentativos de produção de etanol (Kumar, R. *et al.*, 2016). As concentrações destes compostos são variáveis entre as diferentes espécies vegetais. A variação é de aproximadamente 40 - 50% de celulose, 20 - 40% de hemicelulose e 20 - 35% de lignina (Liao *et al.*, 2016).

Figura 2. Estrutura da biomassa lignocelulósica destacando os principais compostos: celulose, hemicelulose e lignina (Microbewiki, 2016).
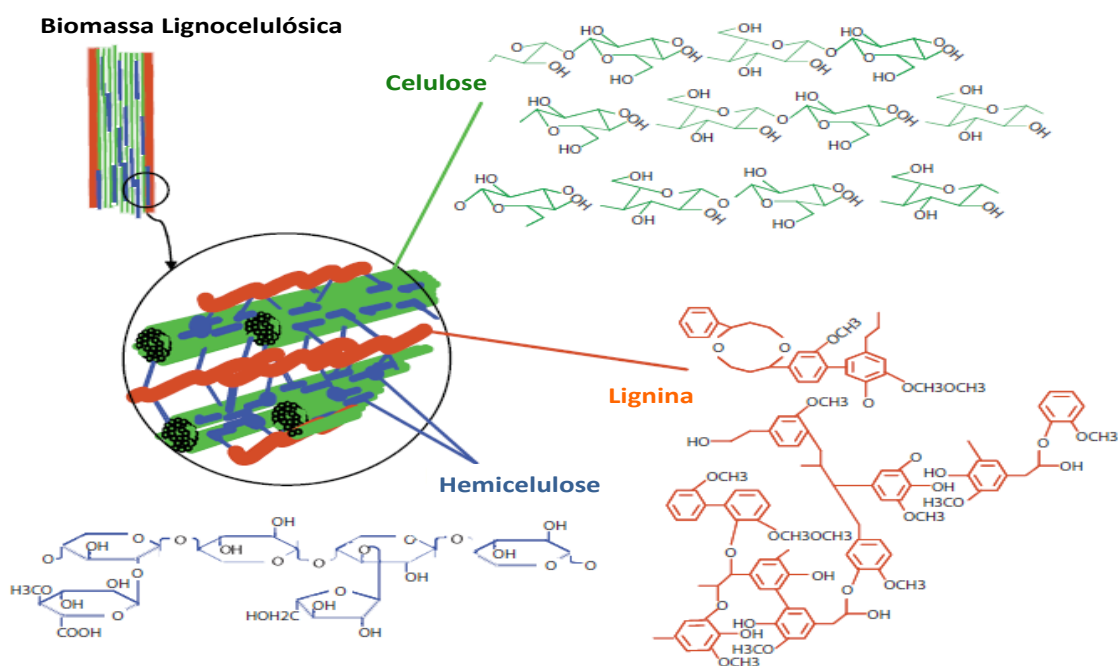
1.2 Compostos Lignocelulósicos

A celulose é um homopolímero composto por cadeias lineares de unidades de glicose. As cadeias de glicose formam microfibrilas, que são empacotadas para formar fibras de celulose. As fibras de celuloses são encaixadas em uma matriz amorfa de hemicelulose e lignina (Kumar, A. *et al.*, 2016). A hemicelulose é um heteropolímero ramificado consistindo de açúcares hexoses (glicose, manose e galactose) e pentoses (xilose e arabinose). Resíduos de xilose formam xilana, o principal componente estrutural da hemicelulose e o segundo mais abundante polissacarídeo na natureza após a celulose (Konishi *et al.*, 2015). A camada de xilana faz interação covalente com a lignina e ligações não covalentes com a celulose (Beg *et*

al., 2001). A lignina consiste de macromoléculas que contém compostos fenólicos ramificados. Sua função é proporcionar rigidez a parede celular. Seus compostos são conectados por ligações ésteres que os ligam firmemente à celulose e hemicelulose (Nanda *et al.*, 2013). Estes compostos da biomassa lignocelulósica formam estruturas complexas, fortemente entrelaçadas e quimicamente ligadas por ligações covalentes (β-1,4 glicosídicas) e pontes de hidrogênio (Kumar, A. *et al.*, 2016).

1.3 Processamento da Biomassa Lignocelulósica

A conversão dos açúcares lignocelulósicos até etanol ocorre a partir de quatro etapas: pré-tratamento da biomassa lignocelulósica, hidrólise enzimática, fermentação e recuperação do etanol formado (Almeida *et al.*, 2011related). Metodologias físicas, químicas e/ou biológicas são usadas para o pré-tratamento e hidrólise dos resíduos agroindustriais para disponibilização dos açúcares, dentre eles a xilose (Kang *et al.*, 2014). Entre os produtos investigados a partir de processos fermentativos utilizando açucares da biomassa lignocelulósica têm etanol, um dos mais investigados, além da produção de ácidos orgânicos, enzimas hidrolíticas entre outros (Kumar, A. *et al.*, 2016).

2. LEVEDURAS FERMENTADORAS DE XILOSE

Diferentes espécies de leveduras tem sido investigadas por causa da sua capacidade de fermentar xilose e produzir etanol (Beg *et al.*, 2001; Barrios-Gonzalez and Miranda, 2010). Os esforços estão concentrados no sentido de entender as propriedades naturais destes microrganismos e melhorar essas características (Kitano, 2002; Parachin *et al.*, 2011). As espécies de leveduras que apresentam metabolismo com a capacidade de fermentar xilose são extremamente relevantes para aumentar a produção de etanol e portanto, de interesse econômico (Eliasson *et al.*, 2000). A Tabela 1, apresenta alguns exemplos de leveduras fermentadoras de xilose que já são estudadas e que apresentam diferentes taxas de rendimento de etanol.

Tabela 1. Leveduras naturalmente consumidoras de xilose e as respectivas taxas de rendimento de etanol alcançadas.

Levedura	Rendimento (g etanol/ g xilose)	Referência
Scheffersomyces stipitis	0.48	(Skoog and Hahn-Hagerdal, 1990)
Spathaspora passalidarum	0.43	(Su *et al.*, 2014)
Spathaspora arborariae	0.37	(Cadete *et al.*, 2009)
Candida tenuis	0.24	(Trausinger *et al.*, 2015)
Candida shehatae	0.35	(Du Preez *et al.*, 1989)
Pachysolen tannophilus	0.28	(Lightelm *et al.*, 1988)
Kluyveromyces marxianus	0.10	(Wilkins *et al.*, 2008)
Hansenula polymorpha	0.08	(Kurylenko *et al.*, 2014)

Para que uma levedura seja utilizada na indústria, ela precisar possuir algumas propriedades como: eficiente utilização de açúcares hexoses e pentose, tolerância aos estresses da fermentação como altas temperaturas, condições de anaerobiose, osmolaridade do meio e baixo pH (Heux *et al.*, 2015; Radecka *et al.*, 2015). Também precisam ter capacidade para fermentar na presença de inibidores liberados durante o processo de pré-tratamento e hidrólise da biomassa lignocelulósica (Almeida *et al.*, 2008; Kang *et al.*, 2014). Além da necessidade de tolerar altas concentrações do etanol produzido (Radecka *et al.*, 2015). Ainda não foi identificado nenhuma levedura com todas as propriedades desejadas e, que apresente compatibilidade com as especificações industriais. Entretanto, através de estudos comparativos é possível identificar as características individuais e usá-las juntas para contribuir com informações para o melhor aproveitamento da xilose.

2.1 Leveduras analisadas

A *S. stipitis* é uma das leveduras fermentadoras de xilose mais investigada. É uma levedura endosimbionte de besouros que habitam e degradam madeira em decomposição (Jeffries *et al.*, 2007). Os genes codificantes para as enzimas xilose reductase (XR) e xilitol desidrogenase (XDH) dessa levedura são frequentemente usados no melhoramento genético de leveduras para fermentar xilose (Moyses *et al.*, 2016). O alto rendimento (Tab. 1) e alta

produtividade são fatores essenciais para a escolha dessa levedura em processo fermentativos de produção de bioetanol. No trabalho que foi avaliado a capacidade fermentativa dessa levedura (Veras *et al.*, 2017), foi observado rendimento de etanol (0.45 g g) similar ao apresentados anteriormente (Skoog and Hahn-Hagerdal, 1990).

No gênero *Spathaspora* contém várias espécies de leveduras fermentadoras de xilose que foram isoladas de madeira em decomposição e/ou intestino de insetos perfuradores de madeira (Cadete *et al.*, 2009). A *S. passalidarum* é uma dessas leveduras que presenta capacidade de utilizar xilose e faz isso melhor em condições limitadas de oxigênio. Além disso, a XR dessa levedura apresenta preferência pelo cofator NADH em vez de NADPH (Hou, 2012). Está característica também foi observada no nosso trabalho (Veras *et al.*, 2017). Outra espécie do gênero *Spathaspora* é a levedura *S. arborariae*, essa levedura foi isolada de madeiras em decomposição presentes em dois ecossistemas brasileiro, a floresta atlântica e o cerrado (Cadete *et al.*, 2009). O estudo dessa levedura irá agregar valor à biodiversidade brasileira, pois caracterizará essa espécie de levedura da nossa biodiversidade.

A levedura *C. tenuis* é outra que vem sendo investigada e também está associada ao intestino de besouros (Wohlbach *et al.*, 2011). No entanto, esta levedura apresenta um desequilíbrio de cofatores que pode levar ao acúmulo de bioprodutos como xilitol e glicerol (Li *et al.*, 2015). No nosso trabalho não foi observado a produção de etanol. Xilitol foi o principal produto detectado. Isto pode estar correlacionado com a atividade da XR dessa levedura que apresentou dependência pelo cofator NADPH (Veras *et al.*, 2017). Outro estudo que avaliou a seletividade de cofatores da enzima XR dessa levedura fez uma dupla mutação (Lys-274 para Arg e Asn-276 para Asp) que alterou a preferência de NADPH para NADH em 6 vezes quando comparado com a linhagem selvagem. A linhagem mutante apresentou maior rendimento de etanol e diminuiu a formação de xilitol (Petschacher and Nidetzky, 2005).

3. METABOLISMO DE XILOSE

A habilidade de assimilar xilose presente no metabolismo de dessas leveduras está associada com a expressão alterada de vários genes presentes na via catabólica de assimilação de xilose, na via pentose fosfato e na via glicolítica (Wohlbach *et al.*, 2011). As vias envolvidas no catabolismo de xilose até formar etanol é uma das propriedades naturais que

desejamos entender melhor. A Figura 3 mostra um esquema da via de conversão de xilose até a formação de etanol e outros produtos.

Nas leveduras fermentadoras de xilose, o metabolismo ocorre a partir da entrada da xilose na célula. Na membrana celular destes microrganismos contém transportadores que carregam a xilose para o citoplasma. A eficiência e preferência dos transportadores de carboidratos presentes na membrana das leveduras também é alvo de diferentes estudos (Sedlak and Ho, 2004; Runquist *et al.*, 2010). E já foi observado por exemplo, que o desempenho dos transportadores depende da fonte de carbono e da sua concentração, mostrando que existe uma maior afinidade por glicose comparada com xilose (Runquist *et al.*, 2010).

3.1 Vias Metabólicas

As reações enzimáticas ocorrem a partir da assimilação de xilose, este açúcar é reduzido a xilitol pela atuação da enzima XR. A enzima XR é dependente dos cofatores NADPH e NADH (Rizzi *et al.*, 1988). No primeiro artigo que serve de base para essa tese, o ensaio enzimático para XR da *S. stipitis*, *S. arborariae* e *C. tenuis* demonstrou maior atividade com NADPH para essas leveduras, sendo $NADP^+$ regenerado. Enquanto *S. passalidarum* apresenta atividade enzimática de aproximadamente 1.5 vezes maior com NADH do que com NADPH (Veras *et al.*, 2017). A atividade de XR com NADH é mais vantajosa, pois regenera NAD^+ que pode ser utilizado na próxima reação (Hahn-Hagerdal *et al.*, 2007). Em seguida, o xilitol é convertido em xilulose pela oxidação realizada pela enzima XDH. A enzima XDH utiliza exclusivamente NAD^+ como cofator (Rizzi *et al.*, 1989; Veras *et al.*, 2017). Desta maneira, construir fluxos com balanço equilibrado de cofatores também é um desafio que se busca superar. Com a atuação da enzima xiluloquinase (XK), xilulose é convertida em xilose-5-fosfato. Essas reações ocorrem na via metabólica oxido-redutiva de assimilação de pentoses.

Figura 3. Esquema representativo das vias metabólicas envolvidas na conversão de xilose até a formação de diferentes compostos. O catabolismo de xilose ocorre em quatro vias metabólicas: via oxido-redutiva de assimilação de pentoses; via da pentose fosfato; via da glicólise e via do ciclo do ácido tricarboxílico. As setas contínuas representam as reações enzimáticas de conversão de um metabólito no outro e estão associadas aos respectivos usos de cofatores e ATP. As setas pontilhadas representam o consumo de xilose e produção dos metabólitos extracelulares (vermelho).
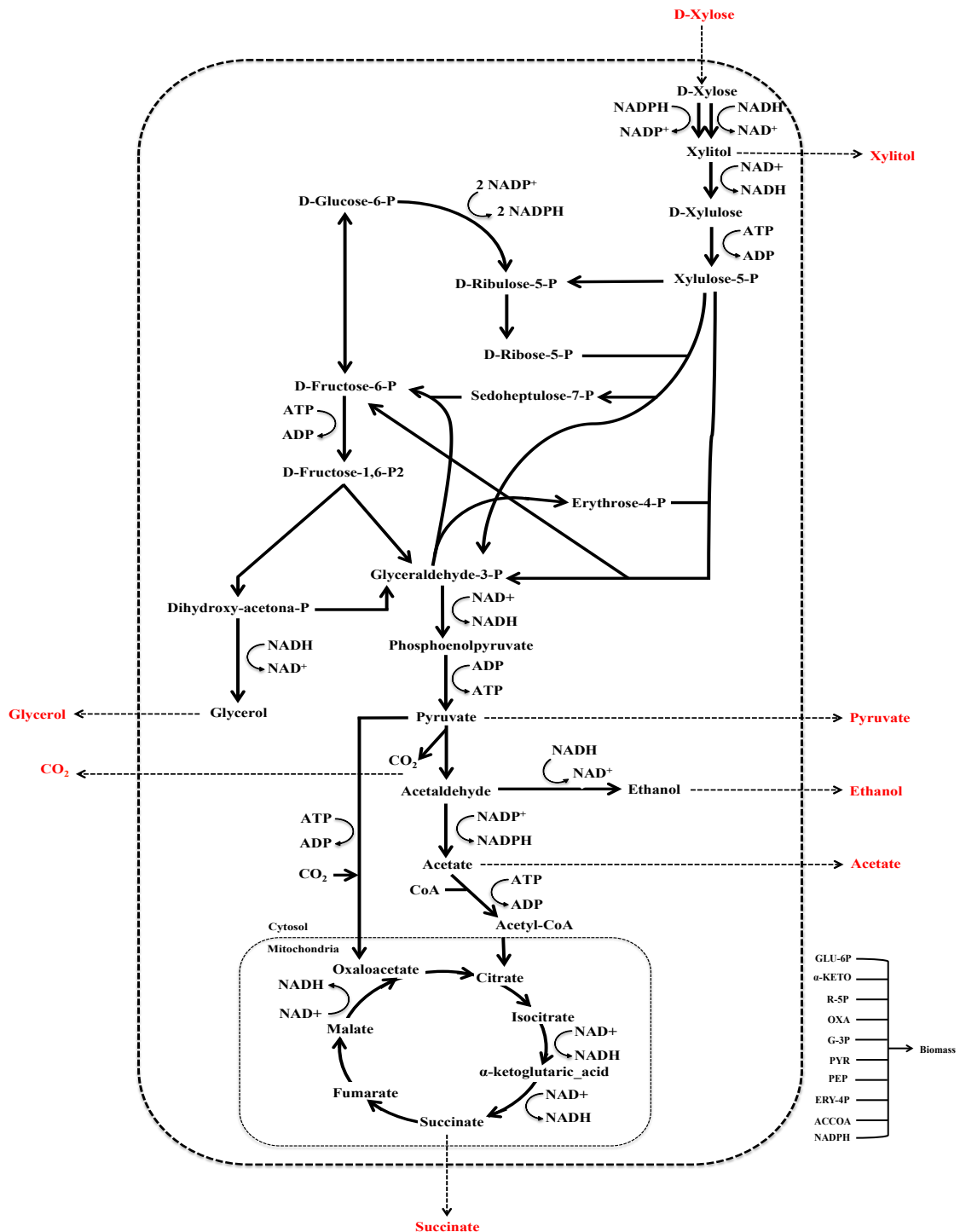
Na reação seguinte, a xilulose-5-fosfato é convertida em ribulose-5-fosfato e, agora, as reações fazem parte da via metabólica da pentose fosfato. Nesta via, os compostos ribulose-5-fosfato, ribose-5-fosfato, eritrose-4-fosfato e sedoeptulose-7-fosfato fazem parte do ciclo da pentose fosfato e a partir deles diferentes rotas metabólicas podem ser seguidas. Uma delas é a entrada na via glicolítica, que pode realizar a reação de regeneração de NAPDH na via da pentose fosfato oxidativa. A outra via é seguir da glicose-6-fosfato até completar as reações da via glicolítica que leva à formação de piruvato, que por sua vez, pode ser convertido pela piruvato descarboxilase em acetaldeído, este último, convertido pela enzima álcool desidrogenase a etanol (Hou, 2012).

4. METABOLOMA

Metabólitos são pequenas moléculas que em conjunto com as enzimas estão envolvidos nas reações bioquímicas integradas em uma rede metabólica. Metabolome, portanto, é a analise que tem como objetivo apresentar um perfil qualitativo e quantitativo de todos os metabolitos de um determinado sistema biológico (Pluskal and Yanagida, 2016). Está analise reflete diretamente a atividade da rede metabólica que leva a produção dos metabólitos. Usando metabólitos alvos as concentrações absolutas e os fluxos de conversão de uma molécula à outra podem ser obtidas (Liu and Locasale, 2017). Os metabólitos e suas mudanças dentro do metabolismo são importantes fatores para entender os efeitos fisiológicos ocorrido nos microrganismos em determinada condição e/ou entre diferentes espécies (Joyce and Palsson, 2006; Yang *et al.*, 2011)

5. FLUXO METABÓLICO

Analise de fluxo metabólico é uma abordagem útil para estimar a distribuição intracelular do fluxo de carbono. A abordagem é baseada em uma rede de reações estequiométricas e no conjunto de metabólitos presentes em vias metabólicas (Lee *et al.*, 2011). As reações estequiométricas são transformadas em um sistema linear de equações matemáticas. E uma das principais metodologia aplicada na analise de fluxo metabólico é usar as taxas medidas de substrato consumido, biomassa e produtos formados como restrições

do modelo (Liang *et al.*, 2013; Li *et al.*, 2017). Com está análise é possível estimar o fluxo metabólico intracelular e identificar as características biológicas como por exemplo: reações limitantes e vias metabólicas mais ativas (O'brien *et al.*, 2015).

OBJETIVOS

Apresentar uma avaliação da capacidade fermentativa das leveduras *Scheffersomyces stipitis*, *Spathaspora passalidarum*, *Spathaspora* arborariae e *Candida tenuis* que consomem xilose como fonte de carbono. Caracterizar a fisiologia dessas leveduras em diferentes condições de oxigênio quanto as taxas de consumo de xilose, rendimento e produtividade de etanol. E determinar a atividade enzimática de XR e XDH que realizam as primeiras reações de assimilação de xilose. Também apresentar o perfil metabólico dessas leveduras através do metaboloma. Está análise foi desenvolvida para a detecção e quantificação dos metabólitos intracelular. E por fim, desenvolver um modelo de reações estequiométrica para estimar o fluxo metabólico intracelular de xilose até a formação de etanol. Entre as leveduras estudadas, *S. passalidarum* e *S. arborariae* tiveram pela primeira vez o fluxo metabólico estimado.

CONCLUSÕES

A avaliação comparativa de quatro leveduras consumidoras de xilose mostra que a *S. stipitis* e *S. passalidarum* têm grande potencial para a produção de etanol a partir da xilose. A análise do fluxo metabólico foi útil para estima a distribuição interna de carbono em um novo modelo de reações estequiométrica envolvendo a conversão de xilose até a formação de etanol. Pela primeira vez foi estimado o fluxo metabólico para as leveduras *S. passalidarum* e *S. arborariae*. O perfil metabólico das leveduras que naturalmente fazem a conversão de xilose foi detalhado. A análise do metaboloma permitiu estimar o perfil metabólico das leveduras com maior acurácia. A partir desta características é proposto que uma alta taxa de assimilação de xilose favorece maior produção de etanol. O fluxo de carbono é dividido igualmente entre a via da pentose fosfato e glicólise. A *S. passalidarum* apresenta maior taxa de fluxo da XR usando NADH, isso demanda menos regeneração de NADPH. Além disso, quando a taxa de fluxo para formar glicerol está inativa, permite melhor balanço de cofatores como $NADH/NAD^+$, permitindo melhor produção de etanol a partir de xilose.

AGRADECIMENTOS

REFERÊNCIAS

Almeida, J. R.; Modig, T.; Roder, A.; Liden, G.; Gorwa-Grauslund, M. F. Pichia stipitis xylose reductase helps detoxifying lignocellulosic hydrolysate by reducing 5-hydroxymethyl-furfural (HMF). **Biotechnol Biofuels,** v. 1, n. 1, p. 12, 2008.

Almeida, J. R.; Runquist, D.; Sanchez I Nogue, V.; Liden, G.; Gorwa-Grauslund, M. F. Stress-related challenges in pentose fermentation to ethanol by the yeast Saccharomyces cerevisiae. **Biotechnology Journal,** v. 6, n. 3, p. 286-99, Mar 2011.

Barrios-Gonzalez, J.; Miranda, R. U. Biotechnological production and applications of statins. **Applied Microbiology and Biotechnology,** v. 85, n. 4, p. 869-883, Jan 2010.

Beg, Q. K.; Kapoor, M.; Mahajan, L.; Hoondal, G. S. Microbial xylanases and their industrial applications: a review. **Applied Microbiology and Biotechnology,** v. 56, n. 3-4, p. 326-338, 2001.

Cadete, R. M.; Melo, M. A.; Dussan, K. J.; Rodrigues, R. C.; Silva, S. S.; Zilli, J. E., . . . Rosa, C. A. Diversity and physiological characterization of D-xylose-fermenting yeasts isolated from the Brazilian Amazonian Forest. **PLoS One,** v. 7, n. 8, p. e43135, 2012.

Cadete, R. M.; Santos, R. O.; Melo, M. A.; Mouro, A.; Goncalves, D. L.; Stambuk, B. U., . . . Rosa, C. A. Spathaspora arborariae sp. nov., a d-xylose-fermenting yeast species isolated from rotting wood in Brazil. **FEMS Yeast Res,** v. 9, n. 8, p. 1338-42, Dec 2009.

Campos, C. G.; Veras, H. C. T.; De Aquino Ribeiro, J. A.; Costa, P.; Araujo, K. P.; Rodrigues, C. M., . . . Abdelnur, P. V. New Protocol Based on UHPLC-MS/MS for Quantitation of Metabolites in Xylose-Fermenting Yeasts. **J Am Soc Mass Spectrom**, Sep 06 2017.

Du Preez, J. C.; Van Driessel, B.; Prior, B. A. D-xylose fermentation by Candida shehatae and Pichia stipitis at low dissolved oxygen levels in fed-batch cultures. **Biotechnology Letters,** v. 11, p. 131-136, 1989.

Eia. US Energy Information Administration p. http://www.eia.gov, 2016.

Eliasson, A.; Boles, E.; Johansson, B.; Osterberg, M.; Thevelein, J. M.; Spencer-Martins, I., . . . Hahn-Hägerdal, B. Xylulose fermentation by mutant and wild-type strains of Zygosaccharomyces and Saccharomyces cerevisiae. **Appl Microbiol Biotechnol,** v. 53, n. 4, p. 376-82, Apr 2000.

Hahn-Hagerdal, B.; Karhumaa, K.; Fonseca, C.; Spencer-Martins, I.; Gorwa-Grauslund, M. F. Towards industrial pentose-fermenting yeast strains. **Appl Microbiol Biotechnol,** v. 74, n. 5, p. 937-53, Apr 2007.

Heux, S.; Meynial-Salles, I.; O'donohue, M. J.; Dumon, C. White biotechnology: State of the art strategies for the development of biocatalysts for biorefining. **Biotechnol Adv,** v. 33, n. 8, p. 1653-70, Dec 2015.

Hou, X. Anaerobic xylose fermentation by Spathaspora passalidarum. **Appl Microbiol Biotechnol,** v. 94, n. 1, p. 205-14, Apr 2012.

Jeffries, T. W.; Grigoriev, I. V.; Grimwood, J.; Laplaza, J. M.; Aerts, A.; Salamov, A., . . . Richardson, P. M. Genome sequence of the lignocellulose-bioconverting and xylose-fermenting yeast Pichia stipitis. **Nature Biotechnology,** v. 25, n. 3, p. 319-26, Mar 2007.

Joyce, A. R.; Palsson, B. O. The model organism as a system: integrating 'omics' data sets. **Nat Rev Mol Cell Biol,** v. 7, n. 3, p. 198-210, Mar 2006.

Kang, Q.; Appels, L.; Tan, T.; Dewil, R. Bioethanol from lignocellulosic biomass: current findings determine research priorities. **ScientificWorldJournal,** v. 2014, p. 298153, 2014.

Kavscek, M.; Strazar, M.; Curk, T.; Natter, K.; Petrovic, U. Yeast as a cell factory: current state and perspectives. **Microb Cell Fact,** v. 14, p. 94, 2015.

Kitano, H. Systems biology: a brief overview. **Science,** v. 295, n. 5560, p. 1662-4, Mar 1 2002.

Konishi, J.; Fukuda, A.; Mutaguchi, K.; Uemura, T. Xylose fermentation by Saccharomyces cerevisiae using endogenous xylose-assimilating genes. **Biotechnol Lett,** v. 37, n. 8, p. 1623-30, Aug 2015.

Kumar, A.; Gautam, A.; Dutt, D. Biotechnological Transformation of Lignocellulosic Biomass in to Industrial Products: An Overview. **Advances in Bioscience and Biotechnology,** v. 07, n. 03, p. 149-168, 2016.

Kumar, R.; Tabatabaei, M.; Karimi, K.; Sárvári H., I. Recent updates on lignocellulosic biomass derived ethanol - A review. **Biofuel Research Journal,** v. 3, n. 1, p. 347-356, 2016.

Kurylenko, O. O.; Ruchala, J.; Hryniv, O. B.; Abbas, C. A.; Dmytruk, K. V.; Sibirny, A. A. Metabolic engineering and classical selection of the methylotrophic thermotolerant yeast Hansenula polymorpha for improvement of high-temperature xylose alcoholic fermentation. **Microbial Cell Factories,** v. 13, 2014.

Lee, S. Y.; Park, J. M.; Kim, T. Y. Application of metabolic flux analysis in metabolic engineering. **Methods Enzymol,** v. 498, p. 67-93, 2011.

Li, M.; Borodina, I. Application of synthetic biology for production of chemicals in yeast Saccharomyces cerevisiae. **FEMS Yeast Res**, Sep 19 2014.

Li, X.; Deng, Y.; Yang, Y.; Wei, Z.; Cheng, J.; Cao, L., . . . Wu, X. Fermentation Process and Metabolic Flux of Ethanol Production from the Detoxified Hydrolyzate of Cassava Residue. **Front Microbiol,** v. 8, p. 1603, 2017.

Li, X.; Yu, V. Y.; Lin, Y.; Chomvong, K.; Estrela, R.; Park, A., . . . Cate, J. H. D. Expanding xylose metabolism in yeast for plant cell wall conversion to biofuels. **eLIFE,** v. 4, 2015.

Liang, M.; Damiani, A.; He, Q. P.; Wang, J. Elucidating Xylose Metabolism of Scheffersomyces stipitis for Lignocellulosic Ethanol Production. **ACS Sustainable Chemistry & Engineering,** v. 2, n. 1, p. 38-48, 2013.

Liao, J. C.; Mi, L.; Pontrelli, S.; Luo, S. Fuelling the future: microbial engineering for the production of sustainable biofuels. **Nat Rev Microbiol**, Mar 30 2016.

Lightelm, M. E.; Prior, B. A.; Du Preez, C. The oxygen requirements of yeasts for the fermentation of D-xylose and D-glucose to ethanol. **Applied Microbiology Biotechnology,** v. 28, p. 63-68, 1988.

Liu, X.; Locasale, J. W. Metabolomics: A Primer. **Trends Biochem Sci,** v. 42, n. 4, p. 274-284, Apr 2017.

Microbewiki. p. https://microbewiki.kenyon.edu/index.php/File:Lignocellulose_structure.png, 2016.

Mme. Análise de Conjuntura do Biocombustíveis p. http://www.mme.gov.br, 2016.

Moyses, D. N.; Reis, V. C.; Almeida, J. R.; Moraes, L. M.; Torres, F. A. Xylose Fermentation by Saccharomyces cerevisiae: Challenges and Prospects. **Int J Mol Sci,** v. 17, n. 3, 2016.

Nanda, S.; Mohammad, J.; Reddy, S. N.; Kozinski, J. A.; Dalai, A. K. Pathways of lignocellulosic biomass conversion to renewable fuels. **Biomass Conversion and Biorefinery,** v. 4, n. 2, p. 157-191, 2013.

O'brien, E. J.; Monk, J. M.; Palsson, B. O. Using Genome-scale Models to Predict Biological Capabilities. **Cell,** v. 161, n. 5, p. 971-987, May 21 2015.

Parachin, N. S.; Hahn-Hagerdal, B.; Bettiga, M. A Microbial Perspective on Ethanolic Lignocellulose Fermentation. **Wastes from Agriculture, Forestry and Food Processing**, p. 605-614, 2011.

Pereira, S. C.; Maehara, L.; Machado, C. M.; Farinas, C. S. 2G ethanol from the whole sugarcane lignocellulosic biomass. **Biotechnol Biofuels,** v. 8, p. 44, 2015.

Petschacher, B.; Nidetzky, B. Engineering Candida tenuis Xylose reductase for improved utilization of NADH: antagonistic effects of multiple side chain replacements and performance of site-directed mutants under simulated in vivo conditions. **Appl Environ Microbiol,** v. 71, n. 10, p. 6390-3, Oct 2005.

Pluskal, T.; Yanagida, M. Metabolomic Analysis of Schizosaccharomyces pombe: Sample Preparation, Detection, and Data Interpretation. **Cold Spring Harb Protoc,** v. 2016, n. 12, p. pdb top079921, Dec 1 2016.

Radecka, D.; Mukherjee, V.; Mateo, R. Q.; Stojiljkovic, M.; Foulquie-Moreno, M. R.; Thevelein, J. M. Looking beyond Saccharomyces: the potential of non-conventional yeast species for desirable traits in bioethanol fermentation. **FEMS Yeast Res,** v. 15, n. 6, Sep 2015.

Rizzi, M.; Erlemann, P.; Buithanh, N. A.; Dellweg, H. Xylose Fermentation by Yeasts .4. Purification and Kinetic-Studies of Xylose Reductase from *Pichia-Stipitis*. **Applied Microbiology and Biotechnology,** v. 29, n. 2-3, p. 148-154, Sep 1988.

Rizzi, M.; Harwart, K.; Erlemann, P.; Bui-Thanh, N.; Dellweg, H. Purification and properties of the NAD+Xylitol-Dehydrogenase from the yeast P stipitis. **Journal of Fermentation and Bioengineering,** v. 67, p. 20-24, 1989.

Runquist, D.; Hahn-Hägerdal, B.; Rådström, P. Comparison of heterologous xylose transporters in recombinant Saccharomyces cerevisiae. **Biotechnol Biofuels,** v. 3, p. 5, 2010.

Sedlak, M.; Ho, N. W. Characterization of the effectiveness of hexose transporters for transporting xylose during glucose and xylose co-fermentation by a recombinant *Saccharomyces* yeast. **Yeast,** v. 21, n. 8, p. 671-84, Jun 2004.

Skoog, K.; Hahn-Hagerdal, B. Effect of oxygenation on xylose fermentation by Pichia stipitis. **Applied and Environmental Microbiology,** v. 56, p. 3389-3394, 1990.

Su, Y.; Willis, L. B.; Jeffries, T. W. Effects of aeration on growth, ethanol and polyol accumulation by Spathaspora passalidarum NRRL Y-27907 and Scheffersomyces stipitis NRRL Y-7124. **Biotechnology and Bioengineering,** v. 112, p. 457-469, 2014.

Trausinger, G.; Gruber, C.; Krahulec, S.; Magnes, C.; Nidetzky, B.; Klimacek, M. Identification of novel metabolic interactions controlling carbon flux from xylose to ethanol in natural and recombinant yeasts. **Biotechnology for Biofuels,** v. 8, 2015.

Veras, H. C. T.; Parachin, N. S.; Almeida, J. R. M. Comparative assessment of fermentative capacity of different xylose-consuming yeasts. **Microb Cell Fact,** v. 16, n. 1, p. 153, Sep 13 2017.

Wahlbom, C. F.; Eliasson, A.; Hahn-Hägerdal, B. Intracellular fluxes in a recombinant xylose-utilizing *Saccharomyces cerevisiae* cultivated anaerobically at different dilution rates and feed concentrations. **Biotechnol Bioeng,** v. 72, n. 3, p. 289-96, Feb 5 2001.

Wilkins, M. R.; Mueller, M.; Eichling, S.; Banat, I. M. Fermentation of xylose by the thermotolerant yeast strains Kluyveromyces marxianus IMB2, IMB4, and IMB5 under anaerobic conditions. **Process Biochemistry,** v. 43, n. 4, p. 346-350, 2008.

Wohlbach, D. J.; Kuo, A.; Sato, T. K.; Potts, K. M.; Salamov, A. A.; Labutti, K. M., . . . Gasch, A. P. Comparative genomics of xylose-fermenting fungi for enhanced biofuel production. **Proc Natl Acad Sci U S A,** v. 108, n. 32, p. 13212-7, Aug 9 2011.

Yang, J. Y.; Karr, J. R.; Watrous, J. D.; Dorrestein, P. C. Integrating '-omics' and natural product discovery platforms to investigate metabolic exchange in microbiomes. **Curr Opin Chem Biol,** v. 15, n. 1, p. 79-87, Feb 2011.

CrossMark

Comparative assessment of fermentative capacity of different xylose-consuming yeasts

Henrique César Teixeira Veras[1,2], Nádia Skorupa Parachin[2,3] and João Ricardo Moreira Almeida[1,3*] iD

Abstract

Background: Understanding the effects of oxygen levels on yeast xylose metabolism would benefit ethanol production. In this work, xylose fermentative capacity of *Scheffersomyces stipitis*, *Spathaspora passalidarum*, *Spathaspora arborariae* and *Candida tenuis* was systematically compared under aerobic, oxygen-limited and anaerobic conditions.

Results: Fermentative performances of the four yeasts were greatly influenced by oxygen availability. *S. stipitis* and *S. passalidarum* showed the highest ethanol yields (above 0.44 g g^{-1}) under oxygen limitation. However, *S. passalidarum* produced 1.5 times more ethanol than *S. stipitis* under anaerobiosis. While *C. tenuis* showed the lowest xylose consumption rate and incapacity to produce ethanol, *S. arborariae* showed an intermediate fermentative performance among the yeasts. NAD(P)H xylose reductase (XR) activity in crude cell extracts correlated with xylose consumption rates and ethanol production.

Conclusions: Overall, the present work demonstrates that the availability of oxygen influences the production of ethanol by yeasts and indicates that the NADH-dependent XR activity is a limiting step on the xylose metabolism. *S. stipitis* and *S. passalidarum* have the greatest potential for ethanol production from xylose. Both yeasts showed similar ethanol yields near theoretical under oxygen-limited condition. Besides that, *S. passalidarum* showed the best xylose consumption and ethanol production under anaerobiosis.

Keywords: Xylose fermentation, Xylose reductase, Bioethanol, Yeast fermentation, Oxygen availability

Background

Conversion of all sugars present at cellulose and hemicellulose fractions of biomass would increase production and reduce cost of second-generation ethanol [1, 2]. *Saccharomyces cerevisiae* is the main yeast used for alcohol production worldwide, but it cannot produce ethanol from xylose, the second most abundant sugar in nature, unless when genetically engineered [3, 4]. Despite the relative success of engineered strains, recombinant *S. cerevisiae* strains show lower fermentation rates and less tolerance to fermentation inhibitors when fermenting xylose instead of glucose [5, 6]. Thus, the isolation, identification and characterization of native xylose-fermenting

yeasts have received great attention in the past years [7–12].

Among the few naturally xylose-fermenting yeasts species, *Scheffersomyces (Pichia) stipitis* is one of the most studied [8, 12, 13]. It has been isolated from the gut of insects and its fermentation capability evaluated in different lignocellulosic hydrolysates [14]. More recently, yeasts from *Spathaspora* and *Candida* genera, as *Spathaspora passalidarum*, *Spathaspora arborariae* and *Candida tenuis*, have been isolated from rotting-wood samples or wood-boring insects and characterized as xylose fermenting yeasts [7, 9, 10]. Like *S. stipitis*, *S. passalidarum* showed xylose fermentation yields above 0.40 g ethanol g^{-1} sugar in both defined and lignocellulosic hydrolyzed medium Slininger [14, 15]. In general, naturally xylose-fermenting yeasts are able to ferment xylose only when the oxygen flow is tightly regulated. High oxygenation level leads to aerobic growth and low ethanol yield, whereas limited dissolved oxygen slows

*Correspondence: joao.almeida@embrapa.br
[1] Brazilian Agricultural Research Corporation, EMBRAPA Agroenergia, Parque Estação Biológica, PqEB-W3 Norte Final-s/nº, Brasília, DF CEP 70.770-901, Brazil
Full list of author information is available at the end of the article

Veras *et al. Microb Cell Fact* (2017) 16:153

Page 2 of 8

the fermentation rate, increases xylitol accumulation and causes poor ethanol productivity [1, 8, 15–17].

In yeasts, xylose is first reduced to xylitol, a reaction catalyzed by a NAD(P)H-dependent xylose reductase (XR). Then, a NAD^+-dependent xylitol dehydrogenase (XDH) oxidises xylitol to xylulose [18–20]. Subsequently, xylulose enters into the pentose phosphate and glycolysis pathways, finally being converted to ethanol. Recently, it was shown that *S. passalidarum* exceptionally harbor two XRs, and one of them, preferentially uses NADH as cofactor [20].

As fermentative conditions like media composition, cell density and oxygen availability are usually different [1, 10, 20] a comparative assessment among xylose-consuming yeasts based on literature data becomes difficult. In addition, few studies on physiology of *C. tenuis* and *S. arborariae* are available [10, 20, 21]. Thus, a systematic comparison of fermentative physiology of *S. stipitis*, *S. passalidarum*, *S. arborariae* and *C. tenuis* is still missing and it might help elucidate important steps on xylose metabolism.

The aim of this study was to compare the alcoholic fermentative capacity of four native xylose-consuming yeasts under different oxygenation conditions. The physiology of *S. stipitis*, *S. passalidarum*, *S. arborariae* and *C. tenuis* in defined mineral medium containing xylose as sole carbon source was assessed under aerobic, oxygen-limited and anaerobic conditions. The results presented clearly distinguished the best performing yeast for each condition and highlights the importance of cofactor usage on ethanol production from xylose.

Methods

Strains

The yeasts employed in this study were *Scheffersomyces (Pichia) stipitis* NRRL Y-7124, *S. passalidarum* NRRL Y-27907, *S. arborariae* NRRL Y-48658 and *C. tenuis* NRRL Y-1498. All yeasts were preserved in 30% glycerol at −80 °C.

Xylose fermentations under different oxygen conditions

The xylose fermentation experiments were carried out in bioreactors (Multifors 2, Infors HT) with 500 mL working volume. Cells from −80 °C stock were initially grown in solid YPD medium (10 g L^{-1} yeast extract, 20 g L^{-1} peptone, 20 g L^{-1} glucose), overnight at 28 °C. One single colony was used to inoculate 50 mL of defined mineral medium [22] containing per litre: $(NH_4)_2SO_4$, 12.5 g; KH_2PO_4, 7.5 g; $MgSO_4 \cdot 7H_2O$, 1.25 g; EDTA, 37.5 mg; $ZnSO_4 \cdot 7H_2O$, 11.25 mg; $MnCl_2 \cdot 2H_2O$, 2.5 mg; $CoCl_2 \cdot 6H_2O$, 0.75 mg; $CuSO_4 \cdot 5H_2O$, 0.75 mg; $Na_2MoO_4 \cdot H_2O$, 1.0 mg; $CaCl_2 \cdot 2H_2O$, 11.25 mg; $FeSO_4 \cdot 7H_2O$, 7.5 mg; H_3BO_3, 2.5 mg; KI, 0.25 mg.

Filter-sterilized vitamins were added after heat sterilization of this medium. Final vitamin concentrations per litre were: biotin, 0.125 mg; Ca-pantothenate 2.5 mg; nicotinic acid 2.5 mg; inositol 62.5 mg; thiamin-HCl 2.5 mg; pyridoxine–HCl 2.5 mg; *P*-aminobenzoic acid 0.5 mg; riboflavin 0.5 g and; folic acid 0.005 g. The carbon source consisted of 40 g L^{-1} xylose.

The start culture at the bioreactor was $OD_{600\ nm}$ of 0.5. Cultures were maintained with pH 5.5, by addition of KOH 3 M, under agitation—stirrer at 400 rpm, and temperature of 28 °C. First, yeast performance was evaluated under aerobic and oxygen-limited conditions. For aerobic experiments, synthetic air (20% pure oxygen and 80% pure nitrogen) was injected in the reactor at 0.5 L min^{-1}. The dissolved oxygen measured in the reactor (Sensors METTLER TOLEDO) was above 60% during the entire fermentation period. For oxygen-limited experiments, the airflow of synthetic air was adjusted for 0.05 L min^{-1}, which resulted in dissolved oxygen below 10% in the first 10 h of fermentation and zero afterwards. But the airflow was kept constant in a minimal rate, indicating that the entire oxygen that was entering the bioreactor was promptly consumed. All fermentations were carried out in biological triplicates.

Anaerobic fermentations with the four yeasts were performed in small cap vials sealed with a rubber stopper, equipped with a needle for carbon dioxide removal. Cells from −80 °C stock were initially grown in solid YPD medium, overnight at 28 °C. One single colony was used to inoculate 50 mL of defined mineral medium as described above. The culture started with a high cell density equal to $OD_{600\ nm}$ of 2.0. The pH was adjusted for 5.5 and, the flasks incubated under agitation—stirrer at 400 rpm and temperature of 28 °C. All experiments were carried out in biological triplicates.

Analytical methods

To monitor yeast growth, samples were withdrawn regularly during fermentations and biomass was measured by optical density at 600 nm using a spectrophotometer (SpectraMax® M3, Molecular Devices). For cell dry weight (CDW) measurement, 5 mL of pre-inoculum culture and of the stationary phase of the growth during all fermentations were withdrawn and centrifuged ($12,000 \times g$, 5 min). Before weighing, the pellet was incubated in glass tube for at least 48 h at 60 °C. The cell dry weight was correlated with $OD_{600\ nm}$ measured in the same time intervals. Each measurement was performed in duplicate.

Sugar consumption and products formed during fermentation experiments were measured using a high-pressure liquid chromatograph (HPLC) system. Initially, samples withdrawn regularly during fermentations were

Veras *et al. Microb Cell Fact* (2017) 16:153

Page 3 of 8

centrifuged (12,000×*g*, 5 min) and the supernatant was transferred to a new tube. Concentrations of xylose, xylitol, glycerol, acetate and ethanol in supernatants were measured using HPLC system (Acquity UPLC H Class, Waters) equipped with a refractive index detector and an Aminex® HPX-87H column (Bio-Rad) at 45 °C. The mobile phase was 5 mM sulfuric acid at a flow rate of 0.6 mL min^{-1}. Results are shown as average ± standard deviations.

Enzymatic assays for XR and XDH

The enzymatic activity of xylose reductase (XR) and xylitol dehydrogenase (XDH) in crude-cell extracts was measured according to [23]. For this, 5 mL of cell suspension of *S. stipitis*, *S. passalidarum*, *S. arborariae* and *C. tenuis* were collected in the middle of the exponential growth phase during aerobic and oxygen-limited fermentations. Cells were pelleted by centrifugation, washed with sterile water, and lysed with Y-PER®—Yeast Protein Extraction Reagent (Pierce, Rockford, USA) to obtain cell-crude extracts. Protein concentrations in cell-free extracts were determined using Quick StartTM Bradford Protein Assay Kit (Bio-Rad Laboratories Ltda., USA), following the manufacture's instruction.

XR reaction mixture contained 100 mM triethanolamine buffer (pH 7.0), 0.2 mM NADH or NADPH, 350 mM xylose. XDH reaction contained 100 mM triethanolamine buffer (pH 7.0), 0.3 mM NAD$^+$, 300 mM xylitol. All reactions were started with addition of limiting substrates. The assays were performed at 30 °C and the oxidation of NADH/NADPH and reduction of NAD$^+$ were followed as the change in absorbance at 340 nm. The value of 6.22 mL (μmol cm)$^{-1}$ was used as the molar absorption coefficient of coenzymes per minute. The specific activities of XR and XDH were given in units per mg protein (U mg^{-1}). Enzyme unit is defined as 1 μmol of cofactor reduced or oxidized per minute. All assays were performed in triplicate and the results are shown as means ± standard deviations.

Results and discussion

Xylose fermentation in defined mineral medium

The fermentative capacity of the four naturally xylose-consuming yeasts, *S. stipitis*, *S. passalidarum*, *S. arborariae* and *C. tenuis* were evaluated under aerobic, oxygen-limited and anaerobic conditions. Xylose consumption varied considerably among the four yeasts both under aerobic and oxygen-limited conditions (Fig. 1). *Scheffersomyces stipitis*, *S. passalidarum* and *S. arborariae* were able to consume xylose completely and showed at least 6 times higher specific xylose consumption rate than *C. tenuis* under aerobic condition (Fig. 1; Table 1). Even after more than 120 h of fermentation,

C. tenuis consumed about 34 and 28 g L^{-1} of xylose under aerobic and oxygen-limited conditions, respectively (Fig. 1d). When cultivated under oxygen limitation, *S. stipitis* and *S. passalidarum* showed similar xylose consumption rates, however the rate was 2 times lower for *S. arborariae* (Table 1). As expected, biomass yields for all yeasts were 2 times higher under aerobic than oxygen-limited condition. However, biomass yield was twofolds higher for *S. passalidarum* than *S. stipitis*. This may explain the lower ethanol productivity rate for this yeast compared to *S. stipitis* under aerobic condition (Table 1).

Growth and ethanol production by these yeasts were strongly influenced by the oxygen availability. Biomass formation was favored in presence of oxygen whereas ethanol production was favored under more strictly oxygen availability. Produced biomass varied from a minimal of 6.7 g L^{-1} for *S. stipitis* to a maximum of 13.9 g L^{-1} to *C. tenuis* under aerobic condition (Fig. 1). Despite the variation in the total biomass, the specific growth rate of *S. stipitis*, *S. passalidarum* and *S. arborariae* ranged from 0.15 to 0.18 h^{-1}. This is about 2 times higher than *C. tenuis* under aerobic conditions, which reached specific growth rate 0.08 h^{-1}. The biomass formation was about 2 times lower under oxygen-limited condition than in aerobic one, varying from 3.0 to 7.0 g L^{-1} (Fig. 1). In anaerobic condition the maximum biomass formation reached was 3.5 g L^{-1} for *S. stipitis*, 2.4 g L^{-1} for *S. passalidarum*, 1.3 g L^{-1} for *S. arborariae* and 1.2 g L^{-1} for *C. tenuis* (Fig. 2).

Scheffersomyces stipitis, *S. passalidarum* and *S. arborariae* produced predominantly ethanol from xylose (Fig. 1a–c). Oxygen limitation increased ethanol production and yields by *S. stipitis*, *S. passalidarum* and *S. arborariae*. Indeed, the concentrations increased approximately twofold when compared to aerobic condition (Table 1). *Scheffersomyces stipitis* and *S. passalidarum* reached the highest ethanol yields (0.45 and 0.44 g g^{-1}) among the four xylose-consuming yeasts employed in this study (Table 1). These values are in good agreement with previous studies, which showed ethanol yields varying from 0.40 to 0.48 g g^{-1} to *S. stipitis* [16, 24] and from 0.43 to 0.48 g g^{-1} to *S. passalidarum* [17, 20] under limited oxygenation levels. In turn, ethanol yield for *S. arborariae* was only of 0.31 g g^{-1} (Table 1), which was also observed previously in an independent study [20]. Xylitol, glycerol and acetate formation by *S. stipitis*, *S. passalidarum* and *S. arborariae* was minimal and did not show significant differences among them (Fig. 1; Table 1). On the other hand, *C. tenuis* did not produce ethanol under any condition evaluated. Indeed, it produced mainly xylitol during fermentation under oxygen-limited condition (0.62 g g^{-1}) (Table 1).

Veras *et al. Microb Cell Fact* (2017) 16:153
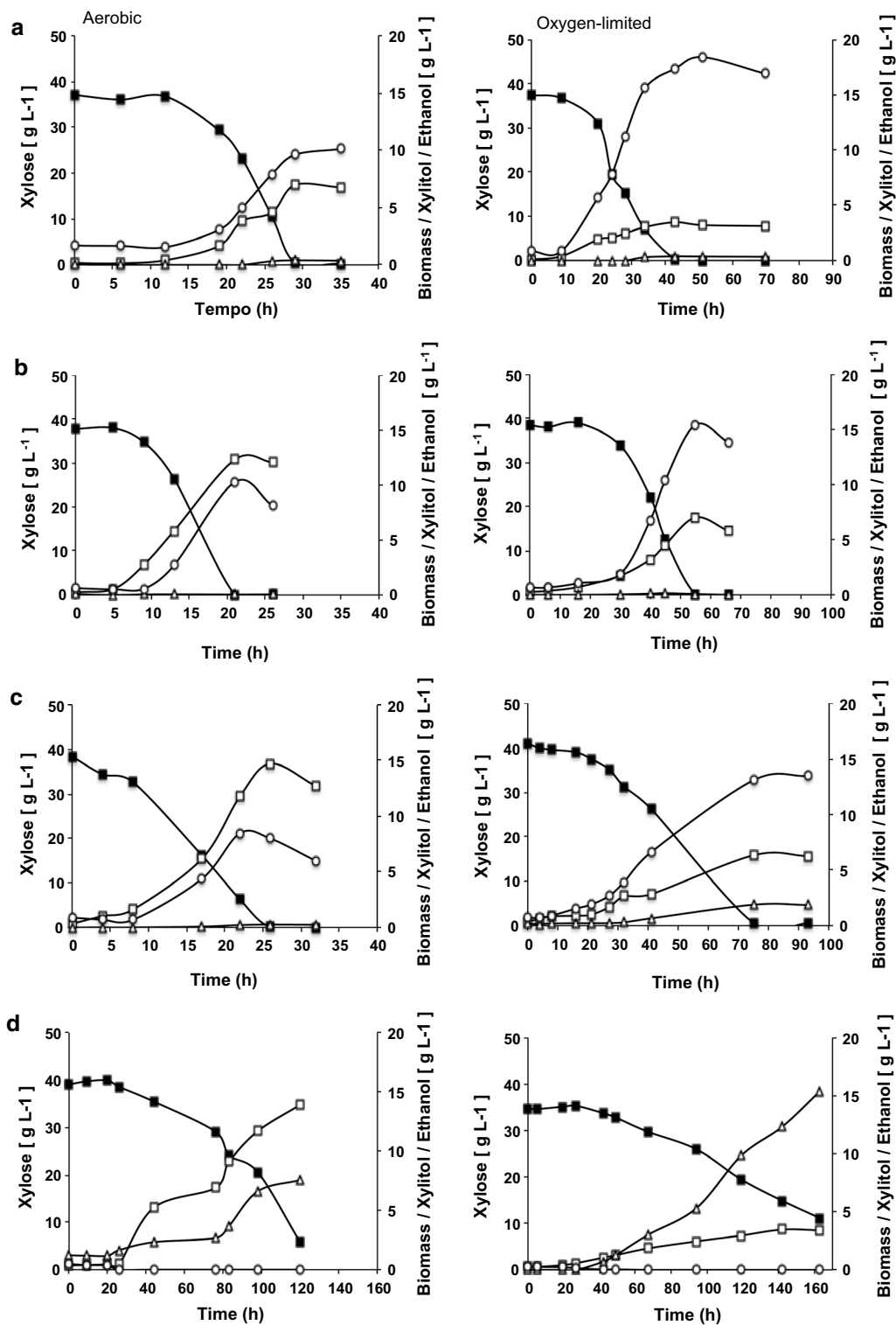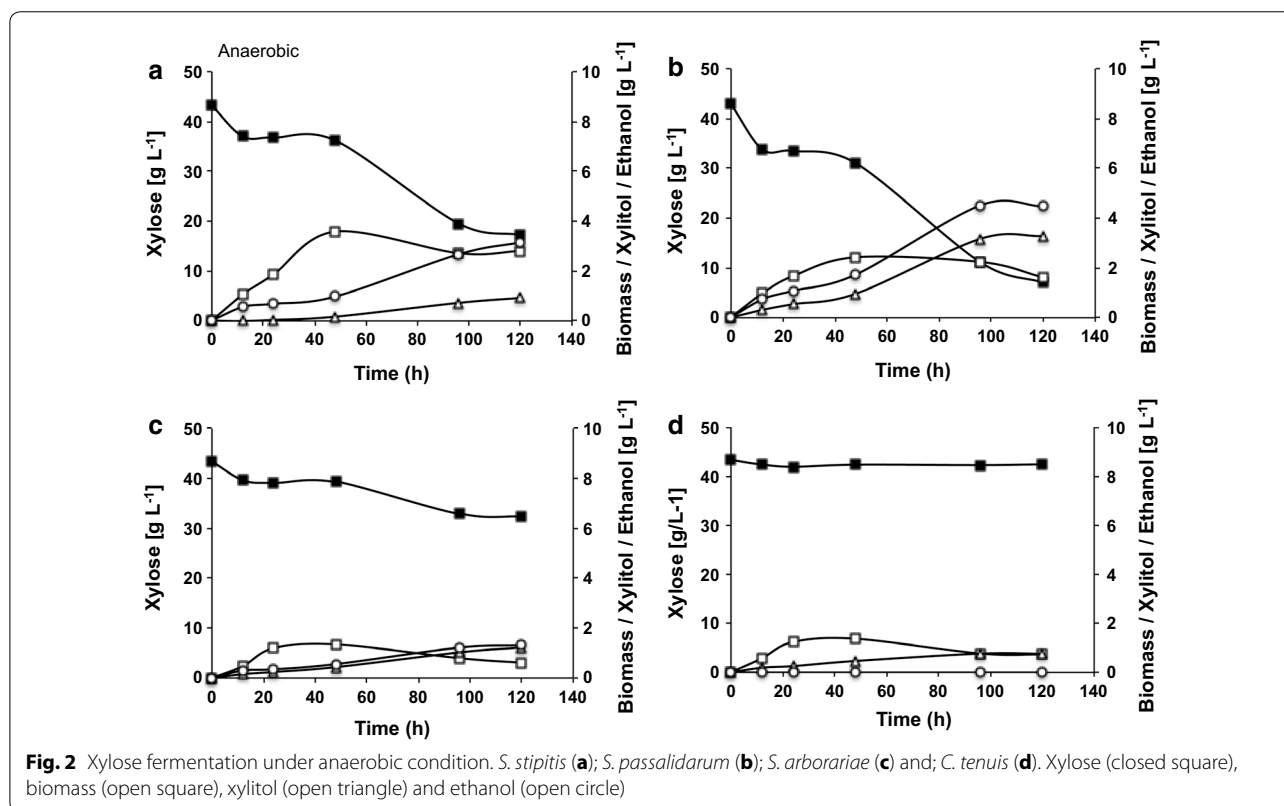
Page 4 of 8

Fig. 1 Xylose fermentation under different oxygen level conditions. Left: aerobic and right: oxygen-limited. *S. stipitis* (**a**); *S. passalidarum* (**b**); *S. arborariae* (**c**) and; *C. tenuis* (**d**). Xylose (closed square), biomass (open square), xylitol (open triangle) and ethanol (open circle). The different scales on x-axis highlight different fermentation rates

Veras *et al. Microb Cell Fact* (2017) 16:153

Page 5 of 8

Table 1 Parameters calculated for xylose fermentation

Yeasts species	Oxygen condition	Xylitol (g L^{-1})	Ethanol (g L^{-1})	Xylitol yield [Y$_{x/s}$ (g g^{-1})]	Ethanol yield [Y$_{e/s}$ (g g^{-1})]	Biomass yield [Y$_{b/s}$ (g g^{-1})]	Specific xylose consumption [(g g$_{cdw}^{-1}$ h^{-1})]	Specific ethanol productivity [(g g$_{cdw}^{-1}$ h^{-1})]
S. stipitis	Aerobic	0.41 ± 0.06	8.05 ± 0.91	0.01 ± 0.00	0.24 ± 0.02	0.16 ± 0.04	0.30 ± 0.09	0.08 ± 0.03
S. passalidarum		0.04 ± 0.00	10.06 ± 0.48	0.00 ± 0.00	0.28 ± 0.02	0.33 ± 0.02	0.13 ± 0.02	0.04 ± 0.01
S. arborariae		0.27 ± 0.08	8.65 ± 1.16	0.01 ± 0.00	0.25 ± 0.02	0.31 ± 0.05	0.13 ± 0.02	0.03 ± 0.01
C. tenuis		8.03 ± 1.48	0.00 ± 0.00	0.30 ± 0.06	0.00 ± 0.00	0.43 ± 0.06	0.02 ± 0.00	0.00 ± 0.00
S. stipitis	Oxygen-limited	0.37 ± 0.01	16.48 ± 0.83	0.01 ± 0.00	0.45 ± 0.04	0.09 ± 0.02	0.29 ± 0.09	0.10 ± 0.02
S. passalidarum		0.05 ± 0.02	16.36 ± 1.40	0.00 ± 0.01	0.44 ± 0.04	0.13 ± 0.04	0.22 ± 0.10	0.10 ± 0.05
S. arborariae		1.82 ± 0.66	11.47 ± 2.37	0.04 ± 0.02	0.31 ± 0.02	0.15 ± 0.01	0.09 ± 0.01	0.03 ± 0.01
C. tenuis		15.43 ± 1.90	0.00 ± 0.00	0.62 ± 0.04	0.00 ± 0.00	0.14 ± 0.01	0.04 ± 0.01	0.00 ± 0.00

The fermentative capacities were measurement under aerobic and oxygen-limited conditions. The values are calculated considering the exponential growth phase

Fig. 2 Xylose fermentation under anaerobic condition. *S. stipitis* (**a**); *S. passalidarum* (**b**); *S. arborariae* (**c**) and; *C. tenuis* (**d**). Xylose (closed square), biomass (open square), xylitol (open triangle) and ethanol (open circle)

The xylose consumption rate was lower under anaerobic condition in all evaluated yeasts (Fig. 2). Only *S. stipitis* and *S. passalidarum* were able to produce ethanol, and even so, xylitol formation also increased when compared to other aerobic and oxygen-limited conditions (Figs. 1a, b, 2a, b). Insufficient oxygen rate was reported to increase xylitol accumulation and to cause poor ethanol productivity in *S. stipitis* and *S. passalidarum* [17]. Despite the similar fermentative performances of *S. stipitis* and *S.*

passalidarum under oxygen-limited condition, *S. passalidarum* consumed more xylose and produced 50% more ethanol than *S. stipitis* in anaerobic condition (Fig. 2a, b). These results are in agreement with those observed in previous work, when *S. passalidarum* showed efficient conversion of xylose into ethanol under anaerobic condition, while the *S. stipitis* almost did not ferment xylose [1]. Another study that assessed the aeration effect on xylose fermentation also showed that *S. passalidarum*

Veras *et al. Microb Cell Fact* (2017) 16:153

Page 6 of 8

(ethanol yield 0.43 g g^{-1}) is a better native xylose-fermenting yeast than *S. stipitis* (ethanol yield 0.39 g g^{-1}) when a smaller oxygen transfer rate is employed [17].

Although it has been proposed that *C. tenuis* is capable of fermenting xylose [10], it showed the poorest xylose consumption rates among the four yeasts assessed and it was not able to produce ethanol in any condition evaluated in this study (Figs. 1, 2). In the previous work, Wohlbach et al. [10] showed that *C. tenuis* produced approximately 2.0 g L^{-1} ethanol during microaerobic fermentation with 8% xylose and high initial cell density (OD$_{600\ nm}$ of 10) in an Erlenmeyer flask. In our study, some change of parameters may have influenced the metabolism of *C. tenuis*, so the xylitol formation by this yeast was significant (up to 15.4 g L^{-1}) and ethanol was not detected (Figs. 1, 2; Table 1). The approximately 20 times lower initial cell density (OD$_{600\ nm}$ of 0.5, equal to 0.2 g L^{-1}), the low flow air rate during oxygen-limited fermentation and the usage of defined mineral medium instead of yeast extract and peptone may have hampered ethanol detection in this work.

Xylose reductase (XR) and xylitol dehydrogenase (XDH) activities

Xylose reductase (XR) and xylitol dehydrogenase (XDH) activities were measured in crude-cell extracts of *S. stipitis*, *S. passalidarum*, *S. arborariae and C. tenuis* from cells growing under aerobic and oxygen-limited conditions. *S. stipitis*, *S. passalidarum* and *S. arborariae* presented NADH and NADPH-dependent XR activity, whereas *C. tenuis* XR were strictly NADPH-dependent (Table 2). While *S. stipitis* and *S. arborariae* showed higher NADPH-dependent XR activity, *S. passalidarum* showed approximately 1.5 times higher NADH-dependent XR activity.

The fermentative performances of yeasts under oxygen-limited condition could be directly correlated with the capability to use NADH on xylose reduction (Tables 1, 2). Indeed, *S. passalidarum* showed the highest ratio of NADH/NADPH XR activity (around 1.30) and the best fermentative performance, i.e. higher xylose consumption rate and higher concentration of ethanol, under anaerobic condition; followed by *S. stipitis* and *S. arborariae* with ratios around 0.6 and 0.4, respectively (Table 2). *Candida tenuis*, which XR prefers 33-fold NADPH over NADH [25] did not produce ethanol at all. Accordingly, it was recently shown that *S. passalidarum* possess two XR (genes XIL1.1 and XIL1.2) and one of them uses preferentially NADH as cofactor [20].

XR NADH-preference was previously correlated with improved ethanol production by engineered *S. cerevisiae* strains [18, 26, 27]. The usage of NADH on xylose reduction is advantageous because the redox balance in the xylose catabolic pathways is optimized, since XDH, the next enzyme in the pathway, is strictly NAD$^+$-dependent (Table 2) [18]. The NAD$^+$ surplus regenerated during xylose reduction would reduce xylitol formation due to higher xylose consumption rate, which impact positively the ethanol yield and productivity [20, 28]. Indeed, strategies aiming to increase NAD$^+$ availability during fermentation increases xylose consumption rate and ethanol production. These include mutations to alter cofactor preference of XRs from NADPH to NADH [29], addition of external electron donor [30] or expression of additional reactions that generated increased NAD$^+$ availability [31]. No enzymatic activity was performed in the anaerobic condition because the growth was very slow and there was no exponential growth phase. Thus, only fermentative capacity was compared.

Conclusion

The comparative assessment of the four-native xylose-consuming yeasts showed that the *S. stipitis* and *S. passalidarum* have the greatest potential for ethanol production from xylose. Both yeasts showed similar ethanol yields near theoretical under oxygen-limited condition. Besides that, *S. passalidarum* showed the best xylose

Table 2 Xylose reductase (XR) and xylitol dehydrogenase (XDH) specific activities in crude-cell extracts of *S. stipitis*, *S. passalidarum*, *S. arborariae* and *C. tenuis*

Yeasts species	Oxygen conditions	XR (U mg^{-1})			XDH (U mg^{-1})
		NADH	NAD(P)H	Ratio$_{NADH/NAD(P)H}$	NAD$^+$
S. stipitis	Aerobic	0.17 ± 0.06	0.23 ± 0.05	0.74 ± 0.13	0.23 ± 0.11
S. passalidarum		2.96 ± 0.40	2.15 ± 0.12	1.38 ± 0.16	0.30 ± 0.05
S. arborariae		0.88 ± 0.13	3.10 ± 0.29	0.29 ± 0.05	0.65 ± 0.07
C. tenuis		–	0.35 ± 0.07	–	0.25 ± 0.05
S. stipitis	Oxygen-limited	0.26 ± 0.07	0.45 ± 0.11	0.59 ± 0.16	0.19 ± 0.08
S. passalidarum		0.60 ± 0.08	0.46 ± 0.04	1.29 ± 0.07	0.21 ± 0.03
S. arborariae		0.77 ± 0.17	1.86 ± 0.25	0.43 ± 0.16	0.12 ± 0.04
C. tenuis		–	0.27 ± 0.05	–	0.28 ± 0.06

Yeasts were grown under aerobic and oxygen-limited conditions and samples were withdrawn in the middle of exponential growth phase

Veras *et al. Microb Cell Fact* (2017) 16:153

Page 7 of 8

consumption and ethanol production under anaerobiosis. The better performing yeasts, i.e. with higher xylose consumption rate and higher concentration of ethanol, during anaerobic xylose showed higher ratio of NADH/NADPH XR activity.

Author details
[1] Brazilian Agricultural Research Corporation, EMBRAPA Agroenergia, Parque Estação Biológica, PqEB-W3 Norte Final-s/nº, Brasília, DF CEP 70.770-901, Brazil. [2] Graduate Program on Molecular Biology, Department of Cellular Biology, University of Brasília, Campus Darcy Ribeiro, Brasília, DF, Brazil. [3] Graduate Program on Chemical and Biological Technologies, Institute of Chemistry, University of Brasília, Campus Darcy Ribeiro, Brasília, DF, Brazil.

Publisher's Note
Springer Nature remains neutral with regard to jurisdictional claims in published maps and institutional affiliations.

References
1. Hou X. Anaerobic xylose fermentation by *Spathaspora passalidarum*. Appl Microbiol Biotechnol. 2012;94:205–14.
2. Arora R, Behera S, Kumar S. Bioprospecting thermophilic/thermotolerant microbes for production of lignocellulosic ethanol: a future perspective. Renew Sustain Energy Rev. 2015;51:699–717.
3. Parachin NS, Hahn-Hägerdal B, Bettiga M. A microbial perspective on ethanolic lignocellulose fermentation. Wastes from agriculture, forestry and food processing. 2011; 605–614.
4. Moyses DN, Reis VC, de Almeida JR, de Moraes LM, Torres FA. Xylose fermentation by *Saccharomyces cerevisiae*: challenges and prospects. Int J Mol Sci. 2016;17:207.
5. Kuyper M, Toirkens MJ, Diderich JA, Winkler AA, van Dijken JP, Pronk JT. Evolutionary engineering of mixed-sugar utilization by a xylose-fermenting *Saccharomyces cerevisiae* strain. FEMS Yeast Res. 2005;5:925–34.
6. Li H, Wu M, Xu L, Hou J, Guo T, Bao X, Shen Y. Evaluation of industrial *Saccharomyces cerevisiae* strains as the chassis cell for second-generation bioethanol production. Microb Biotechnol. 2015;8:266–74.
7. Nguyen NH, Suh SO, Marshall CJ, Blackwell M. Morphological and ecological similarities: wood-boring beetles associated with novel xylose-fermenting yeasts, *Spathaspora passalidarum* gen. sp. nov. and *Candida jeffriesii* sp. nov. Mycol Res. 2006;110:1232–41.
8. Jeffries TW, Grigoriev IV, Grimwood J, Laplaza JM, Aerts A, Salamov A, Schmutz J, Lindquist E, Dehal P, Shapiro H, et al. Genome sequence of the lignocellulose-bioconverting and xylose-fermenting yeast *Pichia stipitis*. Nat Biotechnol. 2007;25:319–26.
9. Cadete RM, Santos RO, Melo MA, Mouro A, Goncalves DL, Stambuk BU, Gomes FC, Lachance MA, Rosa CA. *Spathaspora arborariae* sp. nov., a D-xylose-fermenting yeast species isolated from rotting wood in Brazil. FEMS Yeast Res. 2009;9:1338–42.
10. Wohlbach DJ, Kuo A, Sato TK, Potts KM, Salamov AA, Labutti KM, Sun H, Clum A, Pangilinan JL, Lindquist EA, et al. Comparative genomics of xylose-fermenting fungi for enhanced biofuel production. Proc Natl Acad Sci USA. 2011;108:13212–7.
11. Cadete RM, Melo MA, Zilli JE, Vital MJ, Mouro A, Prompt AH, Gomes FC, Stambuk BU, Lachance MA, Rosa CA. *Spathaspora brasiliensis* sp. nov., *Spathaspora suhii* sp. nov., *Spathaspora roraimanensis* sp. nov. and *Spathaspora xylofermentans* sp. nov., four novel (D)-xylose-fermenting yeast species from Brazilian Amazonian forest. Antonie Van Leeuwenhoek. 2013;103:421–31.
12. Krahulec S, Kratzer R, Longus K, Nidetzky B. Comparison of *Scheffersomyces stipitis* strains CBS 5773 and CBS 6054 with regard to their xylose metabolism: implications for xylose fermentation. MicrobiologyOpen. 2012;1:64–70.
13. Parambil LK, Sarkar D. Probing the bioethanol production potential of *Scheffersomyces (Pichia) stipitis* using validated genome-scale model. Biotechnol Lett. 2014;36:2443–51.
14. Slininger PJ, Shea-Andersh MA, Thompson SR, Dien BS, Kurtzman CP, Balan V, Sousa LC, Uppugundla N, Dale BE, Cotta MA. Envolved strains of *Scheffersomyces stipitis* achieving high ethanol productivity on acid and base pretreated biomass hydrolyzate at high solids loading. Biotechnol Biofuels. 2015;8(60):1–27.
15. Long TM, Su YK, Headman J, Higbee A, Willis LB, Jeffries TW. Cofermentation of glucose, xylose, and cellobiose by the beetle-associated yeast *Spathaspora passalidarum*. Appl Environ Microbiol. 2012;78:5492–500.
16. Skoog K, Hahn-Hagerdal B. Effect of oxygenation on xylose fermentation by *Pichia stipitis*. Appl Environ Microbiol. 1990;56:3389–94.
17. Su Y, Willis LB, Jeffries TW. Effects of aeration on growth, ethanol and polyol accumulation by *Spathaspora passalidarum* NRRL Y-27907 and *Scheffersomyces stipitis* NRRL Y-7124. Biotechnol Bioeng. 2014;112:457–69.
18. Bruinenberg PM, de Bot PHM, van Dijken JP, Scheffers WA. NADH-linked aldose reductase—the key to anaerobic alcoholic fermentation of xylose by yeasts. Appl Microbiol Biotechnol. 1984;19:256–60.
19. Jeffries TW, Jin YS. Metabolic engineering for improved fermentation of pentoses by yeasts. Appl Microbiol Biotechnol. 2004;63:495–509.
20. Cadete RM, de Las Heras AM, Sandstrom AG, Ferreira C, Girio F, Gorwa-Grauslund MF, Rosa CA, Fonseca C. Exploring xylose metabolism in Spathaspora species: XYL1.2 from *Spathaspora passalidarum* as the key for efficient anaerobic xylose fermentation in metabolic engineered *Saccharomyces cerevisiae*. Biotechnol Biofuels. 2016;9(167):1–14.
21. Cadete RM, Melo MA, Dussan KJ, Rodrigues RC, Silva SS, Zilli JE, Vital MJ, Gomes FC, Lachance MA, Rosa CA. Diversity and physiological characterization of D-xylose-fermenting yeasts isolated from the Brazilian Amazonian forest. PLoS ONE. 2012;7:e43135.
22. Verduyn C, Postma E, Scheffers WA, van Dijken JP. Effect of benzoic acid on metabolic fluxes in yeasts: a continuous-culture study on the regulation of respiration and alcoholic fermentation. Yeast. 1992;8:501–17.
23. Smiley KL, Bolen PL. Demonstration of D-xylose reductase and D-xylitol dehydrogenase in *Pachysolen tannophilus*. Biotech Lett. 1982;4:607–20.
24. Papini M, Nookaew I, Uhlén M, Nielsen J. Scheffersomyces stipitis: a comparative systems biology study with the crabtree positive yeast *Saccharomyces cerevisiae*. Microb Cell Factories. 2012;11(136):1–16.
25. Petschacher B, Leitgeb S, Kavanagh KL, Wilson DK, Nidetzky B. The coenzyme specificity of *Candida tenuis* xylose reductase (AKR2B5) explored by site-directed mutagenesis and X-ray crystallography. Biochem J. 2005;385:75–83.
26. Bengtsson O, Hahn-Hägerdal B, Gorwa-Grauslund MF. Xylose reductase from *Pichia stipitis* with altered coenzyme preference improves ethanolic xylose fermentation by recombinant *Saccharomyces cerevisiae*. Biotechnol Biofuels. 2009;2:9.

Veras *et al. Microb Cell Fact* (2017) 16:153

Page 8 of 8

27. Jeffries TW, Shi NQ. Genetic engineering for improved xylose fermentation by yeasts. Adv Biochem Eng Biotechnol. 1999;65:118–61.
28. Hahn-Hägerdal B, Karhumaa K, Fonseca C, Spencer-Martins I, Gorwa-Grauslund MF. Towards industrial pentose-fermenting yeast strains. Appl Microbiol Biotechnol. 2007;74:937–53.
29. Dasgupta D, Bandhu S, Adhikari DK, Ghosh D. Challenges and prospects of xylitol production with whole cell bio-catalysis: a review. Microbiol Res. 2017;197:9–21.
30. Wahlbom CF, Hahn-Hagerdal B. Furfural, 5-hydroxymethyl furfural, and acetoin act as external electron acceptors during anaerobic fermentation of xylose in recombinant *Saccharomyces cerevisiae*. Biotechnol Bioeng. 2002;78:172–8.
31. Almeida JR, Bertilsson M, Hahn-Hagerdal B, Liden G, Gorwa-Grauslund MF. Carbon fluxes of xylose-consuming *Saccharomyces cerevisiae* strains are affected differently by NADH and NADPH usage in HMF reduction. Appl Microbiol Biotechnol. 2009;84:751–61.

CrossMark

RESEARCH ARTICLE

New Protocol Based on UHPLC-MS/MS for Quantitation of Metabolites in Xylose-Fermenting Yeasts

Christiane Gonçalves Campos,[1,2] Henrique César Teixeira Veras,[1,3]
José Antônio de Aquino Ribeiro,[1] Patrícia Pinto Kalil Gonçalves Costa,[1]
Katiúscia Pereira Araújo,[1] Clenilson Martins Rodrigues,[1]
João Ricardo Moreira de Almeida,[1,4] Patrícia Verardi Abdelnur[1,2]

[1]Brazilian Agricultural Research Corporation, Embrapa Agroenergy, W3 Norte, PqEB, Brasília, DF 70770-901, Brazil
[2]Chemistry Institute, Federal University of Goiás, Campus Samambaia, Goiânia, GO 74690-900, Brazil
[3]Postgraduate Program in Molecular Biology, Department of Cellular Biology, University of Brasília, Campus Darcy Ribeiro, Brasília, DF, Brazil
[4]Postgraduate Program in Chemical and Biological Technologies, Institute of Chemistry, University of Brasília, Campus Darcy Ribeiro, Brasília, DF, Brazil
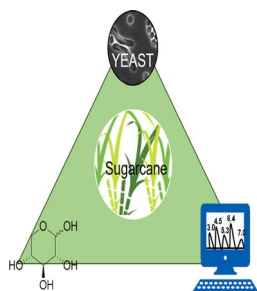
Abstract. Xylose fermentation is a bottleneck in second-generation ethanol production. As such, a comprehensive understanding of xylose metabolism in naturally xylose-fermenting yeasts is essential for prospection and construction of recombinant yeast strains. The objective of the current study was to establish a reliable metabolomics protocol for quantification of key metabolites of xylose catabolism pathways in yeast, and to apply this protocol to *Spathaspora arborariae*. Ultra-high performance liquid chromatography coupled to tandem mass spectrometry (UHPLC-MS/MS) was used to quantify metabolites, and afterwards, sample preparation was optimized to examine yeast intracellular metabolites. *S. arborariae* was cultivated using xylose as a carbon source under aerobic and oxygen-limited conditions. Ion pair chromatography (IPC) and hydrophilic interaction liquid chromatography-tandem mass spectrometry (HILIC-MS/MS) were shown to efficiently quantify 14 and 5 metabolites, respectively, in a more rapid chromatographic protocol than previously described. Thirteen and eleven metabolites were quantified in *S. arborariae* under aerobic and oxygen-limited conditions, respectively. This targeted metabolomics protocol is shown here to quantify a total of 19 metabolites, including sugars, phosphates, coenzymes, monosaccharides, and alcohols, from xylose catabolism pathways (glycolysis, pentose phosphate pathway, and tricarboxylic acid cycle) in yeast. Furthermore, to our knowledge, this is the first time that intracellular metabolites have been quantified in *S. arborariae* after xylose consumption. The results indicated that fine control of oxygen levels during fermentation is necessary to optimize ethanol production by *S. arborariae*. The protocol presented here may be applied to other yeast species and could support yeast genetic engineering to improve second generation ethanol production.

Keywords: Xylose fermentation, Mass spectrometry, UHPLC-MS/MS, Metabolomics, *Spathaspora arborariae*

Introduction

The increased demand for alternative energy sources together with concerns about the environmental impacts of fossil fuels has motivated studies into the production of biofuels from lignocellulosic biomass such as second generation ethanol (Ethanol 2G) [1, 2]. Currently, a few pilot plants worldwide are producing ethanol 2G from different types of biomass, such as feedstock, however, high-capacity ethanol

production using current technologies is not fully achievable, and some improvements are still required. In the fermentation process, for example, xylose, the second most abundant sugar in sugarcane bagasse [3], is not converted to ethanol by *S. cerevisiae*, the yeast used in commercial ethanol production [4, 5]. Therefore, recombinant *S. cerevisiae* strains capable of fermenting xylose have been produced by the expression of xylose-catabolic pathways from naturally xylose-consuming microorganisms [6, 7]. In addition, naturally xylose-fermenting yeasts have been identified and evaluated for industrial ethanol production. Despite this, the relative success in obtaining strains able of producing ethanol through these xylose-conversion strategies is still limited by our understanding of the constraints in xylose metabolism by yeast [7]

Naturally xylose-fermenting yeasts or recombinant strains obtained by overexpression of xylose catabolic pathways are capable of producing ethanol, though with low yield, due to xylitol formation. This happens because xylose is first reduced to xylitol by a NAD(P)H-dependent xylose reductase (XR), followed by xylitol oxidation to xylulose by the NAD^+-dependent xylitol dehydrogenase (XDH) [7, 8]. Thus, other modifications have been proven to be necessary in order to increase process productivity [9–14]. These strategies involve the collection, analysis, and quantitative integration of biological data on a large scale through OMICs tools (genomics, transcriptomics, proteomics, fluxomics, and metabolomics). This may help in the construction of more relevant and predictive models to identify limiting steps in xylose metabolism [12].

Metabolomics analysis allows qualitative and quantitative analysis of metabolites [15, 16]. Targeted metabolomics has been widely used to quantify metabolites in specific pathways, providing kinetic information regarding production and consumption rates that could be further used in metabolic engineering [17, 18]. However, to get a reliable "metabolite picture" of a system using metabolomics, certain steps should be carefully followed: (1) careful choice of material, (2) sample preparation and extraction, (3) analytic methods, (4) data processing, and (5) data analysis and interpretation [19, 20]. An important challenge in metabolomics studies is choosing the ideal analytical method, where specific analytic tools capable of simultaneously analyzing a large number of compounds with high sensitivity and selectivity are required, especially for biological samples containing a large variety of low-abundance metabolites [21, 22]. In this context, liquid chromatography coupled to mass spectrometry has been widely used in targeted metabolomics of polar compounds [23, 24].

Furthermore, ultra-high performance liquid chromatography-mass spectrometry (UHPLC-MS) allows high-throughput efficient analysis, reduces solvent use, improves peak resolution, and consequently, metabolite separation, resulting in better quantification analysis [25]. There is a wide variety of chromatographic separation methods available to separate specific classes of compounds, such as polar, non-polar, and ionic compounds. LC-MS/MS methods based on ion pair chromatography (IPC) have been described in the literature for quantifying metabolites of glycolysis, the pentose phosphate pathway (PPP), and the

tricarboxylic acid (TCA) cycle [26–28]. However, they are limited to phosphorylated compounds, carboxylic acids, nucleotides, and coenzyme-A esters. Moreover, high concentrations of tributylamine (TBA) are used in the mobile phase as an ion pair reagent, which results in mass spectrometer contamination [26]. Hydrophilic interaction liquid chromatography-tandem mass spectrometry (HILIC-MS/MS) allows the use of a range of stationary phases for analyzing polar molecules that are weakly retained in the reverse phase [29]. BEH amide column-based methods are used to quantify sugars [30] but they still require improvements in order to perform faster chromatographic runs with better peak resolution.

Here, we present two complementary chromatographic methods, IPC and HILIC, coupled to tandem mass spectrometry (MS/MS), which together allow complete separation and quantification of 19 intracellular metabolites from central carbon metabolism. Furthermore, sample preparation methods were optimized for the quenching of cellular metabolites and for metabolite extraction steps for yeast sample preparation. The final metabolomics protocol developed here was successfully applied for metabolite quantification in the naturally xylose-fermenting yeast *S. arborariae* during cultivation on xylose as the sole carbon source, under aerobic and oxygen-limited conditions. The metabolomics protocol presented here may be applied to other yeast strains.

Experimental

Standards and Chemicals

All metabolite standards were purchased from Sigma-Aldrich (St. Louis, MO, USA) with purity superior to 95%: acetyl coenzyme-A (ACCOA), acetaldehyde (Acald), alpha ketoglutaric acid (AKG), D-malic acid (L-MAL), oxaloacetic acid (Oaa), D-(+)-glucose, xylose, glucose-6-phosphate (G6P), fructose-6-phosphate (F6P), dihydroxy acetone phosphate (DHAP), erythrose-4-phosphate (E4P), glyceraldehyde-3-phosphate (GAP), glycerol-3-phosphate (GLY3P), ribose-5-phosphate (R5P), ribulose-5-phosphate (RU5P), xylulose (Xylu), phospho(enol)pyruvate (PEP), glycerol, sodium pyruvate (PYR), sedoheptulose-7-phosphate (S7P) and xylitol. Solvents used for development of chromatography and mass spectrometry, such as formic acid, ammonium formate, tributylamine, triethylamine, acetonitrile, and methanol, were also purchased from Sigma-Aldrich (St. Louis, MO, USA) at the highest available purity. Ammonium acetate was acquired from Vetec (St. Louis, MO, USA) and ammonium hydroxide from Fluka (St. Louis, MO, USA). Deionized water (18.2 MΩ) was obtained from a Direct 16 Milli-Q purification system (Millipore, Bedford, MA, USA).

Biological Material

The xylose-fermenting yeast *Spathaspora arborariae* NRRL Y-48658 was grown on a YPD plate overnight, and then one single colony was transferred to pre-inoculum containing 50

mL of mineral medium, 2.5 times concentrated, and supplemented with 40 g/L of xylose as the carbon source [31]. For the fermentation process, a bioreactor was used (Multifors 2 Infors) with working volume of 500 mL of the same mineral medium used in the pre-inoculum. Fermentation was carried out under aerobic and oxygen-limited conditions. The cultures were grown at 28 °C, with agitation (400 rpm), and pH 5.5 adjusted with 3M KOH. Yeast samples were collected in triplicate, during the exponential growth phase between 20 h of aerobic and 40 h oxygen-limited fermentations. Ideal growth rates were estimated using optical density (OD_{600}).

Quenching and Extraction Steps

The quenching of cellular activity and metabolite extraction procedures were optimized for the yeast samples based on previously described protocols [32, 33].

For the quenching step, 2 mL of cell culture were added to 8 mL of 60% (v/v) methanol buffered with 10 mM ammonium acetate (pH 7.4), in a –40 °C thermostatic bath (FP 50-MA, Julabo, Germany). The samples were then centrifuged at 5000 rpm, –9 °C for 5 min. The supernatant was discarded and the resulting pellet was immediately frozen in liquid nitrogen and stored at –80 °C until the extraction step. Frozen cell pellets were kept in a thermostatic bath at –40 °C for 5 min before the extraction procedure.

The boiling ethanol method was used for metabolite extraction [33]. A total of 2 mL of 75% (v/v) ethanol buffered with 10 mM ammonium acetate (pH 7.4) solution at 85 °C was added to the pellet. The samples were homogenized in a vortex and then transferred to a 2 mL tube for 3 min incubation at 85 °C with constant shaking (Thermoximer comfort, Eppendorf). Subsequently, cells were cooled at –40 °C using a thermostatic bath and centrifuged (5424-R, Eppendorf) at 5000 rpm, –9 °C for 3 min. The supernatant was collected in a 2 mL tube and dried under vacuum (Centrivap DNA concentrator, Labconco). Samples were storage at –80 °C until UHPLC-MS/MS analysis.

UHPLC-MS/MS

All experiments were performed using an Acquity UPLC system (Waters, Milford, MA, USA) coupled to a triple quadrupole mass spectrometer (Xevo TQD, Waters) equipped with an electrospray ionization source. Data were acquired and processed with MassLynx 4.1 software (Waters). The MS was operated in the negative ionization mode, ESI(–)-MS, using multiple reaction monitoring (MRM). The instrument parameters were as follows: capillary voltage 3500 V, desolvation temperature: 450 °C, source temperature: 130 °C, cone gas flow: 20 L/h, and desolvation gas flow: 700 L/h. MRM transition channels and collision cell voltages were optimized for each metabolite after direct infusion into the MS.

Hydrophilic interaction liquid chromatography (HILIC) was performed using a BEH amide column (2.1 × 150 mm × 1.7 µm) (Waters) at 50 °C, with eluent A (0.1% ammonium hydroxide aqueous solution) and eluent B (acetonitrile with 0.1% ammonium hydroxide). Five metabolites were analyzed

by this method: glucose, xylose, glycerol, xylitol, and xylulose. Ion pair chromatography (IPC) was performed using a reverse phase column, HSS-T3 (2.1 × 150 mm × 1.8 µm) (Waters) at 45 °C, with eluent A (5 mM tributylamine, 10 mM acetic acid, and 5% (v/v) methanol, pH 4.8), and eluent B (methanol). Fourteen metabolites were analyzed by this method: ACCOA, AKG, L-MAL, G6P, F6P, DHAP, E4P, GAP, GLY3P, R5P, RU5P, PEP, PYR, S7P. The gradient flow rates for both methods are shown in Tables 1 and 2, respectively.

Quantification of Targeted Metabolites

A standard solution (SS) was prepared for each metabolite (1 mg/mL in water). Then, dilutions of SS, 0.1, 0.25, 0.5, 1.0, 2.5, 5.0, 10, and 50 µg/mL were used for calibration curve construction and quality control (QC) experiments. The limit of detection (LOD) and quantitation (LOQ) were established based on signal/noise ratio of 3:1 and 10:1, respectively [34]. The definitive analytical calibration curve was constructed with six levels of standard mixture solutions and obtained by plotting the area against the concentration of each compound, using second-order polynomial regression. Calibration curves and samples of exponential growth phases were analyzed in triplicate, using UHPLC-MS/MS.

Results and Discussion

A total of 19 commercially available metabolites of central carbon metabolism (Figure 1) related to the glycolysis, PPP, and TCA pathways were used for method development. Although these are not the only metabolites involved in these metabolic pathways, each molecule analyzed is key to at least one pathway, and therefore they together represent the metabolic flux of conversion of xylose to ethanol in yeast.

UHPLC-MS/MS

Mass spectrometry is a fast and simple method for detecting metabolites. However, prior chromatographic separation is required in order to avoid ion suppression effects and to identify isomers. A highly sensitive and selective method based on mass spectrometry, the multiple reactions monitoring (MRM) strategy, was used in this study. To perform UHPLC-MS/MS using MRM, first, mass spectrometer parameters such as ionization source and mass analyser (Q1 and Q3 channels) were

Table 1. UHPLC Conditions Using HILIC Mode with Mobile Phase (Eluent) A: 0.1% Ammonium Hydroxide, and B: Acetonitrile with 0.1% Ammonium Hydroxide, Applied to Glycerol, Xylulose, Xylose, Xylitol, and Glucose Analyses

Time (min)	Flow (mL/min)	Eluent A (vol. %)	Eluent B (vol. %)
0.0	0.2	15	85
6.5	0.2	50	50
7.5	0.4	50	50
8.0	0.2	15	85
12.0	0.2	15	85

Table 2. UHPLC Conditions Using IPC Mode with Mobile Phase (Eluent) A: 5 mM Tributylamine, 10 mM Acetic Acid, and 5% (v/v) Methanol, and B: Methanol, Applied to Glucose-6-Phosphate, Fructose-6-Phosphate, Ribose-5-Phosphate, Ribulose-5-Phosphate, Sedoheptulose-7-Phosphate, Glycerol-3-Phosphate, Erytrose-4-Phosphate, Glyceraldehyde-3-Phosphate, Dihydroxyacetone Phosphate, Sodium Pyruvate, Malic Acid, Alpha Ketoglutaric Acid, Phospho(enol)pyruvate, and acetyl co-enzyme-A Analyses

Time (min)	Flow (mL/min)	Eluent A (vol. %)	Eluent B (vol. %)
0.0	0.4	100	0
10.0	0.4	89.5	10.5
18.0	0.4	47.4	52.6
19.0	0.4	47.4	52.6
20.0	0.4	100	0
26.0	0.4	100	0

optimized, followed by chromatographic parameters, such as the mobile phase.

Mass Spectrometry Direct infusion mass spectrometry (DIMS) was used to optimize the ionization source and

collision cell voltages for each metabolite. Although ESI(+)-MS and ESI(−)-MS were tested, all metabolites were detected with better sensitivity using ESI(−)-MS, which was therefore selected for further analyses. After ionization, each precursor ion was isolated in the first quadrupole (Q1), collided with gas in Q2, and then fragment ions were detected in Q3 (MS/MS experiments). Capillary voltage and collision energy values were optimized for each standard, wherein the capillary voltages were similar for all metabolites (3500 V). The highest and/or most selective fragment ion was selected for MRM analyses (Table 3). No fragmentation ion was detected for acetaldehyde (Acald), probably due to its low molecular weight (44 Da), and as such it was excluded from this study.

After the optimization of mass spectrometer parameters, the next step involved developing a chromatographic method capable of separating all metabolites. Liquid chromatography is crucial for the separation of isomeric compounds, especially for metabolites with same MRM channels (Q1 and Q3).
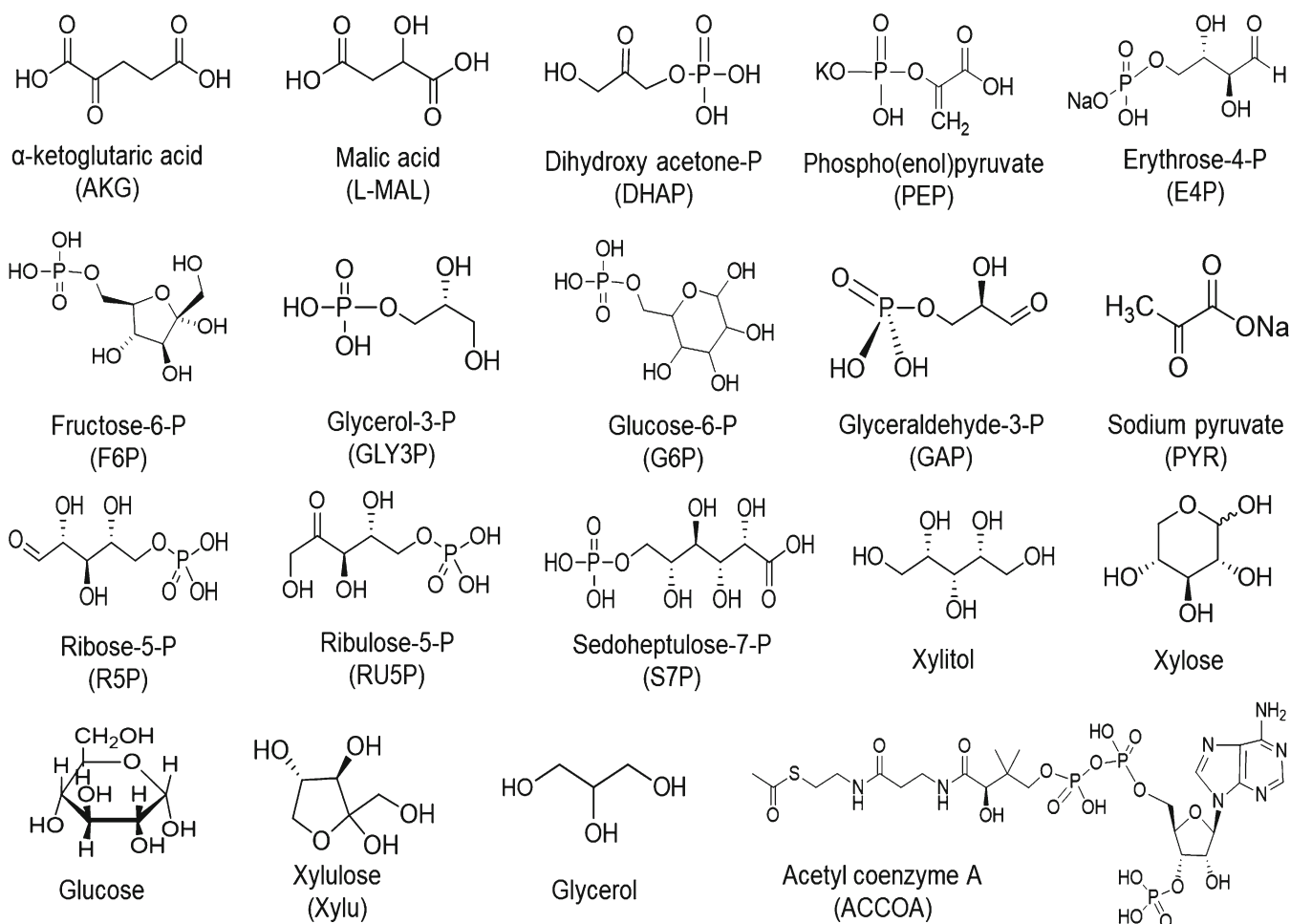
Figure 1. Chemical structures of metabolites from glycolysis, pentose phosphate pathway and tricarboxylic acid cycle analyzed by UHPLC-MS/MS. Metabolites: alpha ketoglutaric acid (AKG), D-malic acid (L-MAL), dihydroxy acetone phosphate (DHAP), phospho(enol)pyruvate (PEP), erythrose-4-phosphate (E4P), fructose-6-phosphate (F6P), glycerol-3-phosphate (GLY3P), glucose-6-phosphate (G6P), glyceraldehyde-3-phosphate (GAP), sodium pyruvate (PYR), ribose-5-phosphate (R5P), ribulose-5-phosphate (RU5P), sedoheptulose-7-phosphate (S7P), xylitol, xylose, D-(+)-glucose, xylulose (Xylu), glycerol and acetyl coenzyme A (ACCOA)

Table 3. The List of Metabolites Quantified by the Developed UHPLC-MS/MS Methods

Method	Metabolite	Cone voltage (V)	Q1 (m/z)	Q3 (m/z)	Collision energy (eV)	Retention time (min)
IPC	ACCOA	60	808.1	408.0	50	18.50
IPC	AKG	18	144.6	56.8	15	15.39
IPC	DHAP	25	169.0	97.0	18	8.37
IPC	E4P	20	198.8	78.8	20	7.52
IPC	F6P	32	258.6	96.8	18	6.66
IPC	G6P	32	258.7	96.8	20	6.16
IPC	GAP	20	168.8	96.8	18	7.27
IPC	GLY3P	30	170.5	78.7	25	6.91
IPC	L-MAL	18	132.6	114.8	10	14.89
IPC	PEP	20	166.6	78.8	10	16.35
IPC	PYR	20	86.8	42.8	8	9.03
IPC	R5P	30	228.8	96.8	20	6.56
IPC	RU5P	30	228.8	79.0	20	7.47
IPC	S7P	32	288.4	138.9	25	6.64
HILIC	Glycerol	18	91.0	59.1	18	3.36
HILIC	Glucose	15	179.1	58.9	18	5.12
HILIC	Xylitol	25	151.0	58.9	20	4.75
HILIC	Xylose	10	149.0	59.0	14	4.57
HILIC	Xylu	10	149.0	59.0	14	3.83

Abbreviations: Ion pair chromatography (IPC), hydrophilic interaction liquid chromatograpy (HILIC), acetyl Co-enzyme A (ACCOA), alpha ketoglutaric acid (AKG), di-hydroxyacetone phosphate (DHAP), erythrose-4-phosphate (E4P), fructose-6-phosphate (F6P), glucose-6-phosphate (G6P), glyceraldehyde-3-phosphate (GAP), glycerol-3-phosphate (GLY3P), malic acid (L-MAL), phospho(enol)piruvate (PEP), sodium pyruvate (PYR), ribose-5-phosphate (R5P), ribulose-5-phosphate (RU5P), sedoheptulose-7-phosphate (S7P), and xylulose, (Xylu).

Ultra-High Performance Liquid Chromatography (UHPLC) Chromatographic parameters such as mobile phase composition, column temperature, and elution modes (gradient and isocratic) were tested to improve peak separation for the 19 metabolites. However, no single set of conditions was able to provide a complete peak separation with good resolution for all metabolites, due to their distinct chemical structures. In metabolomics analyses, a single approach is desirable for measuring all metabolites, but this is a challenge for complex matrix samples with a wide range of chemical classes of metabolites at different concentrations. As such, two main groups were established based on their chemical characteristics: (1) a group
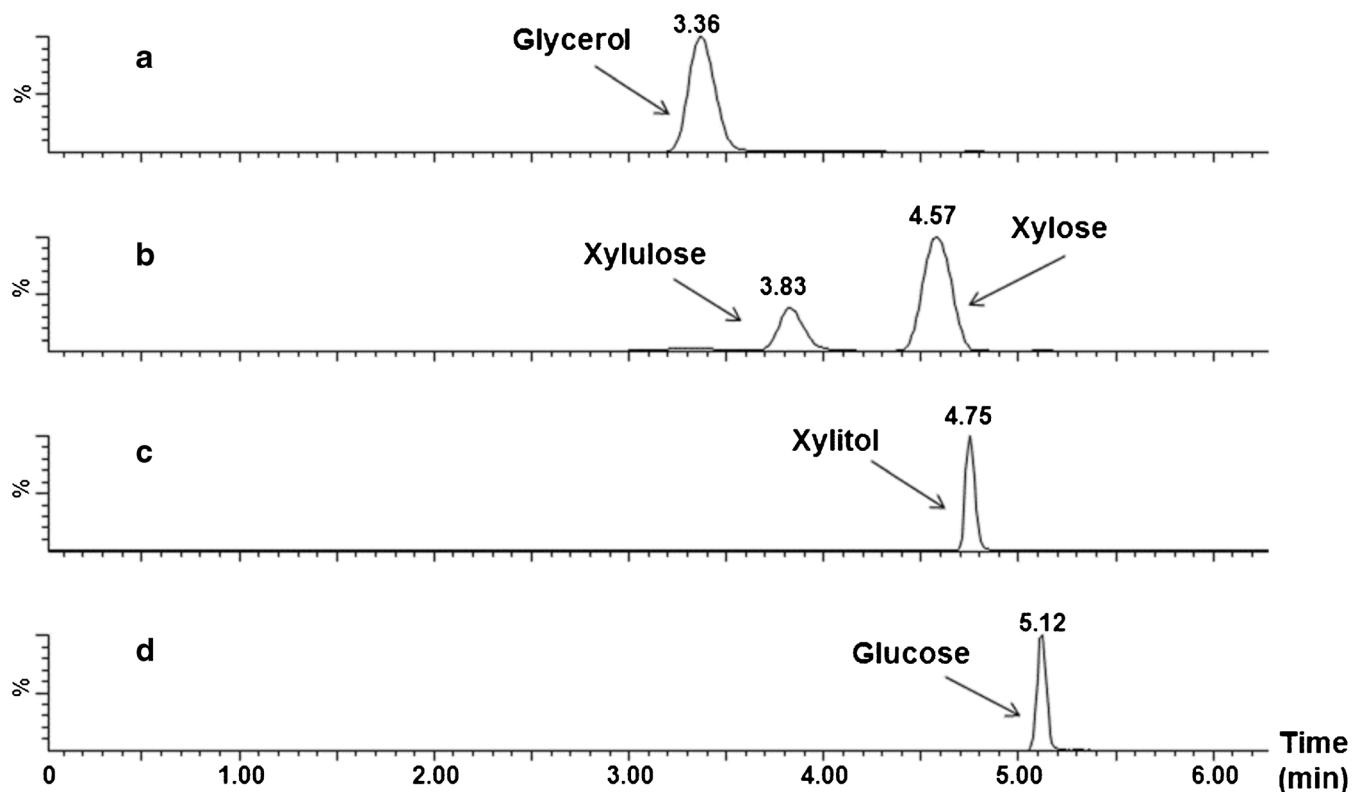

Figure 2. Multiple reaction monitoring (MRM) experiments using HILIC-ESI(-)-MS/MS for channels (Q1 > Q3): a) *m/z* 91 > 59 (glycerol); b) *m/z* 149 > 59 (xylulose and xylose); c) *m/z* 151 > 59 (xylitol) and d) *m/z* 179 > 59 (glucose)
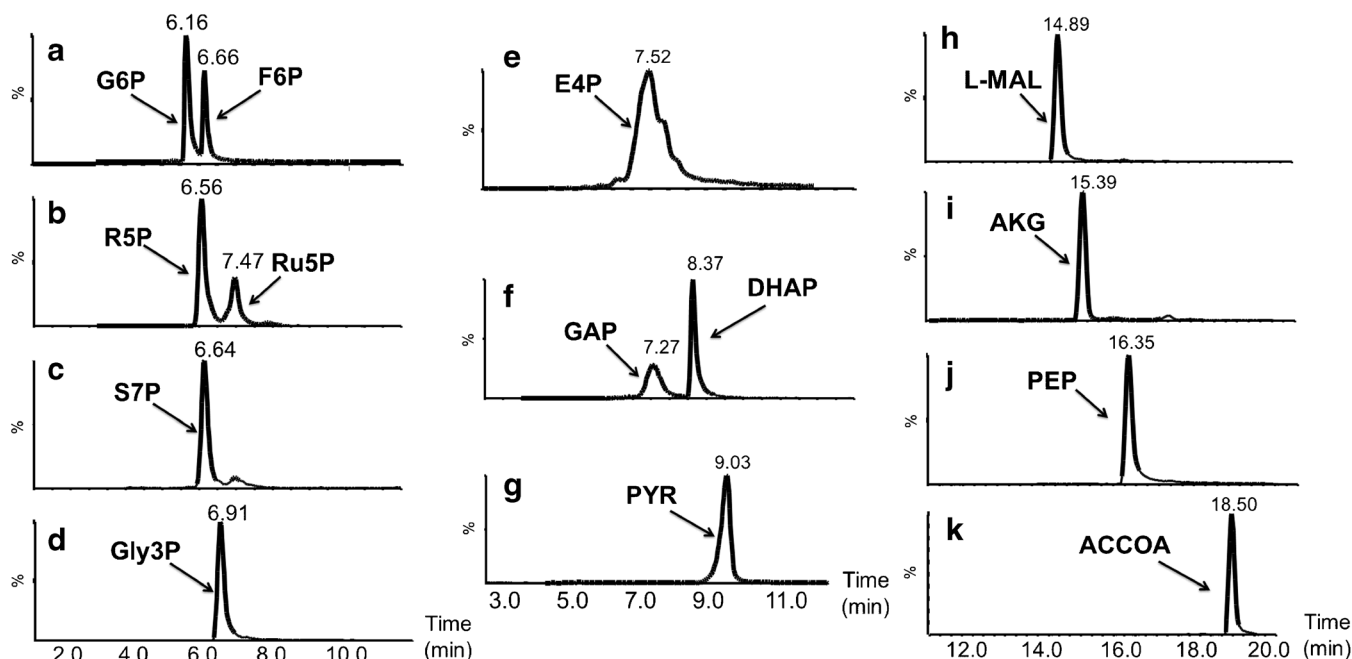
Figure 3. Multiple Reaction Monitoring experiments using IPC-ESI(-)-MS/MS: (**a**) *m/z* 259 > 97 (glucose-6-phosphate and fructose-6-phosphate); (**b**) *m/z* 229 > 97 (ribose-5-phosphate) and *m/z* 229 > 79 (ribulose-5-phosphate); (**c**) *m/z* 288 > 139 (sedoheptulose-7-phosphate); (**d**) *m/z* 170 > 79 (glycerol-3-phosphate); (**e**) *m/z* 199 > 79 (erytrose-4-phosphate); (**f**) *m/z* 169 > 97 (glyceraldehyde-3-phosphate and dihydroxyacetone phosphate); (**g**) *m/z* 87 > 43 (pyruvic acid); (**h**) *m/z* 133 > 115 (malic acid); (**i**) *m/z* 145 > 57 (alpha ketoglutaric acid); (**j**) *m/z* 167 > 79 (phospho(enol)pyruvate); (**k**) *m/z* 808 > 408 (acetyl Co-enzyme-A)

of sugars (monosaccharides) and alcohols; and (2) a group of organic acids and sugar phosphate compounds.

Hydrophilic Interaction Liquid Chromatography (HILIC)
Polar stationary phases, such as chemically modified silica, linked to organic groups, such as amine, amide, diol, cyano, and others, are often used in HILIC. The mechanism of compound separation by HILIC is still poorly understood. Tang and co-workers [35] proposed that water molecules are attracted by polar groups of the stationary phase, resulting in an aqueous layer on the surface. Partition of the analyte between the mobile phase (hydrophobic) and immobilized aqueous layer best explains the HILIC mechanism [29]. In HILIC, the eluting solvent is usually a mixture of water and acetonitrile with a modifier, such as ammonium salts [36]. Initially, the potential of the amide column was tested for separation of 14 metabolites, including phosphate sugars, organic acids, sugars (monosaccharides), and alcohols. Ammonium formate, ammonium acetate, and ammonium hydroxide were tested in different solutions of acetonitrile and water (Supplementary Table S1). The use of ammonium formate as a modifier in isocratic elution mode retained only seven metabolites (Supplementary Figure S1), and the gradient elution mode using ammonium acetate (Supplementary Table S2) provided poor separation, particularly for phosphate compounds (Supplementary Figure S2). The use of ammonium hydroxide, in gradient elution mode (Supplementary Table S3), showed good separation only for the neutral compounds (glycerol, xylulose, xylose, xylitol, and glucose). However, the phosphate compounds and

acids such as malic acid and alpha ketoglutaric were not separated (Supplementary Figure S3).

From these results, metabolites in the study were divided into two groups according to their chemical characteristics and interaction with the chromatography column. The first group consists of sugars (monosaccharides), xylitol, and glycerol, and the second consists of phosphate sugars and organic acids. For this first group the ideal chromatographic condition was observed using the mobile phase: A (0.1% ammonium hydroxide) and B (acetonitrile with 0.1% ammonium hydroxide) at 50 °C (column temperature) in a gradient mode (Table 1). A baseline peak separation of five metabolites: glycerol (91 > 59), xylulose (149 > 59), xylose (149 > 59), xylitol (151 > 59), and glucose (179 > 59) was performed in a 12 min analysis (Figure 2). To our knowledge, this is the first time that an ultrafast chromatography method coupled to mass spectrometry has been reported to detect these compound classes.

The isomers xylose and xylulose have the same values of Q1 (*m/z* 149) and Q3 (*m/z* 59) in the MRM experiment; therefore, chromatography was essential for separation and quantitation (Figure 2b). After the injection of each standard solution, the peaks were assigned to xylulose (3.83 min) and xylose (4.57 min) (data not shown).

Ion-Pair Chromatography (IPC) Ionic compounds are often separated by IPC, which usually uses a hydrophobic stationary phase and an ion pair (IP) reagent as the mobile phase. In general, volatile alkylamines and organic acids are used as IP reagents, and a polar compound, such as methanol or propan-2-
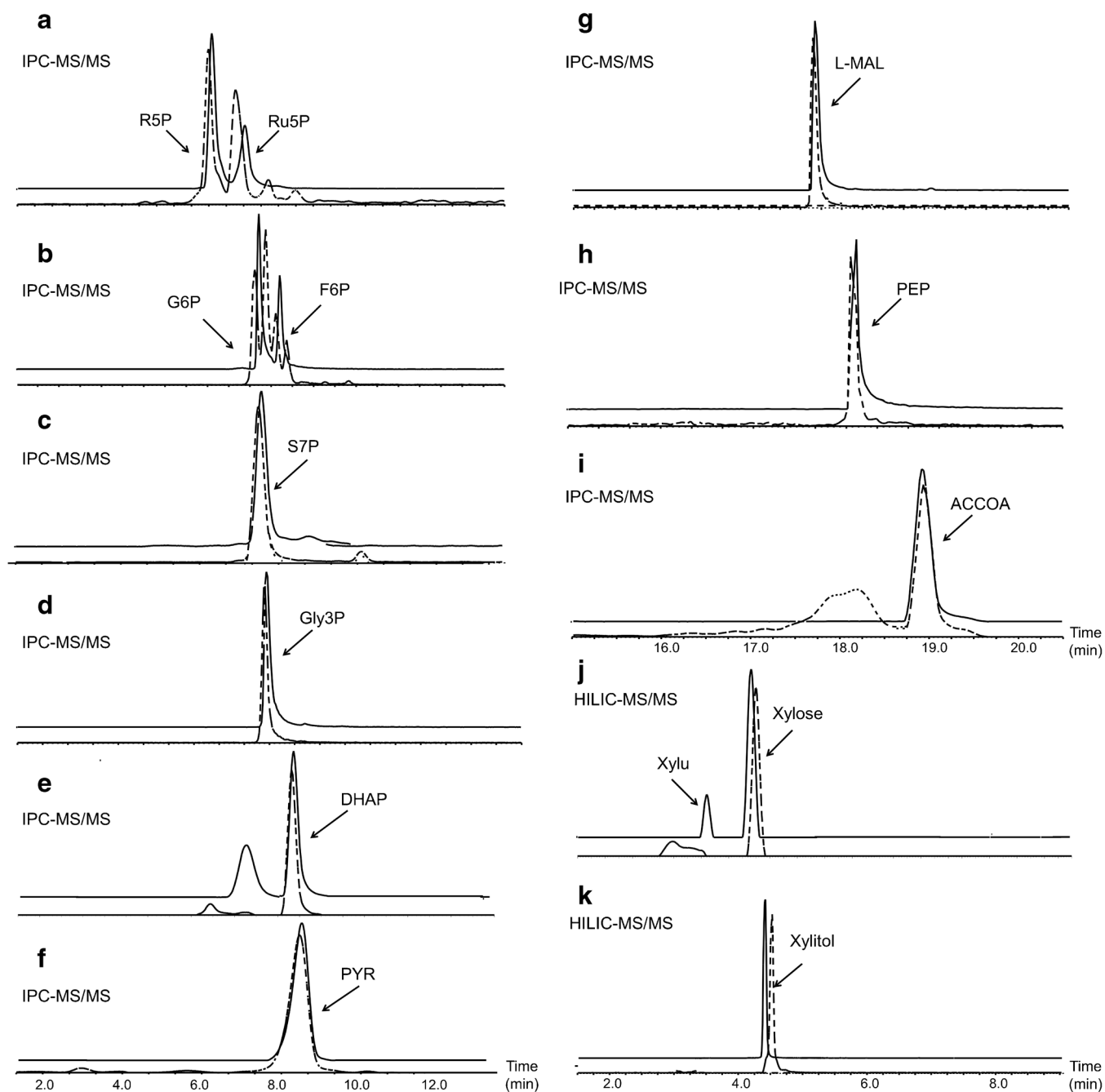
Figure 4. MRM chromatograms of 13 metabolites detected using IPC and HILIC, X axis is retention time in minutes. The upper solid line correspond to the standard mixture of metabolites and lower dashed lines correspond to the metabolites detected in *S. arborariae* cell extracts: (**a**) ribose-5-phosphate (R5P) and ribulose-5-phosphate (Ru5P), (**b**) glucose-6-phosphate (G6P) and fructose-6-phosphate (F6P), (**c**) sedoheptulose-7-phosphate (S7P), (**d**) glycerol-3-phosphate (Gly3P), (**e**) dihydroxy acetone phosphate (DHAP), (**f**) pyruvic acid (PYR), (**g**) malic acid (L-MAL), (**h**) phospho(enol)pyruvate (PEP), (**i**) acetyl Co-enzyme A, (**j**) xylose, (**k**) xylitol

ol, as an organic modifier. IP reagent interacts with the stationary phase, creating an opposite charge to the analyte, thus increasing retention time and selectiveness of the reverse phase column. In the current study, a reverse phase column (HSS-T3- Waters), was tested using two IP reagents, triethylamine (TEA) and tributylamine (TBA), at different concentrations, pH values, temperatures, and elution modes (gradient and isocratic)

(Supplementary Table S6). Acceptable separation of phosphorylated compounds was not seen using TEA (Supplementary Figure S4). However, improved results were seen using TBA, with better peak separation, resolution, and sensitivity, as the alkyl chain size of the IP reagent was directly related to the analyte elution time [27]. Two organic eluents were tested, and a better separation of AKG, L-MAL, DHAP, and GAP was

Table 4. Regression coefficients (R^2), range of calibration curve, limits of detection (LOD), limits of quantification (LOQ), and metabolite concentrations in samples of yeast *Spathaspora arborariae* under aerobic and oxygen- limited condition

#	Metabolite	Range (µg/mL)	R^2	LOD (µg/mL)	LOQ (µg/mL)	Aerobic		Oxygen-limited	
						(µg/mL)	RSD (%)	(µg/mL)	RSD (%)
1	ACCOA	7.4–80	0.9975	2.35	7.12	17.04	7.68	6.61	5.46
2	AKG	3.5–50	0.9958	0.92	3.08	< LOQ	–	< LOQ	–
3	L-MAL	0.2–50	0.9984	0.03	0.11	64.95	18.97	14.03	8.37
4	Gly3P	3.5–50	0.9994	0.09	0.29	7.58	5.77	2.61	15.77
5	G6P	1.5–50	0.9990	0.43	1.43	5.43	10.02	4.45	12.09
6	F6P	3.5–50	0.9980	0.96	3.19	7.77	14.19	6.65	15.38
7	DHAP	2.0–50	0.9992	0.59	1.99	1.90	6.98	< LOQ	–
8	GAP	3.5–50	0.9979	0.92	3.06	ND	–	ND	–
9	R5P	2.0–50	0.9992	0.65	1.99	2.87	13.08	< LOQ	–
10	Ru5P	2.5–50	0.9991	0.61	2.04	21.92	2.72	5.79	15.87
11	E4P	1.0–50	0.9996	0.29	0.98	ND	–	ND	–
12	S7P	1.4–30	0.9983	0.38	1.27	37.33	19.46	20.55	17.23
13	PEP	2.5–50	0.9919	0.66	2.21	18.50	9.91	4.26	13.11
14	PYR	0.5–50	0.9998	0.14	0.43	4.63	9.90	1.65	16.86
15	Xylu	0.5–75	0.9971	0.20	0.50	ND	–	ND	–
16	Xylose	0.5–50	0.9990	0.20	0.50	3275.00	11.26	4896.00	6.10
17	Glucose	0.5–50	0.9991	0.20	0.50	ND	–	ND	–
18	Glycerol	0.5–50	0.9993	0.20	0.50	< LOQ	–	< LOQ	–
19	Xylitol	0.5–75	0.9988	0.20	0.50	1140.00	5.92	401.52	12.16

achieved using methanol instead of acetonitrile, in a gradient mode (data not shown). Variation in pH values (2.8, 4.8, 5.1, and 6.2) (Supplementary Figure S5A–D) showed a greater co-elution at the lower pH value in the separation of phosphates sugars (Supplementary Figure S5B). The separation of ribose-5-phosphate was achieved at pH 4.8, and this pH value improved separation of compounds with carboxylic groups such as malic acid, alpha ketoglutaric acid, and phospho(enol)pyruvate.

Three concentrations of TBA, (2, 5, and 10 mM - Supplementary Table S5), were investigated, and the chromatographic profile was similar using 5 and 10 mM (Supplementary Figure S6). In general, studies in the literature have been performed using 10 mM TBA [26, 27, 37]; however, the use of TBA has the disadvantage of contaminating the mass spectrometer, and it is difficult to remove and requires constant cleaning. As such, 5 mM TBA in the mobile phase was chosen for this study. The best chromatographic condition was achieved using the mobile phases: A (5 mM tributylamine, 10 mM acetic acid, and 5% (v/v) methanol); B (methanol) at 45 °C (column temperature) in a gradient mode (Table 2). A 26 min chromatographic run is described here for the first time, for separation of 14 compounds, including the isomers: G6P and F6P; and R5P and Ru5P (Figure 3). OAA did not show good stability and reproducibility and it was excluded from further study.

A summary table describing the metabolites and most significant UHPLC-MS/MS optimized parameters such as the separation mode, retention time, cone voltage, MRM transitions and collision energy, is presented (Table 3).

Yeast Metabolomics

Quantitative Analysis of Spathaspora arborariae Metabolites
Metabolomics analysis of a naturally xylose-fermenting yeast,

S. arborariae [38], was performed using the UHPLC-MS/MS methods developed here, after the yeast was cultivated in a fermenter under aerobic and oxygen-limited conditions. Optimization of sample preparation was carried out to extract the highest possible quantity of intracellular metabolites using fewer steps in order to avoid loss and chemical degradation, and to increase the sensitivity of analysis. Yeast media volumes of 1-5 mL were collected, processed, and analyzed, and a volume of 2 mL was chosen for further analysis.

An important consideration in metabolomics analysis is the wide range of concentrations for different metabolites in a biological sample, ranging from pmol/L to mol/L. UHPLC-MS/MS injections of *S. arborariae* samples have detected high concentrations of xylose and xylitol, and so samples were diluted 100-fold before HILIC-MS/MS analysis. Furthermore, malic acid and sedohptulose-7-phosphate reached the upper limit of the detection curve, and so a 5-fold dilution was required before IPC-MS/MS analysis.

A total of 13 metabolites (xylitol, xylose, pyruvic acid, sedoheptulose-7-phosphate, glucose-6-phosphate, fructose-6-phosphate, glycerol-3-phosphate, malic acid, phospho(enol)-pyruvate, acetyl co-enzyme-A, ribose-5-phosphate, ribulose-5-phosphate, and dihydroxy acetone phosphate) were quantified in *S. arborariae* samples under aerobic conditions. Figure 4 shows a significant overlap of MRM chromatograms for some of these metabolites identified in yeast samples and standard solutions using IPC and HILIC-MS/MS. The matrix effect exists but was not significant for data interpretation as shown in Figure 4, since the retention times for standards and yeast intracellular metabolites were similar. Furthermore, other isomers, different from the standards, were detected in some MRM channels (Figure 4a and b).

The limit of detection (LOD), limit of quantitation (LOQ), and regression coefficients (R^2) for each metabolite were

a
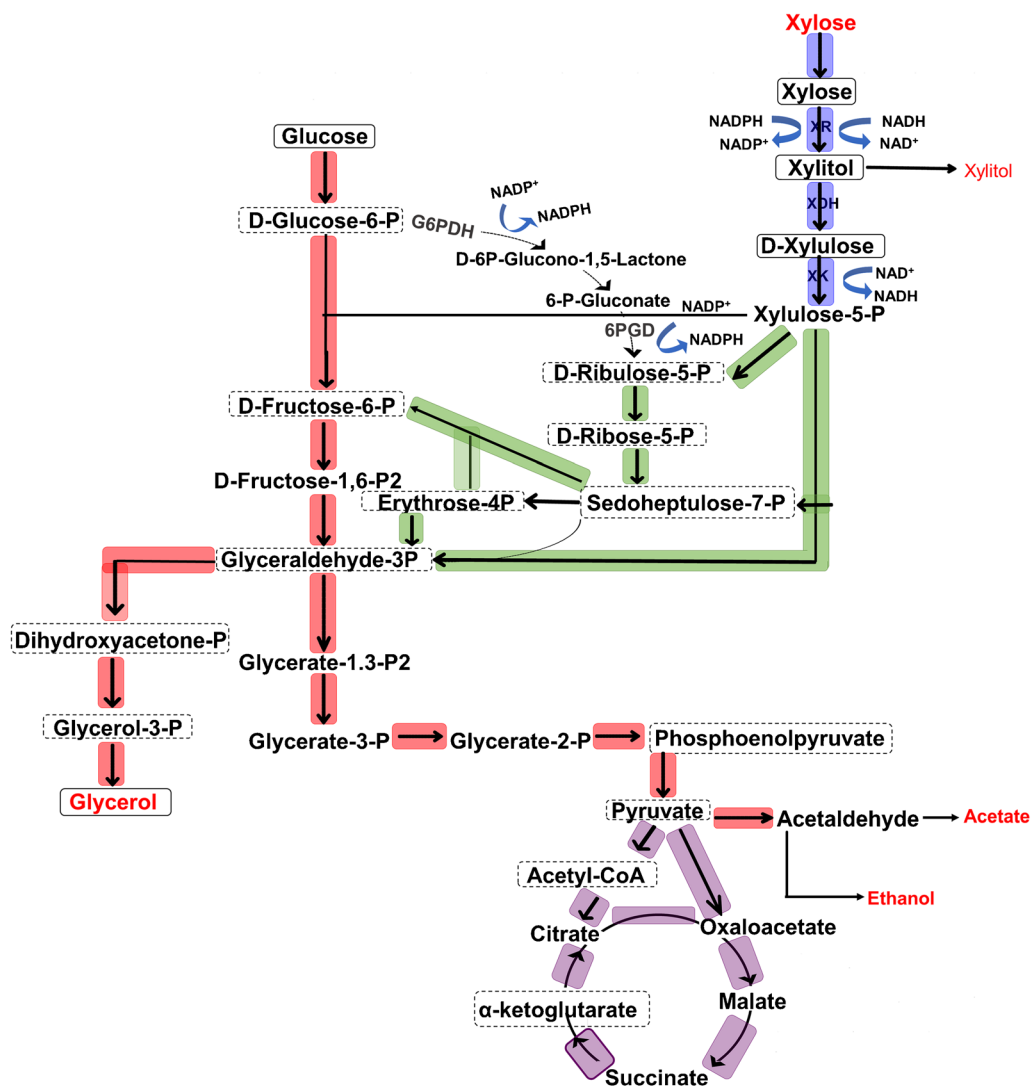
b
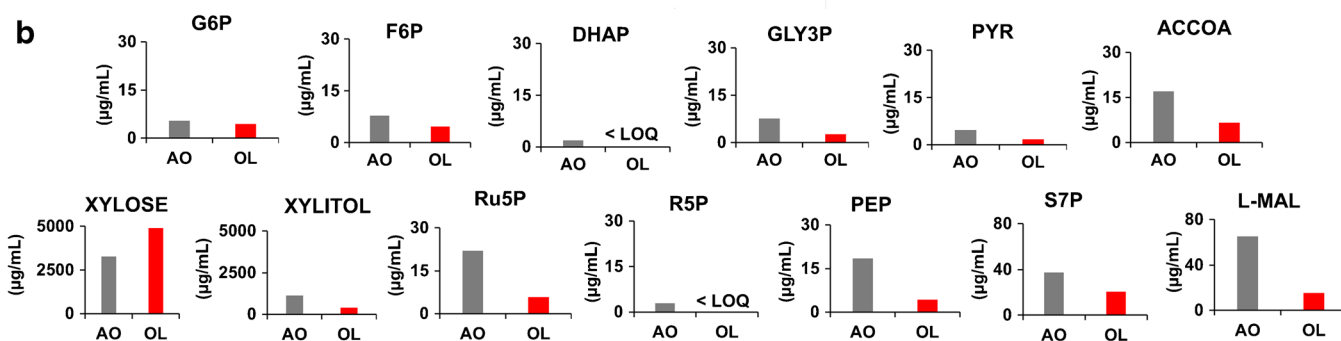
Figure 5. (**a**) Simplified schematic of central carbon metabolism from xylose to ethanol by yeast. Metabolic pathways assigned: oxidoreductive xylose assimilation (blue), pentose phosphate pathway (green); glycolysis (red); and tricarboxylic acid cycle (purple). The dotted boxes indicate which of these metabolites are detected by the HILIC method and the solid boxes indicate those detected by the IPC method. (**b**) Concentrations of 13 metabolites under aerobic (AO) and oxygen-limited (OL) conditions.

established for quantitative analysis (Table 4). Calibration curves ranged from 0.5 to 80 μg/mL (Supplementary Figures S7 and S8); LOD values ranged from 0.03 (L-MAL) to 3.19 μg/mL (ACCOA), and LOQ from 0.11 (L-MAL) to 7.12 μg/mL (ACCOA). Using these parameters, the metabolites detected during exponential growth of *S. arborariae* in

xylose medium were quantified. The concentrations were shown as an average of triplicates (μg/mL), and relative standard deviation (RSD) presented values below 20% as shown in the Table 4.

Concentrations of intracellular metabolites associated with central carbon metabolism in *S. arborariae* were, to

the best of our knowledge, determined for the first time here during xylose fermentation under aerobic and oxygen-limited conditions (Figure 5). Xylose was the most concentrated metabolite, followed by xylitol under both aerobic (3275.00 µg/mL; 1140.00 µg/mL), and oxygen-limited (4896.00 µg/mL; 401.52 µg/mL) conditions (Table 4). Although high concentration of xylose was expected due to this sugar being the substrate for the experiment and cells not being washed before metabolite extraction, the excess of xylitol indicates that the available oxygen was not sufficient for redox balance. Therefore, the accumulation of xylitol can be explained by an imbalance in cofactors required by the enzymes XR and XDH for their respective activities. This is in accordance with data previously reported in the literature, which demonstrated xylitol production, especially when the yeast is cultivated under oxygen-limited conditions [8]. These observations may be explained by the fact that XR from *S. arborariae* uses mainly NADPH as a cofactor in xylose reduction, whereas XDH is strictly NAD^+-dependent. Furthermore, the presence of glucose-6-P (G6P) and fructose-6-P (F6P) (Figure 5) indicates the need for regeneration of the cofactor NADPH in the non-oxidative PPP [39].

In addition, three metabolites of PPP were detected (ribose-5-phosphate (R5P), ribulose-5-phosphate (RU5P), and sedoptulose-7-phosphaste (S7P)), with S7P the most abundant under aerobic and oxygen-limited conditions (Table 4). The excess of S7P in *S. arborariae* can be attributed to insufficient activity of PPP enzymes, as occurs in native *S. cerevisiae* [39]. Overexpression of non-oxidative PPP genes in *S. cerevisiae* was shown to improve xylose conversion to ethanol [9].

As expected, the yeast produced two times more biomass under aerobic (0.31 g g^{-1}) than oxygen-limited (0.15 g g^{-1}) conditions (data not shown). Aerobic metabolism allows carbon flux through the TCA cycle, which in turn results in greater ATP formation [40]. Indeed, higher activity of the TCA cycle under aerobic compared with oxygen-limited conditions was confirmed by the approximately 4.5 and 3.0 times higher concentrations of L-MAL and ACCOA, respectively, (Table 4). In general, all metabolites quantified under oxygen-limited conditions are found at lower concentrations compared with aerobic conditions, and this is possibly related to biomass yield.

Conclusions

Metabolomics studies, although challenging, can contribute to the understanding of xylose metabolism in yeast. Here, we first developed two complementary methods based on ultra-high performance liquid chromatography-tandem mass spectrometry (UHPLC-MS/MS) to quantify 19 metabolites involved in the glycolysis, PPP, and TCA pathways in yeast. A faster run method based on IPC-MS/MS (26 min of total chromatographic run time), using 5 mM TBA concentration (lower than previously described) was capable of separating 14 metabolites with good peak resolution. Furthermore, a new HILIC-MS/MS method was developed to quantify xylose, glucose, glycerol, xylitol, and xylulose in a 12 min chromatographic run. Previous methods described are slower and do not separate all of these metabolites. Analytical parameters such as LOD, LOQ, and calibration curves were established for quantitative analysis of targeted metabolites.

To our knowledge, this is the first time that intracellular metabolites from *S. arborariae* have been successfully quantified using the metabolomics protocol developed in this work, characterizing the metabolic flux after xylose consumption. We showed that the yeast growth under aerobic conditions leads to respiratory metabolism. Analysis under oxygen-limited conditions showed fermentation metabolism, but with imbalance of cofactor regeneration, resulting in xylitol accumulation. These results indicate that fine control of oxygen levels during fermentation is necessary to optimize ethanol production with *S. arborariae*.

The protocol presented here may be further applied to other yeast species, and data generated may be used to identify limiting steps in xylose metabolism, and consequently, support yeast genetic engineering to improve second-generation ethanol production.

Acknowledgments

Compliance with Ethical Standards

Conflict of Interest   Author Christiane Gonçalves Campos declares that she has no conflict of interest.

Author José Antônio de Aquino Ribeiro declares that he has no conflict of interest.

Author Patrícia Pinto Kalil Gonçalves Costa declares that she has no conflict of interest.

Author Katiúscia Pereira Araújo declares that he has no conflict of interest.

Author Henrique César Teixeira Veras declares that he has no conflict of interest.

Author João Ricardo Moreira de Almeida declares that he has no conflict of interest.

Author Clenilson Martins Rodrigues declares that he has no conflict of interest.

Author Patrícia Verardi Abdelnur declares that she has no conflict of interest.

Ethical Approval This article does not contain any studies with human subject or animal participation.

References

1. Alvira, P., Tomás-Pejó, E., Ballesteros, M., Negro, M.J.: Pretreatment technologies for an efficient bioethanol production process based on enzymatic hydrolysis: a review. Bioresor Technol. **101**, 4851–4861 (2010)

2. Dias, M.O.S., Junqueira, T.L., Jesus, C.D.F., Rossell, C.E.V., Maciel Filho, R., Bonomi, A.: Improving second generation ethanol production through optimization of first generation production process from sugarcane. Energy. **43**, 246–252 (2012)

3. Ferreira-Leitão, V., Perrone, C.C., Rodrigues, J., Franke, A.P.M., Macrelli, S., Zacchi, G.: An approach to the utilisation of CO2 as impregnating agent in steam pretreatment of sugar cane bagasse and leaves for ethanol production. Biotechnol. Biofuels. **3**, 7 (2010)

4. Basso, L.C., De Amorim, H.V., De Oliveira, A.J., Lopes, M.L.: Yeast selection for fuel ethanol production in Brazil. FEMS Yeast Res. **8**, 1155–1163 (2008)

5. Hahn-hägerdal, B., Galbe, M., Gorwa-Grauslund, M.F., Lidén, G., Zacchi, G.: Bio-ethanol—the fuel of tomorrow from the residues of today. Trends Biotechnol. **24**, 549–556 (2006)

6. Matsushika, A., Goshima, T., Hoshino, T.: Transcription analysis of recombinant industrial and laboratory *Saccharomyces cerevisiae* strains reveals the molecular basis for fermentation of glucose and xylose. Microb. Cell Fact. **13**, 1–18 (2014)

7. Moysés, D., Reis, V., Almeida, J., Moraes, L., Torres, F.: Xylose fermentation by *Saccharomyces cerevisiae*: challenges and prospects. Int. J. Mol. Sci. **17**, 207 (2016)

8. Cadete, R.M., de Las Heras, A.M., Sandström, A.G., Ferreira, C., Gírio, F., Gorwa-Grauslund, M.-F., Rosa, C.A., Fonseca, C.: Exploring xylose metabolism in *Spathaspora* species: XYL1.2 from *Spathaspora passalidarum* as the key for efficient anaerobic xylose fermentation in metabolic engineered S*accharomyces cerevisiae*. Biotechnol. Biofuels. **9**, 167 (2016)

9. Karhumaa, K.: Investigation of limiting metabolic steps in the utilization of xylose by recombinant *Saccharomyces cerevisiae* using metabolic engineering. Yeast. **22**, 359–368 (2005)

10. Kuiper, I., Lagendijk, E.L., Bloemberg, G.V., Lugtenberg, B.J.J.: Rhizoremediation: a beneficial plant–microbe interaction. Mol. Plant–Microbe Interact. **17**, 6–15 (2004)

11. Parachin, S., Bergdahl, B., Niel, E.W.J., Van Gorwa Grauslund, M.F.: Kinetic modeling reveals current limitations in the production of ethanol from xylose by recombinant *Saccharomyces cerevisiae*. Metab. Eng. **13**, 508–517 (2011)

12. Runquist, D., Hahn-hägerdal, B., Rådström, P.: Comparison of heterologous xylose transporters in recombinant *Saccharomyces cerevisiae*. Biotechnol. Biofuels. **3**, 1–7 (2010)

13. Paes, B.G., Almeida, J.: Genetic improvement of microorganisms for applications in biorefineries. Chem. Biol. Technol. Agric. **1**, 21 (2014)

14. Cordova, L.T., Antoniewicz, M.R.: 13C metabolic flux analysis of the extremely thermophilic, fast growing, xylose-utilizing *Geobacillus* strain LC300. Metab. Eng. **33**, 148–157 (2016)

15. Ricci-silva M, Vaz B, Vasconcelos G, Romão W, Aricetti J, Caldana C, Abdelnur P.: Mass Spectrometry for Metabolomics and Biomass Composition Analyses. In: Vaz, S. (ed.) Anal. Tech. Methods Biomass, pp. 115–141. Springer International Publishing, Cham (2016)

16. Koek, M.M., Jellema, R.H., van der Greef, J., Tas, A.C., Hankemeier, T.: Quantitative metabolomics based on gas chromatography mass spectrometry: status and perspectives. Metabolomics. **7**, 307–328 (2011)

17. Buchholz, A., Hurlebaus, J., Wandrey, C., Takors, R.: Metabolomics: quantification of intracellular metabolite dynamics. Biomol. Eng. **19**, 5–15 (2002)

18. Klavins, K., Neubauer, S., Al Chalabi, A., Sonntag, D., Haberhauer-Troyer, C., Russmayer, H., Sauer, M., Mattanovich, D., Hann, S., Koellensperger, G.: Interlaboratory comparison for quantitative primary metabolite profiling in *Pichia pastoris* metabolomics and metabolite profiling. Anal. Bioanal. Chem. **405**, 5159–5169 (2013)

19. Vargas, L.H.G., Neto, J.C.R., de Aquino Ribeiro, J.A., Ricci-Silva, M.E., Souza, M.T., Rodrigues, C.M., de Oliveira, A.E., Abdelnur, P.V.: Metabolomics analysis of oil palm (*Elaeis guineensis*) leaf: evaluation of sample preparation steps using UHPLC-MS/MS. Metabolomics. (2016). https://doi.org/10.1007/s11306-016-1100-z

20. Abdelnur, P.V., Caldana, C., Martins, M.C.M.: Metabolomics applied in bioenergy. **1**, 1–9 (2014)

21. Bu, M., Czernik, D., Ewald, J.C., Sauer, U., Zamboni, N.: Cross-platform comparison of methods for quantitative metabolomics of primary metabolism cross-platform comparison of methods for quantitative metabolomics of primary metabolism. Metab. Clin. Exp. **81**, 2135–2143 (2009)

22. Dunn, W.B., Bailey, N.J.C., Johnson, H.E.: Measuring the metabolome: current analytical technologies. Analyst. **130**, 606–625 (2005)

23. Pyke, J.S., Callahan, D.L., Kanojia, K., Bowne, J., Sahani, S., Tull, D., Bacic, A., McConville, M.J., Roessner, U.: A tandem liquid chromatography–mass spectrometry (LC-MS) method for profiling small molecules in complex samples. Metabolomics. **11**, 1552–1562 (2015)

24. Wamelink, M.M.C., Struys, E.A., Huck, J.H.J., Roos, B., Knaap, M.S., Van der Jakobs, C., Verhoeven, N.M.: Quantification of sugar phosphate intermediates of the pentose phosphate pathway by LC-MS/MS : application to two new inherited defects of metabolism. **823**, 18–25 (2005)

25. Guillarme, D., Schappler, J., Rudaz, S., Veuthey, J.: Coupling ultra-high-pressure liquid chromatography with mass spectrometry. Trends Anal. Chem. **29**, 15–27 (2010)

26. Buescher, J.M., Moco, S., Sauer, U., Zamboni, N.: Ultrahigh performance liquid chromatography-tandem mass spectrometry method for fast and robust quantification of anionic and aromatic metabolites. Anal. Chem. **82**, 4403–4412 (2010)

27. Luo, B., Groenke, K., Takors, R., Wandrey, C., Oldiges, M.: Simultaneous determination of multiple intracellular metabolites in glycolysis, pentose phosphate pathway, and tricarboxylic acid cycle by liquid chromatography – mass spectrometry. J. Chromatogr. A. **1147**, 153–164 (2007)

28. Seifar, R.M., Ras, C., Deshmukh, A.T., Bekers, K.M., Suarez-Mendez, C.A., da Cruz, A.L.B., van Gulik, W.M., Heijnen, J.J.: Quantitative analysis of intracellular coenzymes in *Saccharomyces cerevisiae* using ion pair reversed phase ultra high performance liquid chromatography tandem mass spectrometry. J. Chromatogr. A. **1311**, 115–120 (2013)

29. Nováková, L., Havlíková, L., Vlcková, H.: Hydrophilic interaction chromatography of polar and ionizable compounds by UHPLC. TrAC Trends Anal. Chem. **63**, 55–64 (2014)

30. Ghfar, A.A., Wabaidur, S.M., Badjah, A.Y., Ahmed, H., Alothman, Z.A., Khan, M.R., Al-Shaalan, N.H.: Simultaneous determination of monosaccharides and oligosaccharides in dates using liquid chromatography-electrospray ionization mass spectrometry. Food Chem. **176**, 487–492 (2015)

31. Petersson, A., Almeida, J.R.M., Modig, T., Karhumaa, K., Hahn-Hägerdal, B., Gorwa-Grauslund, M.F., Lidén, G.: A 5-hydroxymethyl furfural reducing enzyme encoded by the *Saccharomyces cerevisiae* ADH6 gene conveys HMF tolerance. Yeast. **23**, 455–464 (2006)

32. de Koning, W., van Dam, K.: A method for the determination of changes of glycolytic metabolites in yeast on a subsecond time scale using extraction at neutral pH. Anal. Biochem. **204**, 118–123 (1992)

33. Gonzalez, B., François, J., Renaud, M.: A rapid and reliable method for metabolite extraction in yeast using boiling buffered ethanol. Yeast. **13**, 1347–1356 (1997)

34. Shabir, G.: Validation of high-performance liquid chromatography methods for pharmaceutical analysis. Understanding the differences and

similarities between validation requirements of the US Food and Drug Administration, the US Pharmacopeia, and the International Conferemce. J. Chromatogr. A. **987**, 57–66 (2003)

35. Tang, D.Q., Zou, L., Yin, X.X., Ong, C.N.: HILIC-MS for metabolomics: an attractive and complementary approach to RPLC-MS. Mass Spectrom. Rev. **35**, 574–600 (2014)

36. Li, Y., Ptolemy, A.S., Harmonay, L., Kellogg, M., Berry, G.T.: Ultra fast and sensitive liquid chromatography tandem mass spectrometry based assay for galactose-1-phosphate uridylyltransferase and galactokinase deficiencies. Mol. Genet. Metab. **102**, 33–40 (2011)

37. Lu, W., Clasquin, M.F., Melamud, E., Amador-Noguez, D., Caudy, A.A., Rabinowitz, J.D.: Metabolomic analysis via reversed-phase ion-pairing liquid chromatography coupled to a stand alone Orbitrap mass spectrometer. **82**, 3212–3221 (2010)

38. Cadete, R.M., Santos, R.O., Melo, M.A., Mouro, A., Gonçalves, D.L., Stambuk, B.U., Gomes, F.C.O., Lachance, M.A., Rosa, C.A.: *Spathaspora arborariae* sp. nov., a d-xylose-fermenting yeast species isolated from rotting wood in Brazil. FEMS Yeast Res. **9**, 1338–1342 (2009)

39. Bergdahl, B., Heer, D., Sauer, U., Hahn-Hägerdal, B., van Niel, E.W.: Dynamic metabolomics differentiates between carbon and energy starvation in recombinant *Saccharomyces cerevisiae* fermenting xylose. Biotechnol. Biofuels. **5**, 34 (2012)

40. Baumann, K., Carnicer, M., Dragosits, M., Graf, A.B., Stadlmann, J., Jouhten, P., Maaheimo, H., Gasser, B., Albiol, J., Mattanovich, D., Ferrer, P.: A multi-level study of recombinant *Pichia pastoris* in different oxygen conditions. BMC Syst. Biol. **4**, 141 (2010)

Table S1. The mobiles phase tested for separate metabolites from xylose catabolism pathway including phosphate sugars, organic acids, sugars (monosaccharide) and alcohols by Ultra-high performance liquid chromatography (UHPLC) use hydrophilic interaction chromatography (HILIC). Stationary phase used was BEH amide column (Waters).

#	*Mobile phase*	*Elution mode*
1	A: ACN/H$_2$O (90/10) + NH$_4$COOH 5 mM + NH$_4$OH 0.1% B: ACN/H$_2$O (10/90) + NH$_4$COOH 5 mM + NH$_4$OH 0.1%	Isocratic
2	A: CH$_3$COONH$_4$ 10 mM + ACN (50/50) B: CH$_3$COONH$_4$ 10 mM + ACN (90/10)	Gradient
3	A: H$_2$O + NH$_4$OH 0.1% B: ACN + NH$_4$OH 0.1%	Gradient
4	A: ACN/H$_2$O (90/10) + NH$_4$COOH 5 mM + NH$_4$OH 0.1% B: ACN/H$_2$O (10/90) + NH$_4$COOH 5 mM + NH$_4$OH 0.1%	Isocratic
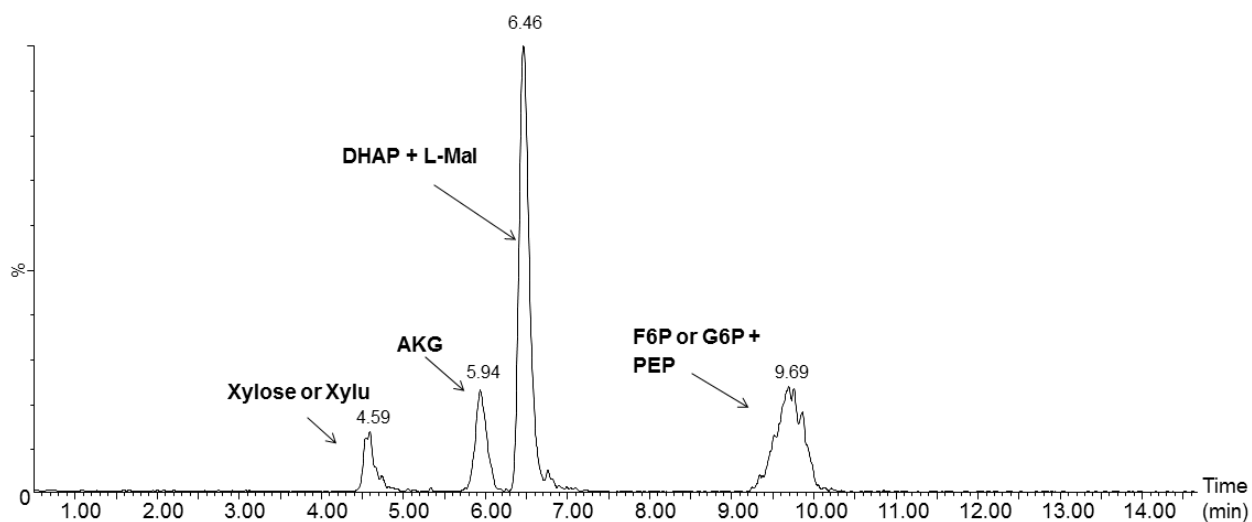
Figure S1. Total ion chromatogram (TIC) of fourteen standards of metabolites mixture: pyruvic acid (PYR), phospho(enol)pyruvate (PEP), malic acid (L-MAL), alpha ketoglutaric acid (AKG), glyceraldehyde-3-phosphate (Velagapudi et al., 2007), di-hydroxyacetone phosphate (DHAP), glucose-6-phosphate (G6P), fructose-6-phosphate (F6P), ribose-5-phosphate (R5P), xylose, xylitol, glucose, glycerol and xilulose (xylu). Mobile phase (A: ACN/H$_2$O (90/10) + NH$_4$COOH 5 mM + NH$_4$OH 0.1% B: ACN/H$_2$O (10/90) + NH$_4$COOH 5 mM + NH$_4$OH 0.1%), using an isocratic mode and BEH amide column (Waters).

Table S2. The gradient tested for separate 14 metabolites from xylose catabolism pathway using mobile phase A: CH_3COONH_4 10 mM + ACN (50/50) and B: CH_3COONH_4 10 mM + ACN (90/10) by Ultra-high performance liquid chromatography (UHPLC) using hydrophilic interaction chromatography (HILIC) and BEH amide column (Waters).

Time (min)	Flow (mL/min)	Eluent A (vol. %)	Eluent B (vol. %)
0.0	0.4	0	100
5.0	0.4	100	0
6.0	0.4	100	0
10.0	0.4	0	100
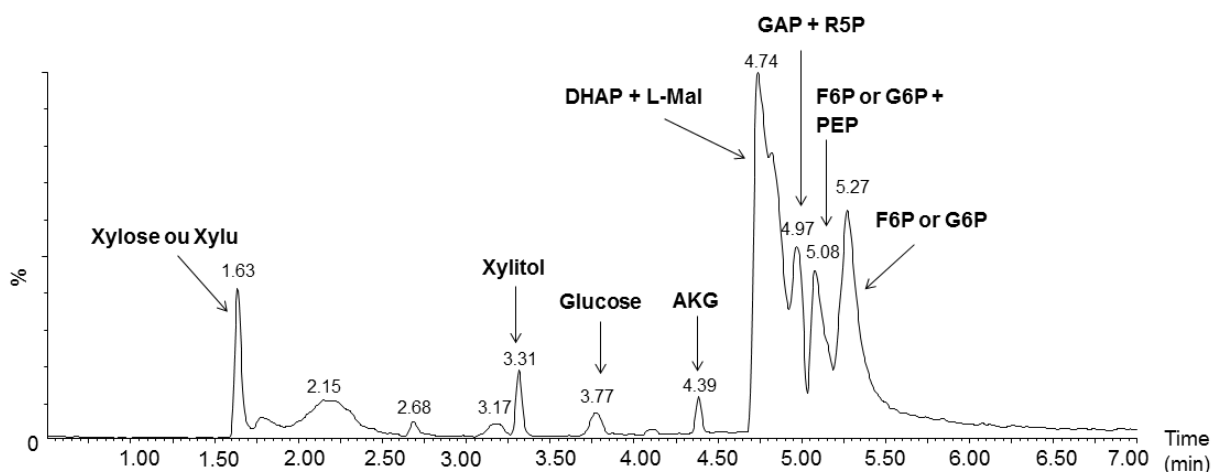
Figure S2. Total ion chromatogram (TIC) of fourteen standards of metabolites mixture: Pyruvic acid (PYR), phospho(enol)pyruvate (PEP), Malic acid (L-MAL), alpha ketoglutaric acid (AKG), glyceraldehyde-3-phosphate (Velagapudi et al., 2007), di-hydroxyacetone phosphate (DHAP), glucose-6-phosphate (G6P), fructose-6-phosphate (F6P), ribulose-5-phosphate (RU5P), xylose, xylitol, glucose, glycerol and xilulose (xylu). Mobile phase (A: CH_3COONH_4 10 mM + ACN (50/50) and B: CH_3COONH_4 10 mM + ACN (90/10)) using a gradient mode and BEH amide column.

Table S3. The gradient tested for separate 14 metabolites from xylose catabolism pathway using mobile phase: A: H_2O + NH_4OH 0.1% and B: ACN + NH_4OH 0.1% by Ultra-high performance liquid chromatography (UHPLC) using to hydrophilic interaction chromatography (HILIC) and BEH amide column (Waters).

Time (min)	Flow (mL/min)	Eluent A (vol. %)	Eluent B (vol. %)
0.0	0.2	24	76
4.5	0.2	50	50
6.0	0.2	50	50
12.5	0.4	24	76
13.0	0.2	24	76
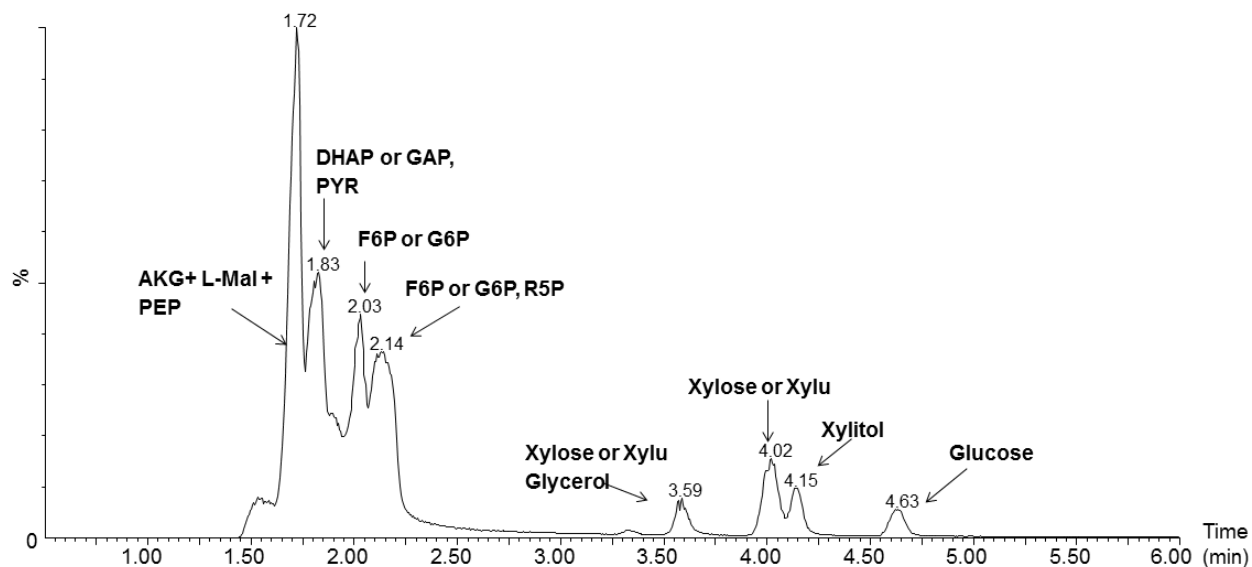
Figure S3. Total ion chromatogram (TIC) of fourteen standards of metabolites mixture: pyruvic acid (PYR), phospho(enol)pyruvate (PEP), malic acid (L-MAL), alpha ketoglutaric acid (AKG), glyceraldehyde-3-phosphate (Velagapudi et al., 2007), di-hydroxyacetone phosphate (DHAP), glucose-6-phosphate (G6P), fructose-6-phosphate (F6P), ribose-5-phosphate (R5P), xylose, xylitol, glucose, glycerol and xilulose (xylu). Mobile phase (A: H_2O + NH_4OH 0.1% and B: ACN + NH_4OH 0.1%), using a gradient mode and BEH amide column.

Table S4. The mobiles phase tested for separation metabolites from xylose catabolism pathway including phosphate sugars and organic acids by Ultra-high performance liquid chromatography (UHPLC) using ion pair chromatography (IPC). Stationary phase used was HSS-T3 column (Waters).

#	Mobile Phase	Elution mode	pH	Temperature (°C)
1	A: TEA 5 mM + FA 10 mM B: MeOH	Isocratic	-	rt
2	A: TEA 10 mM + FA 20 mM B: MeOH	Isocratic	-	rt
3	A: TBA 2 mM + CH3COONH$_4$ 5 mM + 5% MeOH B: MeOH	Gradient	6.2	45
4	A: TBA 2 mM + FA 0.1% + 5% MeOH B: MeOH	Gradient	2.8	45
5	A: TBA 2 mM + Acetic Acid 3 mM + 5% MeOH B: MeOH	Gradient	5.1	45
6	A: TBA 2 mM + Acetic Acid 4 mM + 5% MeOH B: MeOH	Gradient	4.8	45
7	A: TBA 5 mM + Acetic Acid 10 mM + 5% MeOH B: MeOH	Gradient	4.8	45
8	A: TBA 10 mM + Acetic Acid 15 mM B: MeOH	Gradient	5.0	35 / 50

Abbreviations: TEA: triethylamine; TBA: tributylamine; FA: formic acid; rt: room temperature.
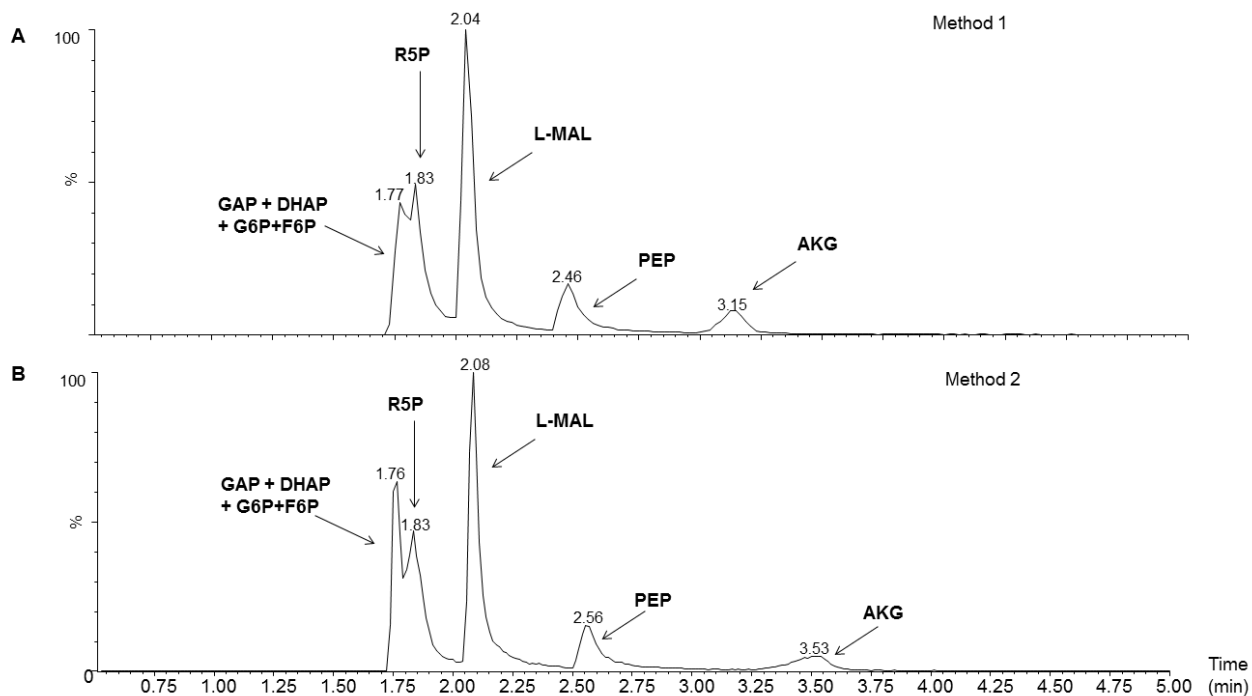
Figure S4. Total ion chromatogram (TIC) of eight standards of metabolites mixture include sugars phosphates and organic acids: malic acid (L-MAL), alpha ketoglutaric acid (AKG), glyceraldehyde-3-phosphate (Velagapudi et al., 2007), di-hydroxyacetone phosphate (DHAP), glucose-6-phosphate (G6P), fructose-6-phosphate (F6P), phospho(enol)pyruvate (PEP) and ribose-5-phosphate (R5P). A) Method 1, isocratic elution mode using mobile phase A: 5 mM triethylamine, 10 mM formic acid and B: methanol, B) Method 2, isocratic elution mode mobile phase A: 10 mM triethylamine, 20 mM formic acid, uses an isocratic mode. The stationary phase was a HSS-T3 column (Waters).
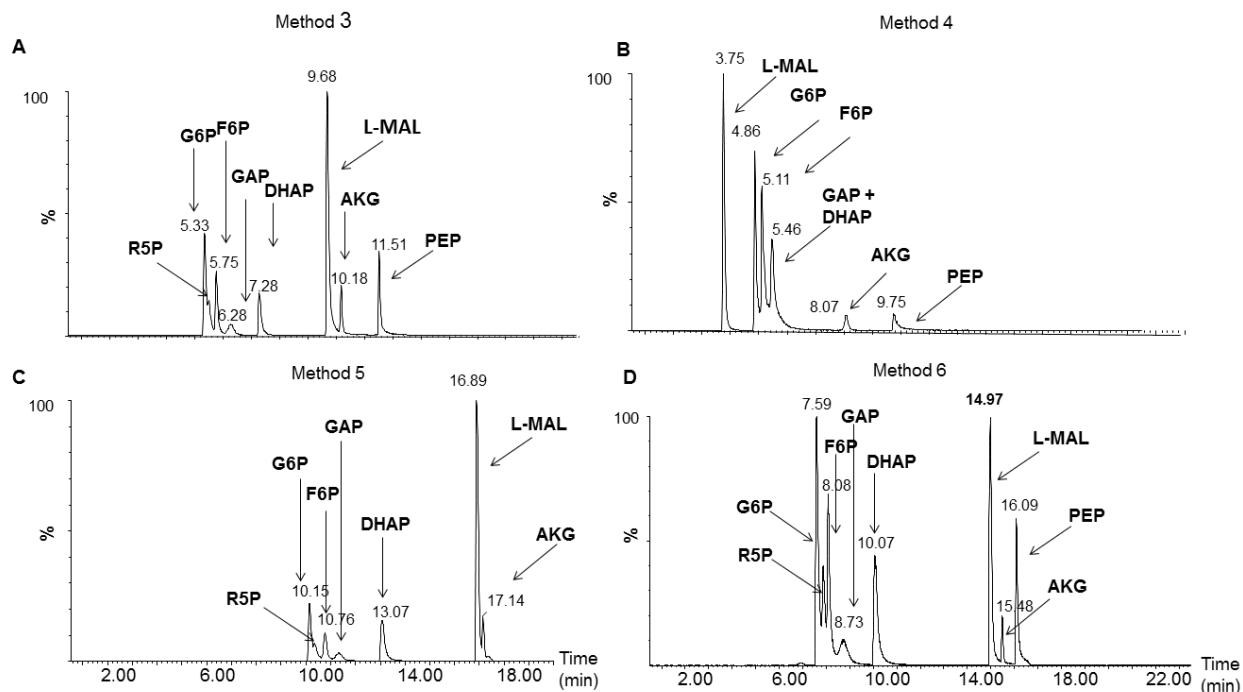
Figure S5. Total ion chromatogram (TIC) of eight standards of metabolites mixture include sugars phosphates and organic acids: malic acid (L-MAL), alpha ketoglutaric acid (AKG), glyceraldehyde-3-phosphate (Velagapudi et al., 2007), di-hydroxyacetone phosphate (DHAP), glucose-6-phosphate (G6P), fructose-6-phosphate (F6P), phospho(enol)pyruvate (PEP) and ribose-5-phosphate (R5P). A) Method 3, gradient elution mode using mobile phase A: TBA 2 mM + CH3COONH4 5 mM + 5% MeOH and B: MeOH, pH 6.2; B) Method 4, gradient elution mode using mobile phase A: TBA 2 mM + FA 0.1% + 5% MeOH and B: MeOH, pH 2.8; C) Method 5, gradient elution mode using mobile phase A: TBA 2 mM + acetic acid 3 mM + 5% MeOH and B: MeOH, pH 5.1; and D) Method 6, gradient elution mode using mobile phase A: TBA 2 mM + acetic acid 4 mM + 5% MeOH and B: MeOH, pH 6.2. The stationary phase was a HSS-T3 column (Waters).

6
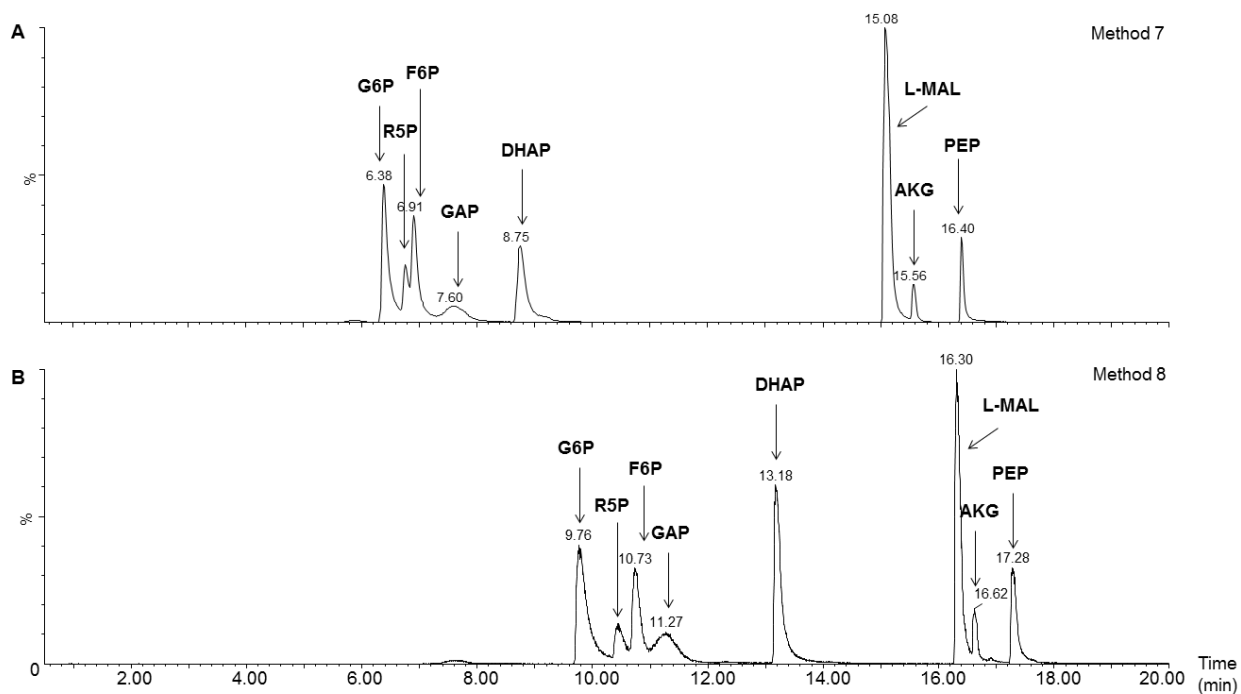
Figure S6. Total ion chromatogram (TIC) of eight standards of metabolites mixture include sugars phosphates and organic acids: malic acid (L-MAL), alpha ketoglutaric acid (AKG), glyceraldehyde-3-phosphate (Velagapudi et al., 2007), di-hydroxyacetone phosphate (DHAP), glucose-6-phosphate (G6P), fructose-6-phosphate (F6P), phospho(enol)pyruvate (PEP) and ribose-5-phosphate (R5P). A) Method 7, gradient elution mode using mobile phase A: TBA 5 mM + acetic cid 10 mM + 5% MeOH and B: MeOH, pH4.8; and B) Method 8, gradient elution mode using mobile phase A: TBA 10 mM + acetic acid 15 mM and B: MeOH, pH 5.0. The stationary phase was a HSS-T3 column (Waters).
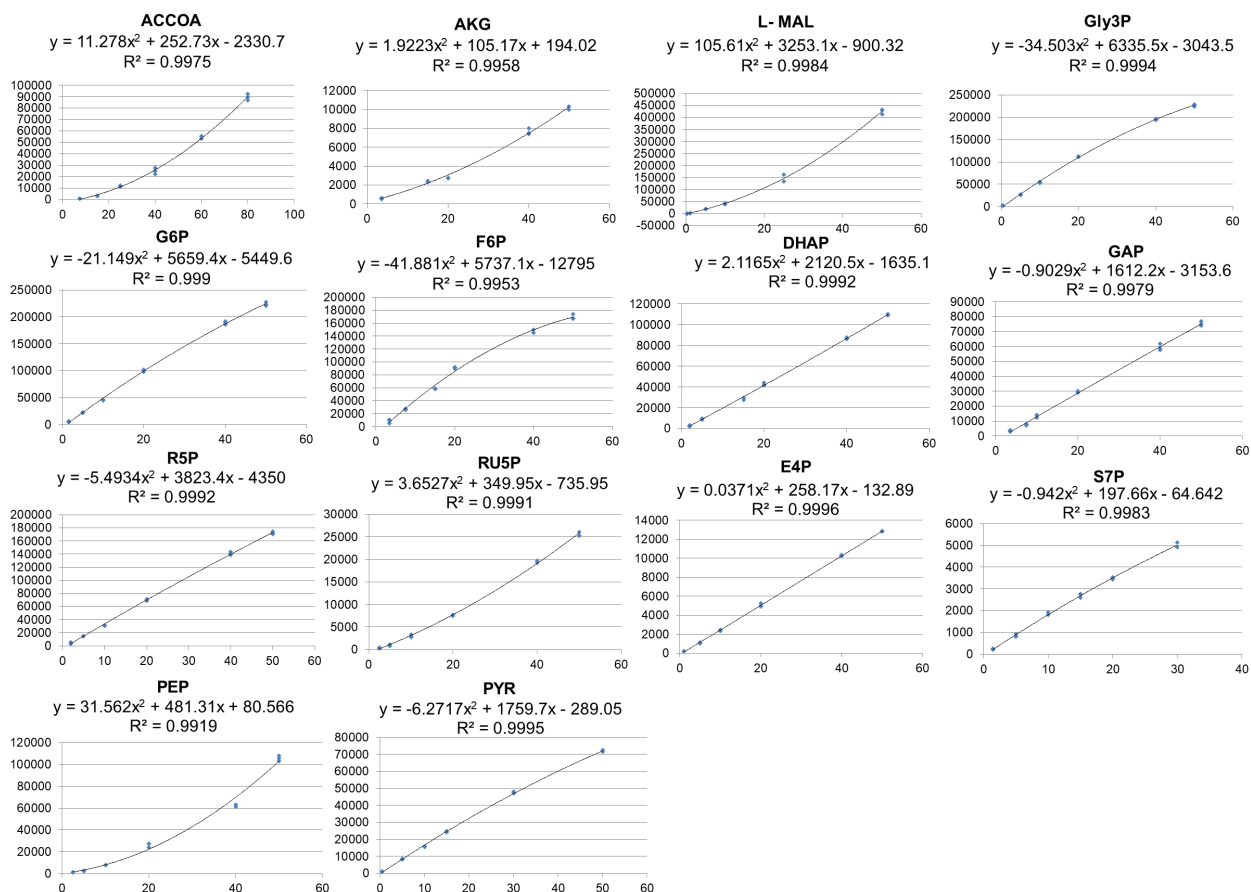
Figure S7. Calibration curves adjustment by quadratic model of fourteen standards of metabolites mixture analyzing by IPC method: acetyl coenzyme A (ACCOA), alpha ketoglutaric acid (AKG), D-malic acid (L-MAL), glycerol-3-phosphate (GLY3P), glucose-6-phosphate (G6P), fructose-6-phosphate (F6P), dihydroxy acetone phosphate (DHAP), glyceraldehyde-3-phosphate (Velagapudi et al., 2007), ribose-5-phosphate (R5P), ribulose-5-phosphate (RU5P), erytrose-4-phosphate (E4P), sedoheptulose-7-phosphate (S7P), phospho(enol)pyruvate (PEP) and pyruvic acid (PYR).

Xylu
$y = -3.1632x^2 + 1020.6x - 756.79$
$R^2 = 0.9971$

Xylose
$y = -2.9621x^2 + 1612.8x - 1884.2$
$R^2 = 0.999$

Glucose
$y = -8.013x^2 + 2782.9x + 2351.9$
$R^2 = 0.9991$

Glycerol
$y = -1.6972x^2 + 483.55x + 191.92$
$R^2 = 0.9993$

Xylitol
$y = 1.7372x^2 + 1535.4x - 1678.2$
$R^2 = 0.9988$
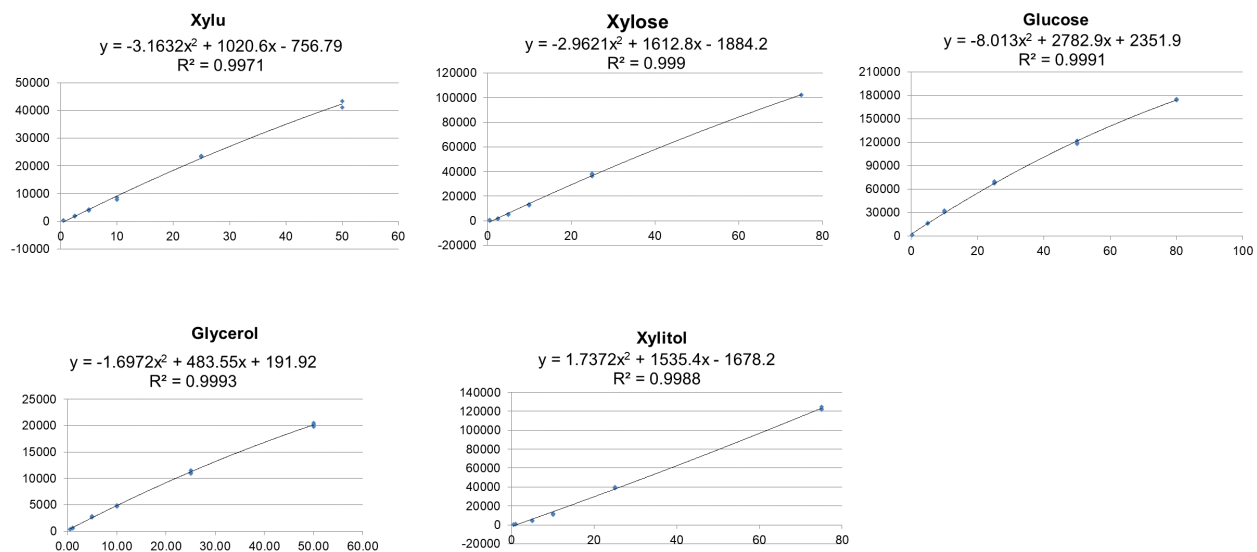
Figure S8. Calibration curves adjustment by quadratic model of five standards of metabolites mixture analyzing by HILIC method: Xylulose (Xylu), Xylose, Glucose, Glycerol and Xylitol.

Research Article

Title:

Utilization of metabolic flux analysis for metabolome data validation of xylose-fermenting yeasts

Henrique C. T. Veras [1, 2]

Christiane C. Gonçalves [1, 3]

Igor F. Nascimento [5]

Patrícia V. Abdelnur [1, 3]

João Ricardo M. Almeida [1, 4]

Nádia S. Parachin [2, 4 , *]

[1] Empresa Brasileira de Pesquisa Agropecuária - EMBRAPA Agroenergia, Brasília-DF, Brasil

[2] Grupo de Engenharia Metabólica Aplicada a Bioprocessos, Universidade de Brasília - UnB Campus Darcy Ribeiro, Instituto de Ciências Biológicas, Bloco K, 1º andar, CEP 70.790-900 Asa Norte - Brasília-DF, Brasil

[3] Instituto de Química, Universidade Federal de Goiás - UFG, Goiânia, Brasil

[4] Programa de Pos-Graduação em Tecnologias Químicas e Biológicas, Instituto de Química Universidade de Brasília - UnB, Brasil

[5] Programa de Pós-Graduação em Administração, Universidade de Brasília – UnB, Brasil

* Correspondence: Nádia Skorupa Parachin

 E-mail: nadiasp@unb.br, nadiasp@gmail.com

Abstract

Metabolic flux analysis (MFA) is used to understand how fluxes are distributed in a metabolic network given a certain substrate. It can predict growth and product distribution based on the stoichiometric reactions within the network adding measured fluxes and production rates as constrains in the mathematical model. In this study, a stoichiometric model was developed using xylose fermentation data for the yeasts *Scheffersomyces stipitis*, *Spathaspora arborariae* and *Spathaspora passalidarum.* Those models were utilized for the first time to validate the quantification of eleven intracellular metabolites within xylose and glucose catabolic pathways. Within the investigated metabolic network, eleven fluxes rates were calculated using the metabolomics data. Among them, nine were validated with a correlation above 90% when compared to the stoichiometric model. Thus confirming that potential of MFA for metabolome data validation. Between intracellular metabolites, fructose-6-phosphate, glucose-6-phosphate, malate and ribulose-5-phosphate were validated in three yeasts. The measured fluxes model with phosphoenolpyruvate and pyruvate could not be correlated with calculated flux. Moreover it was possible to compare metabolism within the three different xylose fermenting yeasts showing that xylose metabolism occurs in higher fluxes rate in *S. stipitis* than *S. passalidarum* and *S. arborariae.* The fluxes rate is divided similarly between pentose phosphate pathway and glycolysis. *S. arborariae* presents 3.0 times higher demand for NADPH regeneration than observed in *S. passalidarum.* The flux rate to glycerol formation in *S. passalidarum* is inactive and this yeast looks like occur a better NADH/NAD$^+$ balance, which permit efficient xylose fermentation.

Keywords: Xylose fermentation, Metabolic flux, Metabolome; Oxygen-limited, Ethanol.

1 Introduction

Metabolic flux analysis (MFA) is one important approach for understanding microbial physiology under a defined metabolic network.[1, 2] It gives insights on how metabolism is balanced, that is, how organisms use substrates for biomass formation and production of other metabolic compounds.[1, 3] Thus MFA allows prediction of novel cellular phenotypes revealing novel targets for genetic engineering.[2, 4, 5]

MFA is based on a stoichiometric model of a defined metabolic network.[6] Those are frequently based on genome annotation and presence of genes coding to enzymes into metabolic pathways.[6] For each metabolic network a set of reactions are defined and converted into a mathematical model.[7] MFA is support by bioinformatics tools that realize the carbon flux distribution calculation, among them, there is the OptFlux, an open-source tool to support *in silico* metabolic engineering.[8]

In a constraints-based flux analysis model the stoichiometric network establishes flux balance constraints for products and consumptions rate. This ensures that the total amount of compounds produced must be equal to the total amount being consumed.[3, 9] To determine the metabolic network model depends of use a certain number of extracellular fluxes measurements. So the metabolic network has to be limited and does not cover all reactions that are noted in the genome. In its turn, is easily obtained extracellular fluxes measurements for substrate consumption, biomass formation and products as such as ethanol, xylitol, and glycerol as well organic acids into a fermentative process.[10, 11]

Intracellular metabolite concentration, on the other hand, have been used far less.[4] Metabolome is a set of metabolites within a biological system and the metabolomics is the analysis that seeks to estimate the quantitative profile of such set of metabolites.[12]

However the analysis of intracellular metabolites is still a challenging task in metabolomics.[13] Mostly due to extracellular/intracellular medium ratio, with high concentration of extracellular that can to cause interference on analysis of low concentration intracellular compounds.[13] Furthermore, the intracellular reactions has a high turnover rates, making sample preparation a critical step for metabolomics.[13]

Therefore, optimize metabolomics analysis is a powerful technique that can provide a detailed quantification of central carbon metabolism (pentose assimilation pathway, pentose phosphate pathway (PPP), glycolysis, and tricarboxylic acid (TCA) cycle) and can greatly aid the construction of specific metabolic and regulatory networks of pathways in microorganisms as yeasts.[14, 15]

In order to improve the stoichiometric models, the intracellular metabolites should also be included to understand the full impact on the physiology of different yeasts.[16] These data can be used separately or combined to identify with increasing precision the true state of the cell metabolism.[7] The main advantage in using intracellular metabolites concentrations is that this measurements are directly linked to the metabolic reactions network and reflected the phenotype of organism.[17]

However, in order to generate accurate intracellular metabolic data, sample preparation, extraction, detection and quantification are crucial steps that need to be carefully analysed to result in statistical representative data of a given microorganism and a specific cultivation condition. For example, biological replicates must be combined to technical replicates into a single value. Once this is done it is necessary to validate that the quantified metabolite corresponds to what is happening *in vivo.* Therefore the combination of MFA analysis and metabolomics

results may be a valuable strategy to assess biological experimental data on microorganism physiology, especially for those not well studied.[12]

Xylose metabolism in yeast has been extensively studied due to the interest in the economic conversion of lignocellulosic biomass to fuels and chemicals.[18-21] However, very little is known about how native xylose-fermenting yeasts mediate the simultaneous metabolic demand for cell growth and ethanol production using this carbon source.[20] For that reason, in this study, three naturally xylose-fermenting yeasts *Scheffersomyces stipitis*, *Spathaspora passalidarum* and *Spathaspora arborariae* were chosen as models for studying metabolic flux distribution within xylose catabolism.

The stoichiometric model included the central carbon metabolism pathways that resulted in 27 genes, 35 metabolites and 39 reactions. Between them, 9 reactions correspondent to fluxes rate for xylose consumption, biomass formation and products measurements into extracellular environment. These data were obtained in a previous work and used as constrains in stoichiometric model.[22]

Due to the availability of genetic and physiological data, the model was initially constructed for *S. stipitis* and then employed for *S. passalidarum* and *S. arborariae*. Moreover eleven intracellular metabolites were quantified during the exponential growth phase of the three yeasts in order to increase the degree of freedom for the MFA analysis. From eleven quantified metabolites, eight has 90% correlation with stoichiometric analysis in all tested yeast. The intracellular metabolites phosphoenolpyruvate and pyruvate could not be validated in none of the tested yeast indicating a limitation in the metabolomics analysis.

To the best of our knowledge, this is the first MFA model that describes carbon distributions for two *Spathaspora* yeasts. The comparison of the three yeasts species allowed identification of key metabolic bottlenecks on xylose metabolism. *S. stipitis* showed 1.5 times higher xylose assimilation rate than were observed in *S. arborariae* and *S. passalidarum*. This feature can be associated with the 3.0 and 1.5 times higher ethanol productions in *S. stipitis* than see in *S. arborariae* and *S. passalidarum* respectively.

In *S. passalidarum* is shown at least 2.0 times less need of NADPH regeneration on oxidative-PPP than *S. stipitis* and *S. arborariae*. This combined with high flux rate in the reaction with XR NADH-dependent, reflects a better cofactor balance and non-accumulation of byproducts as xylitol. Similar rates of carbon fluxes are directed to PPP e glycolysis in three yeasts. Besides then, the inactive reaction for glycerol formation in *S. passalidarum* may also be related with good rate of ethanol production similar to *S. stipitis.*

2 Materials and methods

2.1 Yeasts and culture conditions

The yeasts *Scheffersomyces stipitis* NRRL Y-7124, *Spathaspora arborariae* NRRL Y-48658 and *Spathaspora passalidarum* NRRL Y-27907 were utilized in this study. Those were preserved in 30% glycerol at – 80°C. Cultivations in the bioreactors using xylose as carbon source were performed as described previously.[22] Briefly, the fermentations were carried out in bioreactors (Multifors 2, Infors HT) with defined mineral medium[23] (500 mL), supplemented with 40 g L^{-1} xylose as carbon source. The fermentation started with optical density 600 nm (OD_{600}) equal 0.5. Temperature was set to 28°C, stirrer at 400 rpm, pH maintained at 5.5 by addition 3M KOH. The oxygen-limited condition was maintained with 0.05 L/min airflow injects. Oxygen dissolved in the medium was maintained below 10%. All fermentations were carried out in biological triplicates. Samples for determining xylose

consumption and product formation were withdrawn at regular intervals of time at approximately 8 h of cultivation. For the stoichiometric model construction and metabolite quantification, the samples in the middle exponential phase were utilized since a pseudo-steady state is assumed and therefore all rates can be considered as constant.

2.2 Extracellular metabolites and biomass quantification

Xylose, ethanol, xylitol, glycerol, acetate, pyruvate and succinate were measured by HPLC (Acquity UPLC H Class, Waters) equipped with a HPX-87 H column (Bio-Rad Laboratories) at 45°C and a refractive index detector as previously described.[22] The mobile phase run 0.6 ml/min of 5 mM sulfuric acid (H_2SO_4) for 25 min. The measured products rate in mmol were calculated through transformation the concentration in gram per liter divided by molecular weight of respective compounds. Then, products values are divided by biomass and time. The data show average ± standard deviation in mmol/gCDW. h^{-1}. The carbon and degree of reduction (DR) balances closed to 100% as showed previously.[22] Biomass was measured through OD_{600} using a spectrophotometer (SpectraMax M3, Molecular Devices). For each collected point cell dry weight (CDW) was performed through 5 mL of pre-inoculum and stationary growth phase of all fermentations. Samples were withdrawn and centrifuged (12,000xg, 5 min). Before weighing, the cells were placed in glass tube and incubated to dry at 60°C 48 h. Therefore a correlation between OD_{600} values and CDW could be established.

2.3 Chemicals

The chemicals standards as such as acetate (ACE), acetyl coenzyme A (ACCOA), alpha ketoglutaric acid (AKG), dihydroxy acetone phosphate (DHAP), erythrose-4-phosphate (E4P), ethanol (ETOH), fructose-6-phosphate (F6P), glucose (GLU), glucose-6-phosphate (G6P), glyceraldehyde-3-phosphate (GAP), glycerol (GOL),

glycerol-3-phosphate (GLY3P), malate (MAL), phosphoenolpyruvate (PEP), pyruvate (PYR), ribose-5-phosphate (R5P), ribulose-5-phosphate (RU5P), sedoheptulose-7-phosphate (S7P), succinate (SUC), xylitol (XOL), xylose (XYL), xylulose (XYLU) and all solvents as sulphuric acid, tributylamine, acetonitrile and methanol used in HPLC and UHPLC-MS/MS analysis were purchased from Sigma-Aldrich (St. Louis, MO, USA) in their highest purity. Ultrapure water (18.2 MΩ) was obtained from a Direct 16 Milli-Q purification system (Millipore, Bedford, USA).

2.4 Metabolomics analysis

The experimental planning for acquisition of metabolomics data is shown in supplementary file 01. As mentioned above, all analysis were only done based on the sample collected in the middle of exponential growth phase under oxygen-limited condition. This point is the same used to calculate the measured fluxes rate that carbon recovered were very well balanced. The protocol for sample preparation and analytical data acquisition were previously optimized and described.[15, 24] Briefly preparation of the samples involved the steps of quenching and extraction using cold methanol (–40°C) followed by boiling ethanol (96°C). The analytical method for separation and quantification of metabolites were based on UHPLC-MS/MS. The MS methodology was carried out on an AcQuity[tm] UPLC system (Waters, Milford, MA, USA) coupled to a triple quadrupole mass spectrometer (Xevo TQD, Waters) equipped with an electrospray ionization source. LC was performed on a Hydrophilic Interaction Liquid Chromatography (HILIC) with a BEH amide column (2.1 x 150 mm x 1.7 μm) (Waters Corporation, Milford, MA, USA) and Ion-Pairing Chromatography (IPC) with a reverse phase column, HSS-T3 (2.1 x 150 mm x 1.8 μm) (Waters Corporation, Milford, MA, USA).

2.5 Statistical analysis

As mentioned before, yeasts performed fermentation in biological triplicates and for each replicate was extracted the intracellular metabolites in three points within exponential growth phase. Each point was analyzed by UHPLC-MS/MS method in a three technical replicates, giving a total of twenty-seven samples measurements. So that these data would be converted into a single data the metabolome data set was statistically processed through a measured repeated ANOVA design. RStudio software (http://www.rstudio.org) was used to construct the mathematical models. The following mathematical equation represents how the ANOVA test was performed.

$$y_{ijk} = \mu + \alpha_i + \beta_{j(i)} + \tau_k + (\alpha\tau)_{ik} + e_{ijk}$$

Using this linear model, it was assumed that the data for class i; for yeast j at time k is equal to an overall mean μ plus the treatment effect α_i, the effect of the yeast within that class $\beta_{j(i)}$, the effect of time τ_k, the effect of the interaction between time and class $(\alpha\tau)_{ik}$, and the error e_{ijk}.

Such that:

- μ = overall mean
- α_i = effect of class i
- $\beta_{j(i)}$ = random effect of yeast j receiving class i
- τ_k = effect of time k
- $(\alpha\tau)_{ik}$ = class by time interaction
- e_{ijk} = experimental error

2.6 Construction of stoichiometric model

An overview of the metabolic model is shown in supplementary file 02. The stoichiometric model was constructed based on previously works.[16, 21, 25] It was defined with 39 reactions from xylose assimilation pathway, PPP, glycolysis, pyruvate metabolism and TCA. The TCA cycle was included but the compartmentalization into mitochondria and cytosol were not considered (Supplementary file 2). Biomass reaction was determined as previously described.[26] The biomass reaction includes the macromolecules components of the cell (i.e., proteins, nucleic acid, and polysaccharides).[27] The construction of stoichiometric model was based on the information available at Kyoto Encyclopedia of Genes and Genomes (KEGG). Genomic and biochemical information of *S. stipitis* (Entry T01023) was used as reference. The genes coding to enzymes on carbohydrate metabolism present into the respective genome could be determined using KEGG pathway, based on genome information, were identified the enzymes of metabolic reactions in defined pathways. With this information, the most important reactions in carbon central metabolism were selected for the construction of the stoichiometric model network.

2.7 Metabolic Flux Analysis using OptFlux

Once the model was uploaded into OptFlux, degrees of freedom of the system were calculated from the properties of the stoichiometric model. The accurate number of degrees of freedom was obtained by difference between the number of metabolites of the system and number of linearly independent equations of the system.[3] For differentiate internal and external reactions, external metabolites were identified with "[e]" and intracellular metabolites occurring in cytosolic subsystems with "[c]". Biomass reaction was used as an objective function.[8, 26] The extracellular measured fluxes rate of xylose fermentations obtained from middle exponential growth phase of a previously study were

added to the model.[22] The simulations were run using the algebraic method with least square fitting as properties.

2.8 Fluxes distribution simulations

The extracellular fluxes rates measurements were utilized as constrain to calculate the carbon flux distribution through the stoichiometric model. The model was classified in overdertermined system. It contains 39 reactions, 35 metabolites, 27 genes and, 04 degrees of freedom. Nine extracellular fluxes were measured (xylose consumption, ethanol, carbon dioxide, xylitol, glycerol, acetate, pyruvate, succinate and biomass productions) during xylose fermentations as previously described.[22] Seven of them were used as constrain to the initial metabolic model resolution. Xylose consumption and biomass production were maintained fixed during all simulations. In order to validate the metabolic flux distribution was simulated without two others measured fluxes rate (ethanol and carbon dioxide). So, these measured fluxes obtained experimentally were used to compare and validate the calculated fluxes for these two compounds.

2.9 Improving accuracy of metabolome data with metabolic flux

Concentrations of intracellular metabolites measurements were added directly on stoichiometric model. The supplementary file 03 shown the concentrations obtained through metabolomics analysis. After that simulations were performed aiming at determining flux distribution under the influence of the intracellular metabolites concentrations. Initially, the simulations were performed with addition of one metabolite concentration by time. Thus, eleven measured fluxes distribution were obtained, one to each metabolite concentration measured. Then, the fluxes obtained from stoichiometric calculations and the ones with addition of metabolome data were correlated using the Pearson correlation coefficient (R^2). The correlation coefficient was used to determine the

relationship between the calculated and measured fluxes distributions. The metabolites whose correlation was above 90% were added together to the stoichiometric model for novel simulations. Thus it was possible to estimate the percentage of error between calculated and measured fluxes.

3 Results and discussion

3.1 MFA for three xylose-fermenting yeasts

Initially a stoichiometric model was constructed for *S. stipitis*, *S. arborariae* and *S. passalidarum* containing 39 reactions and 35 metabolites. The metabolic network involved the pathways on central carbon metabolism such as xylose assimilation, pentose phosphate pathway, glycolysis, metabolism tricarboxylic acid cycle and biomass formation (Supplementary file 02). All reactions and metabolites included in the model are detailed in the supplementary files 04 and 05. The measured fluxes rate in the three xylose-fermenting yeasts cultivated under oxygen-limited condition were obtained for extracellular metabolites (Table 01).

Table 01. Rates of xylose consumption and products formation. Measured fluxes show average and standard deviations in mmol/gCDW.h^{-1} of biological growth in triplicate. These values were used in the stoichiometric model for calculated the carbon fluxes distribution. Growth rates (μ); carbon recovered (%); and redox balance (%) were also showed.

ID	Constrain	Formula	Molar Weight g.mol^{-1}	*S. stipitis* (28h)	*S. arborariae* (32h)	*S. passalidarum* (40h)
XYL[cons]	D-Xylose[cons]	$C_5H_{10}O_5$	150.13	-2.1552 ± 0.4760	-0.8991 ± 0.0732	-1.3709 ± 0.3986
ETOH[e]	Ethanol[e]	C_2H_6O	46.07	3.0482 ± 0.2552	0.8928 ± 0.1911	1.9721 ± 0.7427
ACE[e]	Acetate[e]	$C_2H_4O_2$	59.04	0.0000 ± 0.0000	0.0000 ± 0.0000	0.0000 ± 0.0000
CO2[e]	Carbon_dioxide[e]	CO_2	44.01	3.0521 ± 0.2555	0.8939 ± 0.1913	1.9746 ± 0.7437
XOL[e]	Xylitol[e]	$C_5H_{12}O_5$	152.15	0.0000 ± 0.0000	0.0297 ± 0.0063	0.0000 ± 0.0000
GROL[e]	Glycerol[e]	$C_3H_8O_3$	92.09	0.0448 ± 0.0094	0.0241 ± 0.0013	0.0000 ± 0.0000
PYR[e]	Pyruvate[e]	$C_3H_4O_3$	88.06	0.0000 ± 0.0000	0.0038 ± 0.0012	0.0000 ± 0.0000
SUC[e]	Succinic[e]	$C_4H_6O_4$	118.09	0.0000 ± 0.0000	0.0000 ± 0.0000	0.0000 ± 0.0000
	Biomass	$CH_{1.8}O_{0.5}N_{0.2}$	24.63	1.4500	1.2688	1.0150
	Growth Rates (μ)			0.0991	0.0500	0.1127
	Carbon Balance (%)			98	93	100
	Redox Balance (%)			100	94	100

Afterwards, these data were used to calculate the carbon flux distributions using the MFA model. All constructed models had its calculated fluxes under oxygen-limited condition, where the carbon and redox balances closed at least more than 93% recovery (Table 01).

Ethanol was the main product secreted by the three yeasts. The fluxes rate for ethanol formation observed in *S. stipitis* and *S. passalidarum* were 3.0 and 2.0 times highest than observed in a previous work that assessed another interesting yeast as *Candida tropicalis* for xylose fermentation.[11] As byproducts of xylose fermentation, xylitol and pyruvate were detected and quantified only in *S. arborariae*. Glycerol was quantified in *S. stipitis* and *S. arborariae*, being concentration rate in *S. stipitis* 1.8 times higher than *S. arborariae*. Acetate and succinate were not detected in any yeast investigated under oxygen-limited condition (Table 01).

Since four degrees of freedom were obtained from the difference between the number of reactions and metabolites, the ethanol flux rate was used to validate the fluxes obtained experimentally. As can be seen in figure 1 comparison between measured and calculated fluxes for ethanol in three yeasts showed very similarity. The prediction of ethanol calculated fluxes aligned with experimental measurements results, having a correlation above 95%. The experimental value for metabolic flux distribution in *S. stipitis* realizing xylose fermentative process are scarce.[19] Became the systemic analysis employed in this work a very useful approach for better understanding the xylose metabolism in the yeasts.
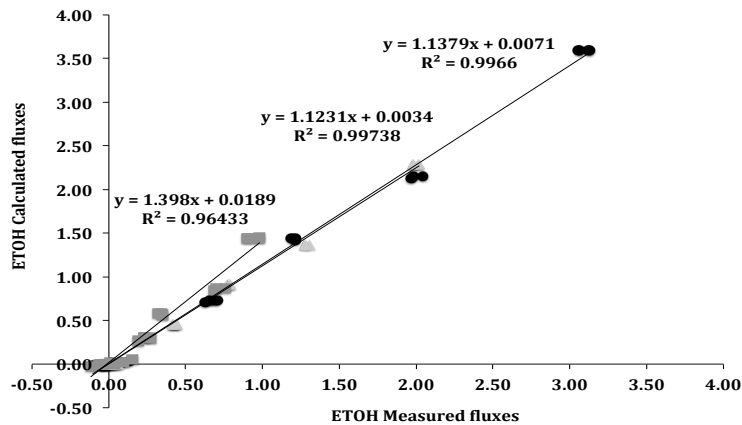
Figure 01. Correlation between measured and calculated ethanol fluxes. The points represent the measured fluxes (x-axis), calculated fluxes (y-axis) rates in three yeasts. *S. stipitis* (black cycle), *S. arborariae* (dark grey square) and *S. passalidarum* (light grey triangle).

3.2 Intracellular metabolites concentration

Metabolomics is a rapidly developing field that provides a powerful tool to efficiently identify and quantitate a large number of metabolites simultaneously.[28] Thus, metabolome allows obtainment of a set of metabolites with their respective concentrations. A previous metabolomics study showed some regulatory mechanisms of metabolic flux in central metabolism of different strains of *Saccharomyces cerevisiae* in distinct steady state conditions.[29] Among them, was observed that citrate accumulation inhibited the pyruvate kinase, causing reduction of glycolytic flux and ethanol production in nitrogen-limited yeast. Therefore, demonstrating that metabolite concentration is the main determinant of the metabolic flux in central metabolism of yeast.[29]

In this study, the concentrations of eleven metabolites measurements are shown in figure 02 for *S. stipitis*, *S. arborariae* and *S. passalidarum*. ANOVA analysis indicated that the minimal variation between biological and technical replicates and what the significance level of variance between quantification metabolites with respective p-values

(Supplementary file 06). Intracellular metabolomics data has been used in combination with flux analysis to classify and understand metabolism profiles in yeasts.

In our analysis, acetyl-CoA (ACCOA) and erytrose-4-phosphate (E4P) could not be detected in *S. stipitis* and *S. arborariae*, respectively (Figure 02). Sedoheptulose-7-phosphate (S7P) has four times higher concentration in *S. passalidarum* than others yeasts. E4P and S7P are precursor of amino acids as such as phenylalanine, tyrosine and tryptophan.[30] Concentration of D-ribulose-5-phosphate (RU5P) is twice higher than D-ribose-5-phosphate (R5P) in *S. stipitis* and *S. passalidarum*. The metabolomics analysis employed in our study was able to separate and quantify these two metabolites efficiently, overcoming the limitation observed is a previous metabolomics analysis for xylose fermentation performed by *S. passalidarum*.[30] Pyruvate (PYR) present five times higher concentration in *S. stipitis*. Dihydroxy acetone-phosphate (DHAP), D-glucose-6-phosphate (G6P), D-fructose-6phosphate (F6P), phosphoenolpyruvate (PEP) and malate (MAL) presented different concentrations among the three yeasts, range of 0.005 to 0,06 mmol (Figure 02).

Our metabolomics analysis was also able to efficiently separate isomers of sugar phosphate as glucose-6-phosphate and fructose-6-phosphate, solving a challenge observed previously.[31, 32] In *S. passalidarum* is observed equal or highest concentrations of almost all metabolites measured (Figure 02).
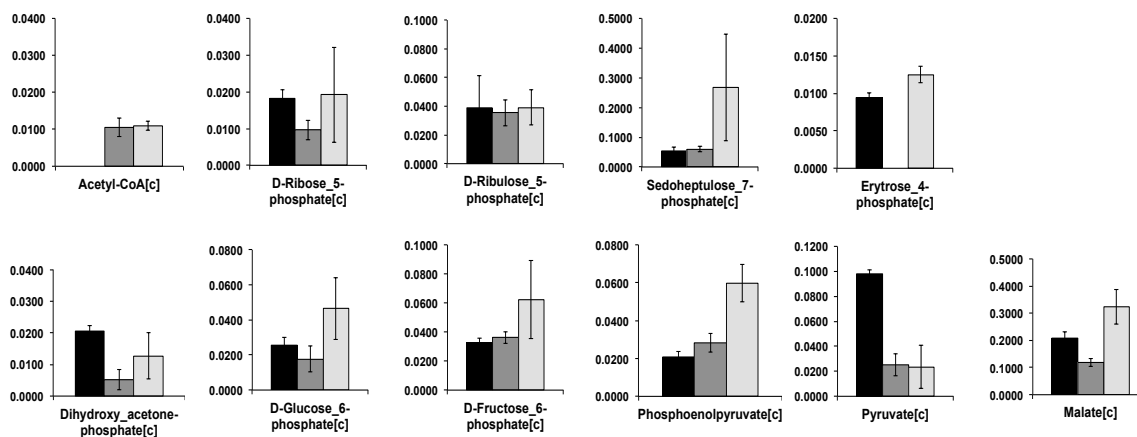
Figure 02. Measured intracellular metabolites concentrations (mmol) during exponential phase of xylose fermentation experiments. *S. stipitis* (black column), *S. arborariae* (dark grey column) and *S. passalidarum* (light grey column). Experiments were performed in biological triplicates. The presented values are men of ANOVA analysis for 3 biological replicates and 9 technical replicates.

The concentration changes do not readily allow conclusions on metabolic fluxes, or the direction of the flux changes, since an increase in metabolite concentration can both be indicative of increased activity of metabolite producing enzymes, but also decreased activity of metabolite consuming enzymes.[10] But the addition of the metabolite concetration in the model was useful to compare distribution measured fluxes with calculated flux. Thus, these data were added in the model and a simulations set of measured fluxes could be estimated.

3.3 Correlation between calculated and measured metabolic flux

It was investigated if the addition intracellular metabolites concentrations in the model keep the fluxes distributions rates. The model maintains the constraints utilized to estimate the calculated flux. Intracellular fluxes distributions were simulated again, now with addition intracellular metabolite concentration measurement per simulation. In *S. stipitis* and *S. arborariae* were quantified ten intracellular metabolites, consequently ten simulations were realized. While in *S. passalidarum* was quantified one intracellular

metabolite more than *S. stipitis* and *S. arborariae*, thus were obtained eleven simulations of flux distribution.

Pearson correlation test (R^2) were used to evaluate the consistence of the each measured flux to calculated flux (Supplementary file 06). It was assumed that R^2 greater than 0.90 and 0.95 were satisfactory to determine correlation between measured and calculated fluxes. In *S. stipitis* it was observed that from ten metabolites, eight (i.e. 80%) shown $R^2 >$ 0.90 between measured and calculated fluxes (Supplementary file 07a). 50% of them (E4P, F6P, G6P, MAL and RU5P) showed that the measured fluxes are aligned with calculated fluxes, presenting $R^2 > 0.95$ (Figure 03a). In *S. arborariae* it was observed that from ten metabolites seven (i.e. 70%) shown $R^2 > 0.90$ (Supplementary file 07b) and 50% of them (ACCOA, F6P, G6P, MAL and RU5P), presents $R^2 > 0.95$ (Figure 03b) between measured and calculated fluxes. While, in *S. passalidarum* it was observed that from eleven metabolites nine (i.e. 82%) shown $R^2 > 0.90$ between measured and calculated fluxes (Supplementary file 07c). Moreover 54% of the measure metabolites (ACCOA, E4P, F6P, G6P, MAL and RU5P) presents $R^2 > 0.95$ (Figure 03c). The correlation higher 0.90 between fluxes with metabolites measurements and calculated fluxes could not be established for PEP and PYR in any of the tested yeasts (Supplementary file 7). The fluxes rate for PEP and PYR formation are the highest estimated. These highest fluxes rate can demand faster procedures for sample preparation and data processing steps to avoid degradation and lost of information. However, a study that assessed metabolome of *S. passalidarum* in xylose fermentation founded similar concentrations of PEP and PYR.[30] But this work not use the metabolome data in a metabolic flux, do not been possible make comparison.

Other measured metabolites that could not be correlated with calculated fluxes was acetyl-CoA. As seen in *S. stipitis* (Figure 02), ACCOA was not quantified, probably because

the fluxes rates in this yeast were higher than observed in *S. arborariae* and *S. passalidarum*. Acetyl-CoA is involved in 34 compartmentalized metabolic reactions and used for acetylation of macromolecules.[32] To balance the use of these precursor metabolites, cells have evolved several levels of tight regulation, especially to control biosynthesis of amino acids, lipids, nucleotides, and carbohydrates needed for cell growth, homeostasis, and maintenance.[32]
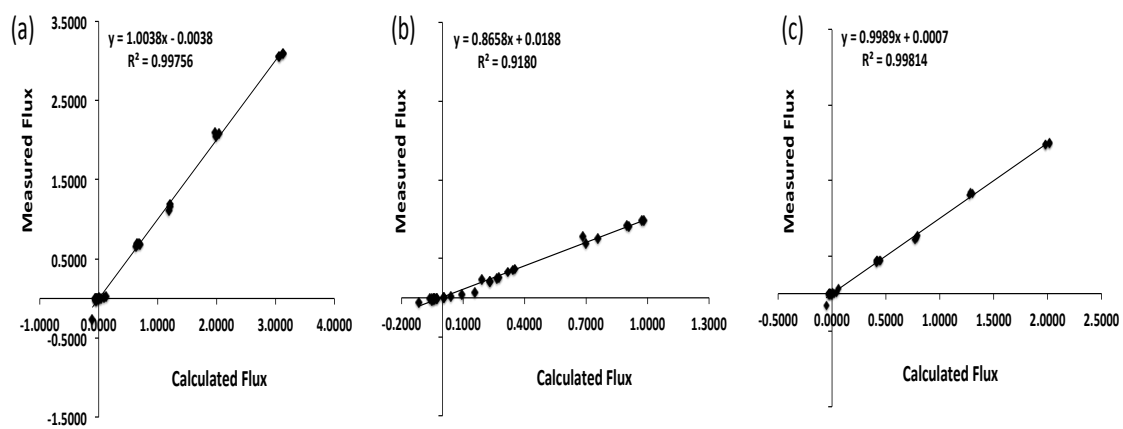
Figure 03. Correlation rate (R^2) between calculated and measured flux. The relationship were assess with all metabolites measured that present R^2 higher than 0.95. (a) *S. stipitis* with E4P, F6P, G6P, MAL and RU5P; (b) *S. arborariae* with ACCOA, F6P, G6P, MAL and RU5P; and (c) *S. passalidarum* with ACCOA, E4P, F6P, G6P, MAL and RU5P.

3.4 Intracellular carbon flux distribution of xylose metabolism in yeasts

One of the drawbacks of measuring the intracellular metabolites experimentally is the impossibility to distinguish metabolites in different compartments, e.g. pyruvate in the cytoplasm and pyruvate in mitochondria will be considered as the same species in a metabolome experiment.[33] For that reason, in the model developed here cellular compartmentalization is not considered.

In the present study, carbon flux distribution had a correlation above 90% between experimental data and calculated flux obtained for *S. stipitis* (Figure 04), *S. arborariae*

(Figure 05) and *S. passalidarum* (Figure 06). The calculated and measured fluxes showed that xylose assimilation in *S. stipitis, S. arborariae* and *S. passalidarum* is realized by XR enzyme using both NADPH and NADH (R01 e R02) cofactors.[23, 27, 33, 41] As also seen in previous studies.[22, 34-36] Two reactions represent this first step in xylose metabolism in the model. Xylose reduction reaction NADH-dependent showed higher fluxes rates for *S. stipitis* and *S. passalidarum* (R02 Figures 04 and 06). In *S. arborariae* the xylitol production is higher than other two yeasts, confirming the literature data and our previous study.[22, 33] *S. passalidarum* possess two XR (genes XIL1.1 and XIL1.2) and one of them uses preferentially NADH as cofactor.[37] Its enzymatic activity presents higher NADH-dependent XR.[23] Although is observed in enzymatic assays for XR that *S. stipitis* and *S. arborariae* presents higher NADPH-dependent activity, the calculated fluxes rate were higher with reactions that use NADH. Probably this difference between enzymatic activities and calculated fluxes rate can be explained by optimal condition and concentration determined in enzymatic activities, not necessarily these occurs *in vivo*. Same results is also observed in work conducted by Wahlbom et al., that assessed the intracellular fluxes in a recombinant xylose-utilizing *Saccharomyces cerevisiae*.[26]

The cofactor imbalance in XR and XDH reactions can cause byproducts formation as xylitol how observed in *S. arborariae*. The production of xylitol is a consequence of the differences in cofactor specificity in the XR and XDH reactions.[16] Xylitol production was not detected in cultivations with *S. stipitis* and *S. passalidarum*. These results are in good agreement with previous work that showed that higher NADH dependent XR activity resulted in less xylitol production.[38]

In *S. arborariae* (Figure 05) was observed in reaction that uses NADPH as cofactor (R01) rate 3.0 times higher than was observed in *S. passalidarum* (Figure 06). This characteristic

in *S. arborariae* can be associated with flux rate for oxidative-PPP (R10) in 3.0 times higher than observed in *S. passalidarum*. This metabolism characteristic in *S. arborariae* is to regenerate the NADPH cofactor on oxidative pentose phosphate pathway (R10). *S. arborariae* has the slower flux rate to consume xylose and smaller growth rate (Figure 05). Due to the decreased cell growth, the requirement of NADPH has been reduced and caused the down-regulation of fluxes through pentose phosphate pathway (PPP).[21, 39] The flux rate in oxidative pentose phosphate pathway (R10) responsible by regenerating NADPH was 3.0 times higher in *S. arborariae* than *S. passalidarum*. Probably, this flux characteristic can be associated with high flux rates observed in R01 that also present high flux rate in *S. arborariae* (Figure 05).

D-Xylose

R30
-2.1551
-2.1551

D-Xylose

R01
0.1316
0.0177

R02
1.9662
2.0966

Xylitol - - - - - - - - - - - - → **Xylitol**

R03
2.0435
2.0808

R31
0.0000
0.0000

R10
0.0831
0.0131

D-Xylulose

R05
0.6290
0.6605

R04
1.9863
2.0400

D-Glucose-6-P

R11
-0.1054
-0.2666

D-Ribulose-5-P

Xylulose-5-P

R08
0.7012
0.6820

D-Ribose-5-P

D-Fructose-6-P

Sedoheptulose-7-P

R12
1.1851
1.1134

R09
0.6563
0.6820

R07
0.6901
0.6900

D-Fructose-1,6-P2

Erythrose-4-P

R13
1.2091
1.1626

R06
0.6564
0.6979

Glyceraldehyde-3-P

Dihydroxy-acetona-P

R16
3.1213
3.0863

R15
-0.0111
-0.0059

R14
1.2100
1.1932

Phosphoenolpyruvate

R17
3.1295
3.1024

Glycerol ← - - - - - Glycerol

R32
0.0265
0.0265

Pyruvate - - - - - - - - - - - - → **Pyruvate**

R18
3.0561
3.0670

R19
3.0651
3.0559

R35
0.0000
0.0000

CO₂ ← - - - -

R33
3.0520
3.0520

CO_2

Acetaldehyde → Ethanol - - - - - - - - → **Ethanol**

R22
0.0330
0.000

R20
-0.0291
-0.0041

R34
3.0481
3.0481

CO_2 →

Acetate - - - - - - - - - - - - - - → **Acetate**

CoA

R21
-0.0517
-0.0263

R36
0.0000
0.0000

Acetyl-CoA

Cytosol

Mitochondria

R23
-0.0440
-0.0200

R29
-0.0601
-0.0057

Oxaloacetate

Citrate

R24
-0.0418
-0.0173

Malate

Isocitrate

R25
-0.0396
-0.0147

R28
-0.0484
-0.0066

α-ketoglutaric_acid

Fumarate

R26
-0.0254
-0.0055

R27
-0.0372
-0.0064

Succinate

GLU-6P

α-KETO

R-5P

OXA

G-3P

PYR

PEP

ERY-4P

ACCOA

NADPH

R38
Biomass
0.0080
0.0093

Biomass

R37
0.0000
0.0000

Succinate

Figure 04. Metabolic flux in *S. stipitis*. Carbon distribution comparison between calculated (top line) and measured (bottom line) fluxes rate. Intracellular metabolites highlight in red had the concentration added in the model and were validated through of simulation the measured fluxes rate. External metabolites had the fluxes rate used as constrains.
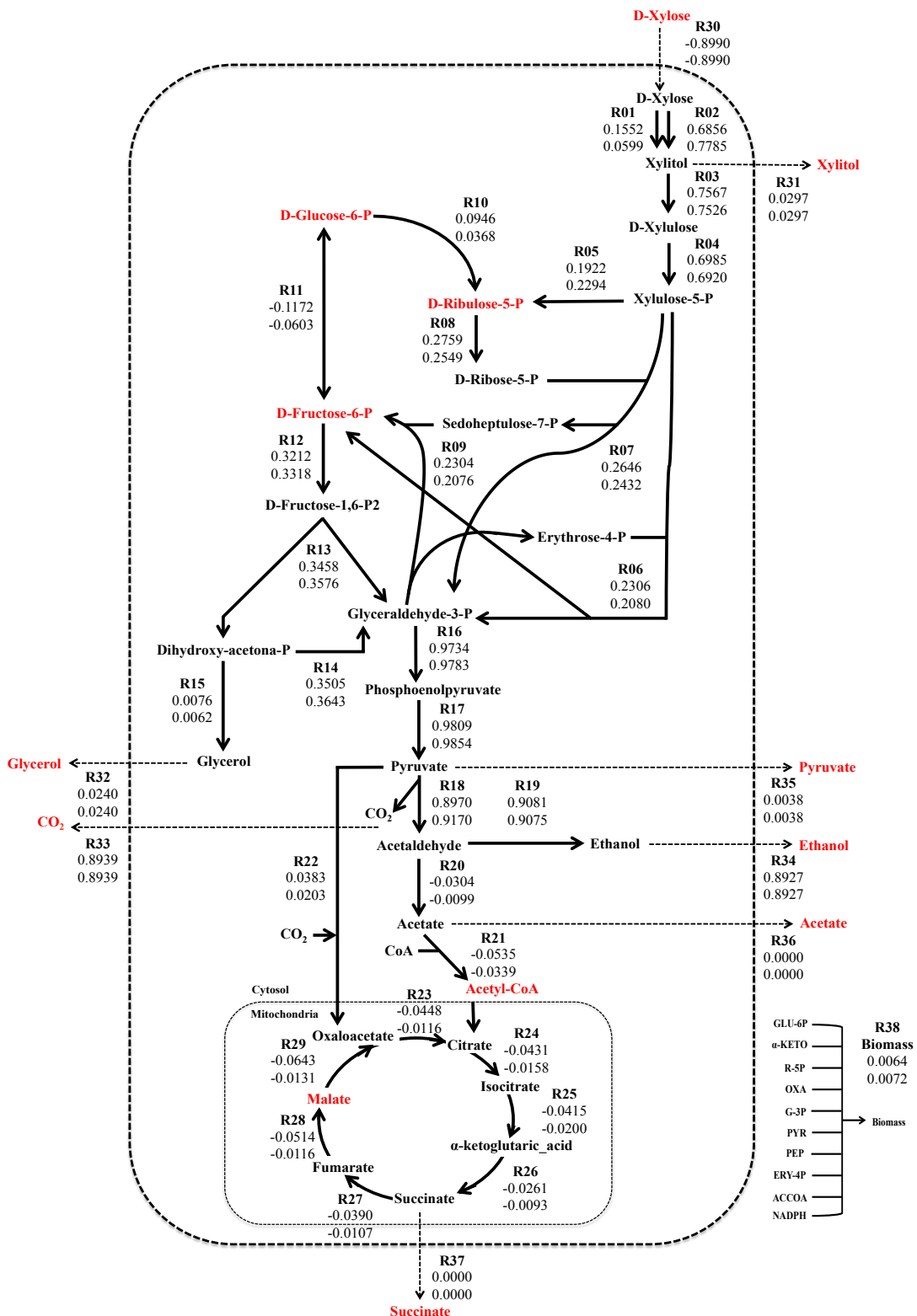
Figure 05. Metabolic flux in *S. arborariae*. Carbon distribution comparison between calculated (top line) and measured (bottom line) fluxes rate. Intracellular metabolites highlight in red had the concentration added in the model and were validated through of simulation the measured fluxes rate. External metabolites had the fluxes rate used as constrains.
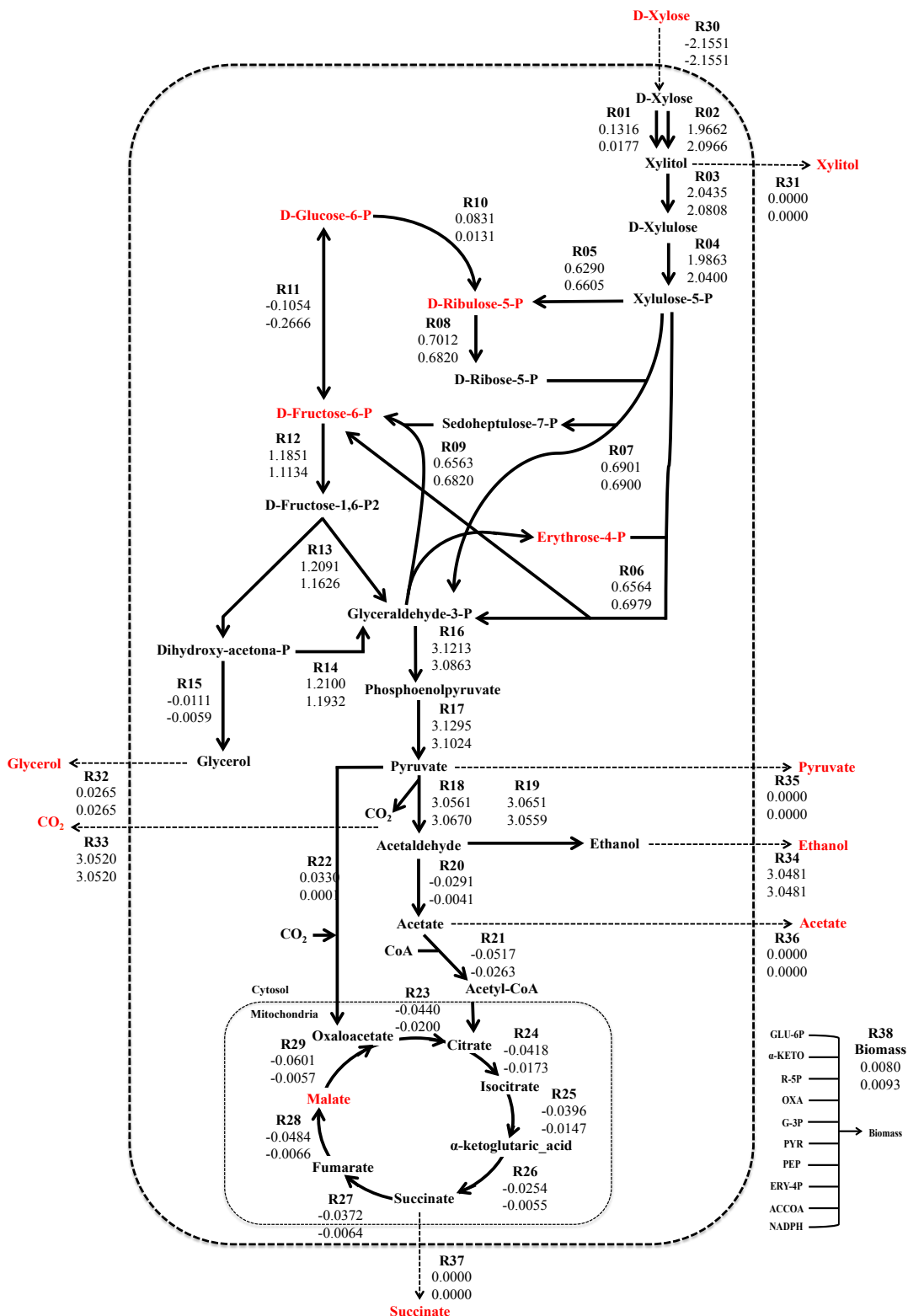
Figure 06. Metabolic flux in *S. passalidarum*. Carbon distribution comparison between calculated (top line) and measured (bottom line) fluxes rate. Intracellular metabolites highlight in red had the concentration added in the model and were validated through of simulation the measured fluxes rate. External metabolites had the fluxes rate used as constrains.
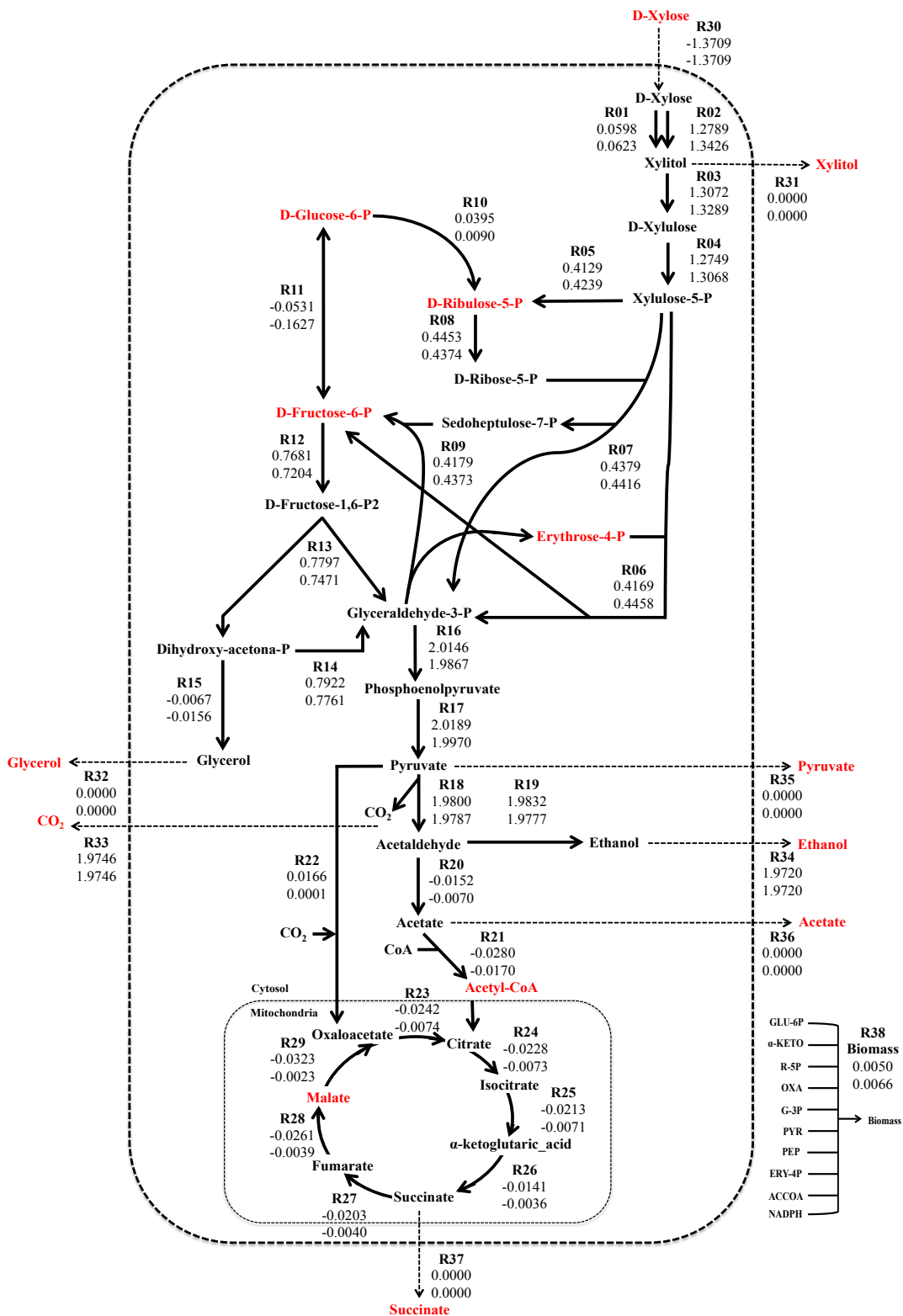
Besides then, this conversion of glucose-6-phosphate into ribulose-5-phosphate in S. passalidarum was 3.0 times slower than *S. stipitis* and *S. arborariae.* The yeasts evaluated here, predominantly showed pyruvate reactions to acetaldehyde and consequently ethanol production (Figures 04 – 06). The pyruvate represents one of the most important regulation points in carbon metabolism. Carbon can either follow catabolic reactions (acetaldehyde production) or anabolic pathways (oxaloacetate production).[39] In *S. passalidarum* (Figure 06) was not observed flux rate for glycerol formation (R32), this is another important characteristic in the carbon flux distribution that distinguishes itself from of others yeasts and can be associated with better NADH/NAD+ balance.

To our knowledge, for first time is proposed a metabolic flux model to *S. arborariae* and *S. passalidarum*. In addition, metabolic flux combined with intracellular metabolites concentration was useful to improve the accuracy of metabolomics analysis. Metabolome data increase the precision of the true state of the cell metabolism.[7] Using intracellular metabolites concentrations its measurement can be directly linked to the metabolic reactions network.[17] The percentage of errors between calculated and measured fluxes was determined to check the accuracy of the model (Figure 07).
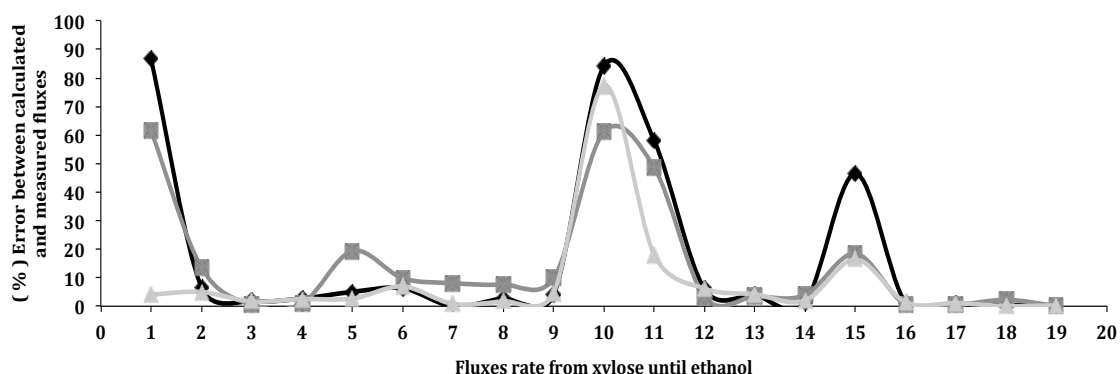

Figure 07. Percentage errors between calculated and measured fluxes rates. Points represent the fluxes rates from xylose to ethanol. *S. stipitis* (black line), *S. arborariae* (grey dark line) and *S. passalidarum* (gray light line).

The reactions present in xylose assimilation pathway (R01 – 04), is observed that only the R01 in *S. stipitis* and *S. arborariae* the error is of 85% and 60%, respectively. In pentose phosphate pathway (R05 – R09) the error is less than 10%, except for R05 in *S. passalidarum*. The reaction R10, responsible by regenerate NADPH in oxidative pentose phosphate pathway and the reversible reaction R11 also showed error higher than 60%. In general, from twenty metabolic fluxes rates that are involved xylose conversion to ethanol, four of them (R01, R05, R10, R11 and R15) were not predicted accurately in the metabolic model proposed. Thus showing that our analysis was able to predict 74% of fluxes rate with accuracy above 90%.

Conclusions

The present work shows a detailed metabolic profile of natural xylose-fermenting yeasts. A new stoichiometric reactions model from xylose until ethanol was useful to estimate the metabolic flux distribution in *Spathaspora* yeasts for first time. The metabolic flux model was useful to improve accuracy metabolome data through the metabolic flux model. Based on the flux analysis *S. stipitis* and *S. passalidarum* are the two promise yeasts with better metabolic characteristics able to perform xylose fermentation. It is proposed that the high xylose assimilation rates allow high ethanol production. The carbon distribution is divided among PPP and glycolysis pathways similarly. In *S. passalidarum* the highest flux rate of XR NADH-dependent demanded less NADPH regeneration. And inactive flux rate to glycerol production are metabolic characteristics that allows better $NADH/NAD^+$ balance, thus allowing improves ethanol production from xylose.

Conflict of interest

The authors declare no financial or commercial competing interest.

References

1.   Stephanopoulos, G. N., Aristidou, A. A., and Nielsen, J. (1998) Metabolic engineering: Principles and Methodologies, *Academic Press - San Diego-CA*, 725p.
2.   Bideaux, C., Montheard, J., Cameleyre, X., Molina-Jouve, C., and Alfenore, S. (2016) Metabolic flux analysis model for optimizing xylose conversion into ethanol by the natural C5-fermenting yeast Candida shehatae, *Applied microbiology and biotechnology 100*, 1489-1499.
3.   Carreira, R., Evangelista, P., Maia, P., Vilaça, P., Pont, M., Tomb, J., Rocha, I., and Rocha, M. (2014) CBFA: phenotype prediction integrating metabolic models with constraints derived from experimental data, *BMC systems biology 8:123*.
4.   Sánchez, B. J., and Nielsen, J. (2015) Genome scale models of yeast: towards standardized evaluation and consistent omic integration, *Royal Society of Chemistry 7*, 846-858.
5.   Jones, J. A., Toparlak, O. D., and Koffas, M. A. (2015) Metabolic pathway balancing and its role in the production of biofuels and chemicals, *Current opinion in biotechnology 33*, 52-59.
6.   Lee, S. Y., Park, J. M., and Kim, T. Y. (2011) Application of metabolic flux analysis in metabolic engineering, *Methods in enzymology 498*, 67-93.
7.   O'Brien, E. J., Monk, J. M., and Palsson, B. O. (2015) Using Genome-scale Models to Predict Biological Capabilities, *Cell 161*, 971-987.
8.   Rocha, I., Maia, P., Evangelista, P., Vilaça, P., Soares, S., Pinto, J. P., Nielsen, J., Patil, K. R., Ferreira, E. C., and Rocha, M. (2010) OptFlux: an open-source software platform for in silico metabolic engineering, *BMC systems biology 4:45*.
9.   Buescher, J. M., Antoniewicz, M. R., Boros, L. G., Burgess, S. C., Brunengraber, H., Clish, C. B., DeBerardinis, R. J., Feron, O., Frezza, C., Ghesquiere, B., Gottlieb, E., Hiller, K., Jones, R. G., Kamphorst, J. J., Kibbey, R. G., Kimmelman, A. C., Locasale, J. W., Lunt, S. Y., Maddocks, O. D., Malloy, C., Metallo, C. M., Meuillet, E. J., Munger, J., Noh, K., Rabinowitz, J. D., Ralser, M., Sauer, U., Stephanopoulos, G., St-Pierre, J., Tennant, D. A., Wittmann, C., Vander Heiden, M. G., Vazquez, A., Vousden, K., Young, J. D., Zamboni, N., and Fendt, S. M. (2015) A roadmap for interpreting (13)C metabolite labeling patterns from cells, *Current opinion in biotechnology 34*, 189-201.
10.   Tummler, K., and Klipp, E. (2018) The discrepancy between data for and expectations on metabolic models: How to match experiments and computational efforts to arrive at quantitative predictions?, *Current Opinion in Systems Biology 8*, 1-6.
11.   Li, X., Deng, Y., Yang, Y., Wei, Z., Cheng, J., Cao, L., Mu, D., Luo, S., Zheng, Z., Jiang, S., and Wu, X. (2017) Fermentation Process and Metabolic Flux of Ethanol Production from the Detoxified Hydrolyzate of Cassava Residue, *Frontiers in microbiology 8*, 1603.
12.   Pluskal, T., and Yanagida, M. (2016) Metabolomic Analysis of Schizosaccharomyces pombe: Sample Preparation, Detection, and Data Interpretation, *Cold Spring Harbor protocols 2016*, pdb top079921.

13.   Granucci, N., Pinu, F. R., Han, T. L., and Villas-Boas, S. (2015) Can we predict the intracellular metabolic state of a cell based on extracellular metabolite data?, *Molecular bioSystems 11, 3297*.

14.   Buchholz, A., Hurlebaus, J., Wandrey, C., and Takors, R. (2002) Metabolomics: quantification of intracellular metabolite dynamics.pdf>, *Biomolecular Engineering 19*, 5 - 15.

15.   Campos, C. G., Veras, H. C. T., de Aquino Ribeiro, J. A., Costa, P., Araujo, K. P., Rodrigues, C. M., de Almeida, J. R. M., and Abdelnur, P. V. (2017) New Protocol Based on UHPLC-MS/MS for Quantitation of Metabolites in Xylose-Fermenting Yeasts, *Journal of the American Society for Mass Spectrometry*.

16.   Wahlbom, C. F., Eliasson, A., and Hahn-Hägerdal, B. (2001) Intracellular fluxes in a recombinant xylose-utilizing *Saccharomyces cerevisiae* cultivated anaerobically at different dilution rates and feed concentrations, *Biotechnology and bioengineering 72*, 289-296.

17.   Bogaerts, P., Mhallem Gziri, K., and Richelle, A. (2017) From MFA to FBA: Defining linear constraints accounting for overflow metabolism in a macroscopic FBA-based dynamical model of cell cultures in bioreactor, *Journal of Process Control 60*, 34-47.

18.   Sonderegger, M., Jeppsson, M., Hahn-Hägerdal, B., and Sauer, U. (2004) Molecular basis for anaerobic growth of *Saccharomyces cerevisiae* on xylose, investigated by global gene expression and metabolic flux analysis, *Applied and environmental microbiology 70*, 2307-2317.

19.   Balagurunathan, B., Jonnalagadda, S., Tan, L., and Srinivasan, R. (2012) Reconstruction and analysis of a genome-scale metabolic model for Scheffersomyces stipitis, *Microbial cell factories 11*, 27.

20.   Trausinger, G., Gruber, C., Krahulec, S., Magnes, C., Nidetzky, B., and Klimacek, M. (2015) Identification of novel metabolic interactions controlling carbon flux from xylose to ethanol in natural and recombinant yeasts, *Biotechnology for biofuels 8*.

21.   Liang, M., Damiani, A., He, Q. P., and Wang, J. (2013) Elucidating Xylose Metabolism of Scheffersomyces stipitis for Lignocellulosic Ethanol Production, *ACS Sustainable Chemistry & Engineering 2*, 38-48.

22.   Veras, H. C. T., Parachin, N. S., and Almeida, J. R. M. (2017) Comparative assessment of fermentative capacity of different xylose-consuming yeasts, *Microbial cell factories 16*, 153.

23.   Verduyn, C., Postma, E., Scheffers, W. A., and Van Dijken, J. P. (1992) Effect of Benzoic Acid on Metabolic Fluxes in Yeasts: A Continuous-Culture Study on the Regulation of Respiration and Alcoholic Fermentation, *Yeast 8*, 501-517.

24.   Bergdahl, B., Heer, D., Sauer, U., Hahn-Hagerdal, B., and van Niel, E. W. (2012) Dynamic metabolomics differentiates between carbon and energy starvation in recombinant Saccharomyces cerevisiae fermenting xylose, *Biotechnology for biofuels 5*, 34.

25.   Almeida, J. R., Bertilsson, M., Hahn-Hagerdal, B., Liden, G., and Gorwa-Grauslund, M. F. (2009) Carbon fluxes of xylose-consuming Saccharomyces cerevisiae strains are affected differently by NADH and NADPH usage in HMF reduction, *Applied microbiology and biotechnology 84*, 751-761.

26.   Wahlbom, C. F., Eliasson, A., and Hahn-Hagerdal, B. (2001) Intracellular Fluxes in a Recombinant Xylose-Utilizing Saccharomyces cerevisiae Cultivated Anaerobically at Different Dilution Rates and Feed Concentration, *Biotechnology and bioengineering 72*.

27.   Senger, R. S. (2010) Biofuel production improvement with genome-scale models: The role of cell composition, *Biotechnology journal 5*, 671-685.

28.   Riekeberg, E., and Powers, R. (2017) New frontiers in metabolomics: from measurement to insight, *F1000Research 6*, 1148.

29.   Hackett, S. R., Zanotelli, V. R., Xu, W., Goya, J., Park, J. O., Perlman, D. H., Gibney, P. A., Botstein, D., Storey, J. D., and Rabinowitz, J. D. (2016) Systems-level analysis of mechanisms regulating yeast metabolic flux, *Science 354*.

30.   Long, T. M., Su, Y. K., Headman, J., Higbee, A., Willis, L. B., and Jeffries, T. W. (2012) Cofermentation of glucose, xylose, and cellobiose by the beetle-associated yeast Spathaspora passalidarum, *Applied and environmental microbiology 78*, 5492-5500.

31.   Matsuda, F., Toya, Y., and Shimizu, H. (2017) Learning from quantitative data to understand central carbon metabolism, *Biotechnology advances 35*, 971-980.

32.   Nielsen, J., and Keasling, J. D. (2016) Engineering Cellular Metabolism, *Cell 164*, 1185-1197.

33.   Österlund, T., Nookaew, I., Bordel, S., and Nielsen, J. (2013) Mapping condition-dependent regulation of metabolism in yeast through genome-scale modeling, *BMC systems biology 7:36*.

34.   Bruinenberg, P. M., de BOT, P. H. M., van DIJKEN, J. P., and SCHEFFERS, W. A. (1984) NADH-linked aldose reductase - the key to anaerobic alcoholic fermentation of xylose by yeasts, *Applied Microbiology Biotechnology 19*, 256-260.

35.   Bengtsson, O., Hahn-Hagerdal, B., and Gorwa-Grauslund, M. F. (2009) Xylose reductase from Pichia stipitis with altered coenzyme preference improves ethanolic xylose fermentation by recombinant Saccharomyces cerevisiae, *Biotechnology for biofuels 2:9*, 1-10.

36.   Jeffries, T. W., and Shi, N. Q. (1999) Genetic engineering for improved xylose fermentation by yeasts, *Advances in Biochemical Engineering/Biotechnology 65*, 118-161.

37.   Cadete, R. M., de Las Heras, A. M., Sandstrom, A. G., Ferreira, C., Girio, F., Gorwa-Grauslund, M. F., Rosa, C. A., and Fonseca, C. (2016) Exploring xylose metabolism in Spathaspora species: XYL1.2 from Spathaspora passalidarum as the key for efficient anaerobic xylose fermentation in metabolic engineered Saccharomyces cerevisiae, *Biotechnology for biofuels 9:167*, 1-14.

38.   Mortensen, J., Poulsen, T. S., Grove, E. L., Refsgaard, J., Nielsen, H. L., Pedersen, S. B., Thygesen, S. S., Hvas, A. M., and Kristensen, S. D. (2008) Monitoring aspirin therapy with the Platelet Function Analyzer-100, *Scandinavian journal of clinical and laboratory investigation 68*, 786-792.

39.   Quiros, M., Martinez-Moreno, R., Albiol, J., Morales, P., Vazquez-Lima, F., Barreiro-Vazquez, A., Ferrer, P., and Gonzalez, R. (2013) Metabolic flux

analysis during the exponential growth phase of Saccharomyces cerevisiae in wine fermentations, *PloS one 8*, e71909.

SUPPLEMENTARY FILES

Utilization of metabolic flux analysis for metabolome data validation of xylose-fermenting yeasts

Supplementary file 01. Experimental planning for the metabolomics samples in the three species of xylose-fermenting yeasts.
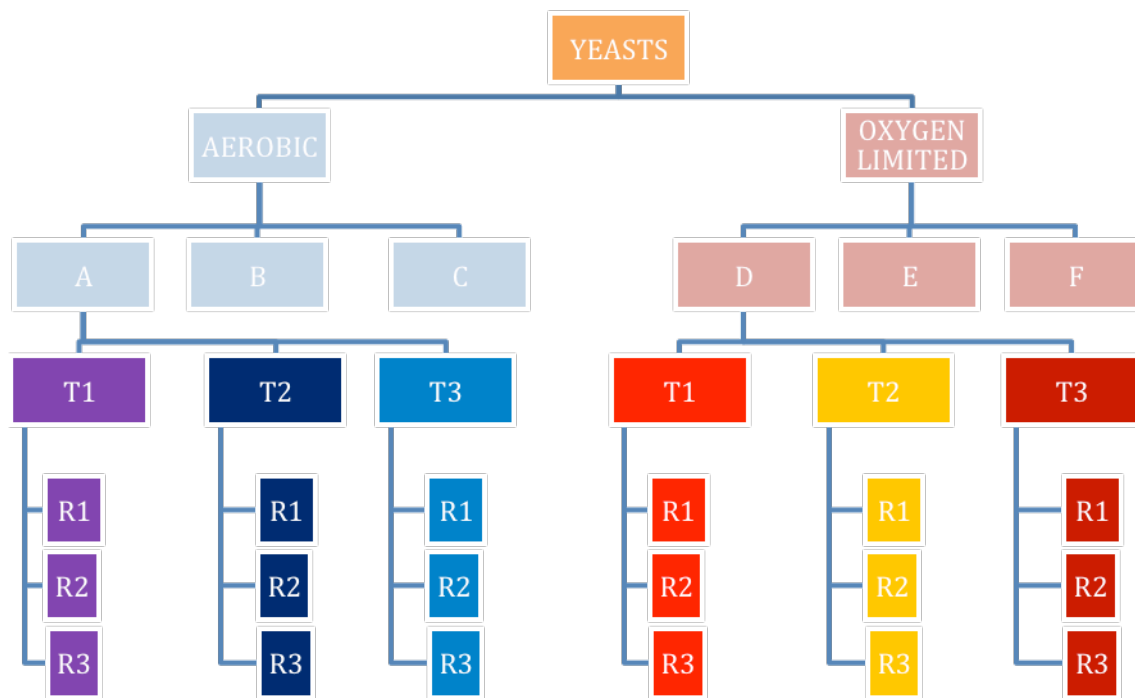
Supplementary file 02. Overview of metabolic network model with the direction of reactions and cofactor (NADPH/NADP$^+$ and NADH/NAD$^+$) used by enzymes.

D-Xylose

D-Xylose
NADPH   NADH
NADP$^+$ NAD$^+$
Xylitol - - - - - - - - -> Xylitol
NAD+
NADH
D-Xylulose
ATP
ADP
2 NADP$^+$
D-Glucose-6-P
2 NADPH
D-Ribulose-5-P <- Xylulose-5-P
D-Ribose-5-P
Sedoheptulose-7-P
D-Fructose-6-P
ATP
ADP
Erythrose-4-P
D-Fructose-1,6-P2
Glyceraldehyde-3-P
NAD+
NADH
Dihydroxy-acetona-P
Phosphoenolpyruvate
ADP
ATP
NADH
NAD$^+$
Glycerol <- - - - - - Glycerol
Pyruvate - - - - - - - -> Pyruvate
CO$_2$
CO$_2$ <- - - - -
NADH
NAD$^+$
Acetaldehyde -> Ethanol - - - - - -> Ethanol
ATP
ADP
NADP$^+$
NADPH
CO$_2$ ->
Acetate - - - - - - - - - -> Acetate
CoA
ATP
ADP
Acetyl-CoA

Cytosol
Mitochondria

Oxaloacetate -> Citrate
NADH
NAD+
Malate
Isocitrate
NAD+
NADH
α-ketoglutaric_acid
NAD+
NADH
Fumarate
Succinate

Succinate

GLU-6P
α-KETO
R-5P
OXA
G-3P
PYR
PEP
ERY-4P
ACCOA
NADPH

Biomass

Supplementary file 03. Metabolites concentration. Average (μg/mL) of samples in exponential growth phase on oxygen-limited condition with respective standard deviation (s).

Metabolites	*S. stipitis*		*S. arborariae*		*S. passalidarum*	
	(µg/mL)	*s*	*(µg/mL)*	*s*	*(µg/mL)*	*s*
ACCOA	-	-	8.5733	2,067	10.115	0.035
AKG	-	-	-	-	-	-
MAL	28.090	2.880	15.7400	1,922	56.330	0.552
G6P	6.6100	1.180	4.5867	1,940	16.605	2.171
F6P	8.4967	0.812	5.5500	1,030	21.100	0.891
DHAP	3.5000	0.297	-	0,544	3.3300	0.014
GAP	-	-	-	-	-	-
R5P	4.1900	0.523	-	0,608	6.6900	0.806
Ru5P	11.8050	1.66	8.1533	2,095	11.9300	0.523
E4P	1.8900	0.135	-	-	2.6650	0.021
S7P	19.9433	3.91	17.3967	2,735	140.060	11.851
PEP	3.5267	0.423	4.7333	0,820	13.8150	0.389
PYR	8.6100	0.283	1.4233	0,775	5.0950	0.827
XYLU	-	-	-	-	-	-
XYL	3389.29	841.2	5116.46	312,05	1632.65	504.82
GLU	-	-	-		-	-
GLY	-	-	-		-	-
XOL	221.58	79.43	422.62	29,84	227.74	132.56

Supplementary file 04.

Reactions in stoichiometric model input in OptFlux to MFA approach.

ID	Reactions equation	EC number	Pathways
R01	D-Xylose[c] + NADPH[c] --> Xylitol[c] + NADP[c]	1.1.1.307	Xylose Assimilation Pathway
R02	D-Xylose[c] + NADH[c] --> Xylitol[c] + NAD[c]	1.1.1.307	Xylose Assimilation Pathway
R03	Xylitol[c] + NAD[c] --> D-Xylulose[c] + NADH[c]	1.1.1.9	Xylose Assimilation Pathway
R04	D-Xylulose[c] + ATP[c] --> D-Xylulose_5-phosphate[c] + ADP[c]	2.7.1.17	Xylose Assimilation Pathway
R05	D-Xylulose_5-phosphate[c] --> D-Ribulose_5-phosphate[c]	5.1.3.1	Pentose Phosphate Pathway
R06	D-Xylulose_5-phosphate[c] + D-Erythrose_4-phosphate[c] --> D-Fructose_6-phosphate[c] + D-Glyceraldehyde_3-phosphate[c]	2.2.1.1	Pentose Phosphate Pathway
R07	D-Xylulose_5-phosphate[c] + D-Ribose_5-phosphate[c] --> Sedoheptulose_7-phosphate[c] + D-Glyceraldehyde_3-phosphate[c]	2.2.1.1	Pentose Phosphate Pathway
R08	D-Ribulose_5-phosphate[c] --> D-Ribose_5-phosphate[c]	5.3.1.6	Pentose Phosphate Pathway
R09	Sedoheptulose_7-phosphate[c] + D-Glyceraldehyde_3-phosphate[c] --> D-Erythrose_4-phosphate[c] + D-Fructose_6-phosphate[c]	2.2.1.2	Pentose Phosphate Pathway
R10	D-Glucose_6-phosphate[c] + 2 NADP[c] --> D-Ribulose_5-phosphate[c] + CO2[c] + 2 NADPH[c]	1.1.1.49	Pentose Phosphate Pathway
R11	D-Glucose_6-phosphate[c] <--> D-Fructose_6-phosphate[c]	5.3.1.9	Glycolisis Pathway
R12	D-Fructose_6-phosphate[c] + ATP[c] <--> D-fructose-1-6-bisphosphate[c] + ADP[c]	2.7.1.11	Glycolisis Pathway
R13	D-fructose-1-6-bisphosphate[c] --> Dihydroxyacetone_phosphate[c] + D-Glyceraldehyde_3-phosphate[c]	4.1.2.13	Glycolisis Pathway
R14	Dihydroxyacetone_phosphate[c] --> D-Glyceraldehyde_3-phosphate[c]	5.3.1.1	Glycolisis Pathway
R15	Dihydroxyacetone_phosphate[c] + NADH[c] --> Glycerol[c] + NAD[c]	1.1.1.156	Glycolisis Pathway
R16	D-Glyceraldehyde_3-phosphate[c] + NAD[c] --> Phosphoenolpyruvate[c] + NADH[c]	1.2.1.12	Glycolisis Pathway
R17	Phosphoenolpyruvate[c] + ADP[c] --> Pyruvate[c] + ATP[c]	2.7.1.40	Pyruvaye Metabolism
R18	Pyruvate[c] --> Acetaldehyde[c] + CO2[c]	4.1.1.1	Pyruvaye Metabolism
R19	Acetaldehyde[c] + NADH[c] --> Ethanol[c] + NAD[c]	1.1.1.1	Pyruvaye Metabolism
R20	Acetaldehyde[c] + NADP[c] --> Acetate[c] + NADPH[c]	1.2.1.5	Pyruvaye Metabolism
R21	Acetate[c] + CoA[c] + ATP[c] --> Acetyl_CoA[c] + ADP[c] + Pi[c]	6.2.1.1	Pyruvaye Metabolism
R22	Pyruvate[c] + CO2[c] + ATP[c] --> Oxaloacetate[c] + ADP[c] + Pi[c]	6.4.1.1	TCA Cicle Pathway
R23	Acetyl_CoA[c] + Oxaloacetate[c] --> Citrate[c] + CoA[c]	2.3.3.1	TCA Cicle Pathway
R24	Citrate[c] --> Isocitrate[c]	4.2.1.3	TCA Cicle Pathway
R25	Isocitrate[c] + NAD[c] --> alpha-Ketoglutaric_acid[c] + CO2[c] + NADH[c]	1.1.1.41	TCA Cicle Pathway
R26	alpha-Ketoglutaric_acid[c] + NAD[c] --> Succinate[c] + NADH[c] + CO2	1.2.4.2	TCA Cicle Pathway
R27	Succinate[c] --> Fumarate[c]	1.3.5.1	TCA Cicle Pathway
R28	Fumarate[c] --> Malate[c]	4.2.1.2	TCA Cicle Pathway
R29	Malate[c] + NAD[c] --> Oxaloacetate[c] + NADH[c]	1.1.1.37	TCA Cicle Pathway
R30	D-Xylose[e] --> D-Xylose[c]		External Metabolite
R31	Xylitol[c] --> Xylitol[e]		External Metabolite
R32	Glycerol[c] --> Glycerol[e]		External Metabolite
R33	CO2[c] --> CO2[e]		External Metabolite
R34	Ethanol[c] --> Ethanol[e]		External Metabolite
R35	Pyruvate[c] --> Pyruvate[e]		External Metabolite
R36	Acetate[c] --> Acetate[e]		External Metabolite
R37	Succinate[c] --> Succinate[e]		External Metabolite
R38	0.300 alpha-Ketoglutaric_acid[c] + 0.287 Oxaloacetate[c] + 0.406 Pyruvate[c] + 0.061 D-Erythrose_4-phosphate[c] + 0.040 D-Ribose_5-phosphate[c] + 0.164 D-Glyceraldehyde_3-phosphote[c] + 0.122 Phosphoenolpyruvate[c] + 0.176 Acetyl_CoA[c] + 1.762 NADPH[c] --> 0.071 Fumarate[c] + 0.026 Acetate[c] + 0.335 NADH[c] + 1.521 Pi[c] + 0.323 CO2[c]		Biomass_reaction
R39	Biomass[c] --> Biomass_formation[e]		Biomass_formation

Supplementary file 05.
Metabolites in the stoichiometric model input in OptFlux.

ID	Metabolites	Formula	Compartment
XYL[c]	D-Xylose[c]	C5H10O5	cytosol
XOL[c]	Xylitol[c]	C5H12O5	cytosol
XYLU[c]	D-Xylulose[c]	C5H10O5	cytosol
XYLU-5P[c]	D-Xylulose_5-phosphate[c]	C5H11O8P	cytosol
ERY-4P[c]	D-Erythrose_4-phosphate[c]	C4H9O7P	cytosol
FRU-6P[c]	D-Fructose_6-phosphate[c]	C6H13O9P	cytosol
F1-6-BP[c]	D-fructose-1-6-bisphosphate[c]	C6H14O12P2	cytosol
GA-3P[c]	D-Glyceraldehyde_3-phosphate[c]	C3H7O6P	cytosol
RIB-5P[c]	D-Ribose_5-phosphate [c]	C5H11O8P	cytosol
SEDO-7P[c]	Sedoheptulose_7-phosphate[c]	C7H15O10P	cytosol
RIBU-5P[c]	D-Ribulose_5-phosphate[c]	C5H11O8P	cytosol
GLU-6P[c]	D-Glucose_6-phosphate[c]	C6H13O9P	cytosol
DHAP[c]	Dihydroxyacetone_phosphate[c]	C3H7O6P	cytosol
3PGT[c]	3-Phosphoglycerate[c]	C3H7O7P	cytosol
GROL[c]	Glycerol[c]	C3H8O3	cytosol
GLY-3P[c]	Glycerol_3-phosphate[c]	C3H9O6P	cytosol
PEP[c]	Phosphoenolpyruvate[c]	C3H5O6P	cytosol
PYR[c]	Pyruvate[c]	C3H4O3	cytosol
ACDH[c]	Acetaldehyde[c]	C2H4O	cytosol
ETOH[c]	Ethanol[c]	C2H6O	cytosol
ACE[c]	Acetate[c]	C2H4O2	cytosol
ACCOA[c]	Acetyl-CoA[c]	C23H38N7O17P3S	cytosol
COA[c]	CoA[c]	C21H36N7O16P3S	cytosol
OXA[c]	Oxaloacetate[c]	C4H4O5	cytosol
CIT[c]	Citrate[c]	C6H8O7	cytosol
ISO[c]	Isocitrate[c]	C6H8O7	cytosol
AKG[c]	alpha-Ketoglutaric_acid[c]	C5H6O5	cytosol
FUM[c]	Fumarate[c]	C4H4O4	cytosol
SUC[c]	Succinate[c]	C4H6O4	cytosol
MAL[c]	Malate[c]	C4H6O5	cytosol
CO2[c]	Carbon_dioxide[c]	CO2	cytosol
Pi[c]	Phosphate[c]	H3PO4	cytosol
H2O[c]	H2O[c]	H2O	cytosol
NADPH[c]	NADPH[c]	C21H30N7O17P3	cytosol
NADP[c]	NADP[c]	C21H29N7O17P3	cytosol
NADH[c]	NADH[c]	C21H29N7O14P2	cytosol
NAD[c]	NAD[c]	C21H28N7O14P2	cytosol
ATP[c]	ATP[c]	C10H16N5O13P3	cytosol
ADP[c]	ADP[c]	C10H15N5O10P2	cytosol
Biomass[c]	Biomass[c]	CH1.8O0.5N0.2	cytosol
XYL[e]	D-Xylose[e]	C5H10O5	external
XOL[e]	Xylitol[e]	C5H12O5	external
GROL[e]	Glycerol[e]	C3H8O3	external
ETOH[e]	Ethanol[e]	C2H6O	external
PYR[e]	Pyruvate[e]	C3H4O3	external
ACE[e]	Acetate[e]	C2H4O2	external
SUC[e]	Succinate[e]	C4H6O4	external
CO2[e]	Carbon_dioxide[e]	CO2	external

Supplementary file 06.
P-values for effects class (C), time (T) and interaction between class and time (ICT) of ANOVA table for yeasts *S. arborariae, S. passalidarum* and *S.stipitis* under oxygen-limited.

Metabolite	*S. stipitis* ρ-value			*S. arborariae* ρ-value			*S. passalidarum* ρ-value		
	C	*T*	*ICT*	*C*	*T*	*ICT*	*C*	*T*	*ICT*
ACCOA				***	**	**			
L-MAL				***			**	**	
G6P									
F6P		*						*	
DHAP		*						**	
R5P		*						*	
RU5P		*		*	*	*		**	
E4P							*	*	
S7P		*		***				*	
PEP	*	*	*	**	**	**	*		
PYR									
XYL		**						***	**
XOL	**	*	*				*	**	

Significance codes: ' ' 0; '***' 0.001; '**' 0.01; '*' 0.05

Supplementary file 07. Correlation (R2) between calculated and measured fluxes.
(a) S. stipitis; (b) S. arborariae; and (c) S. passalidarum. ACCOA (acetyl-CoA), DHAP
(dihydroxy-acetone-phosphate), (E4P) erythrose-4-phosphate), F6P (fructose-6-
phosphate), G6P (glucose-6-phosphate), MAL (malate), PEP (phosphoenolpyruvate), PYR
(pyruvate), R5P (ribose-5-phosphate), RU5P (ribulose-5-phosphate), S7P (sedoheptulose-
7-phosphate) were the metabolites measured. (X-axis) show the calculated flux using the
constrained values of products. (Y-axis) show measured fluxes with respectively
metabolites concentrations. Fluxes rates are in mmol/gCDW.h-1